ON THE THROUGHPUT GAIN OF RAPID SYMBOL DURATION ADAPTATION WITH DYNAMIC SPREADING GAIN CONTROL

by

Song Xue

B.ASc., University of Electronic Science and Technology of China, 1990

A Thesis submitted in partial fulfillment
of the requirements for the degree of
Master of Applied Science
in the School
of
Engineering Science

SIMON FRASER UNIVERSITY
Summer 2010

APPROVAL

Name: Song Xue

Degree: Master of Applied Science

Title of Thesis: On the Throughput Gain of Rapid Symbol Duration Adaptation with Dynamic Spreading Gain Control

Examining Committee:

Dr. Lesley Shannon,
Assistant Professor
Chair

Dr. Daniel C. Lee,
Associate Professor,
Senior Supervisor

Dr. Paul Ho,
Professor,
Supervisor

Dr. Ivan V. Bajic,
Assistant Professor,
Examiner

Date Approved: August 3, 2010

Declaration of
Partial Copyright Licence

Abstract

In [1] [2], methods for symbol-by-symbol (SBS) channel feedback and symbol duration adaptation by rapid dynamic spreading gain control were proposed by the authors. Previous research showed that, in an uncoded system, the symbol-by-symbol duration adaptation can theoretically achieve a throughput gain by orders of magnitude over non-adaptation or a frame-by-frame (FBF) adaptation in a fast time-varying fading environment. This thesis extends the study of the throughput gain to the cases in which, the symbol duration can only be chosen from a discrete finite set, the channel is varying during each symbol duration, and the duration adaption is implemented in a coded system. The results show that for an uncoded system the throughput gain is still significant even within discrete duration sets and over the channel varying during each symbol duration. In coded systems, the performance depends on the coding scheme and the interleaver size. For many commonly used codes without interleaving, symbol-by-symbol duration adaptation can also bring a large throughput gain. However, if the system adopts a superior forward error correction (FEC) code, e.g., DVB-S2 LDPC codes, or if the system employs a large size interleaver to make the channel much less time correlated, there will be little benefit to apply SBS duration adaptation to increase the throughput. This thesis also presents the analysis on the throughput gain with outdated and imperfect channel information. The numerical results illustrates how the throughput gain will diminish as the correlation between the available channel information and the true channel condition decreases.

To my wife, Jun Wang, and my daughter, Lan Xue, for their understanding and support during my degree pursuit

Acknowledgments

It is a pleasure to thank all the people who made this thesis possible even though it is also very difficult to mention all the names.

I would like to present my appreciation to my supervisor, Dr. Daniel C. Lee. He not only offered me this precious opportunity to study, but also supported me with his inspirations, energy , time and patience.

I owe a very special thank to Mr. Muhammad Naeem, a Ph.D candidate in our group. During the past couple years, he generously offers me the guidance, encouragement and support on all aspects of my study and research. I also would like to thank Dr. Jinyun Ren, who is often the first person I seek advices from.

I wish to thank all instructors of the courses I have taken during my study, Dr. John Bird, Dr. Shawn Stapleton, Dr. James K. Cavers, and Dr. Ivan V. Bajic. Their knowledge and insight have enlighten my path. I am also grateful to Dr. Rodney G. Vaughan, who not only gave me instruction when I audited his course but also encourages and inspires me since I knew him.

Most importantly, I wish to thank my family, specially my wife, Maggie Jun Wang, and my daughter, Sherry Lan Xue. They are my constant sources of support and love. To them, I dedicate this thesis.

Contents

Approval ii

Abstract iii

Dedication iv

Acknowledgments v

Contents vi

List of Tables ix

List of Figures x

Nomenclature xiv

1 Introduction 1

1.1 Adaptive transmission 2

1.1.1 History of adaptive transmission 3

1.1.2 Current application of adaptive transmission 4

1.2 Rapid Dynamic spreading gain control 5

1.2.1 Frame-by-frame dynamic spreading gain control 5

1.2.2 Rapid spreading gain control 7

1.2.3 Throughput gain of symbol-by-symbol DGSC 14

1.3 Outline of this thesis 16

2 Throughput Gain within Discrete Duration Set **20**
2.1 System model . . . 20
2.2 Numerical study of throughput gain . . . 24
2.2.1 Non-coherent BFSK . . . 24
2.2.2 M-QAM . . . 27
2.3 Chapter conclusion . . . 29

3 Throughput Gain within Discrete Duration Set over Channels Varying in A Symbol Duration **33**
3.1 System model . . . 33
3.1.1 Throughput of symbol-by-symbol duration adaptation . . . 35
3.1.2 Throughput of frame-by-frame adaptation . . . 36
3.1.3 Throughput gain . . . 37
3.2 Numerical method . . . 38
3.2.1 MGF of received SNR at MRC output . . . 38
3.2.2 Expectation of BEP for NC-BFSK . . . 39
3.2.3 Expectation of BEP for MQAM . . . 40
3.2.4 Computing P_j with MGF . . . 41
3.3 Numerical results . . . 43
3.4 Chapter conclusion . . . 48

4 Throughput Gain Achieved In Coded Systems **54**
4.1 System model . . . 54
4.1.1 Capacity analysis . . . 54
4.1.2 Throughput gain in coded systems . . . 56
4.1.3 Simulation systems . . . 58
4.1.4 Sample size and confidence interval . . . 59
4.2 Numerical results . . . 62
4.2.1 Convolutional codes . . . 62
4.2.2 LDPC codes . . . 69
4.2.3 Other block codes . . . 70
4.2.4 Interleaved channel . . . 70
4.2.5 Impact of f_d, the maximum Doppler shift . . . 74
4.3 Chapter conclusion . . . 76

5 Throughput Gain with Imperfect Channel Information **77**
5.1 System model 78
5.2 Optimization of policy $r_p(\hat{Y}) = q\hat{Y}$ 78
5.3 Suboptimal SBS adaptation policy for BFSK 80
5.4 Chapter conclusion 86

6 Conclusions and Discussion **87**

A Derivation of Channel Power Gain Autocorrelation **91**

B Proof of Equation (5.2) **93**

Bibliography **95**

List of Tables

2.1 The values of κ for Fig. 2.3 28
2.2 The values of Λ, Υ, α and β for (2.18) 28

3.1 The values of Λ, Υ, α and β for (3.21) 40
3.2 the values of N and K for NC-BFSK 44
3.3 the values of N and K for MQAM 44

4.1 The simulation sample size to obtain bit error probability curves for coded systems. The confidence level is set to 99% and the width of the confidence interval is set to be $0.1\varepsilon_b$. 62

List of Figures

1.1 System model of adaptive transmission 2
1.2 Spreading and modulation in a WCDMA downlink dedicated channel (DCH). 6
1.3 Channel power gain of a Rayleigh fading channel. The maximum Doppler shift of the channel is 100Hz. 7
1.4 Example of FOSSIL. 9
1.5 Example of sibling (conjugate) FOSSIL. 10
1.6 RI and FBI code sets. 12
1.7 Throughput gain for NC-BFSK over Rayleigh fading channel. 17
1.8 Throughput gain for MQAM over Rayleigh fading channel. 17

2.1 Receive power thresholds for symbol rate adaptation 21
2.2 The throughput gain achieved by SBS with non-coherent BFSK and the 32-code set, $\kappa = 1$ 26
2.3 Throughput gain for NC-BFSK with different values of κ 26
2.4 Throughput gains for NC-BFSK with the code length only spanning from 2 to 2^{10}, 2 to 2^{16}, 2 to 2^{20} 27
2.5 The BEP bounds for MQAM 31
2.6 The throughput gain for 4QAM within the 28-code set and $\kappa = 1$ 31
2.7 The throughput gain for 16QAM within the 28-code set and $\kappa = 1$ 32
2.8 The throughput gain for 64QAM within the 28-code set and $\kappa = 1$ 32

3.1 The throughput gain achieved by SBS duration adaptation with 12-code duration set ($N = 12$) for NC-BFSK modulation. The throughput gain curves for different values of κ are plotted for comparison. 45

3.2 The throughput gain achieved by SBS duration adaptation with 12-code duration set ($N = 12$) for NC-BFSK modulation. The throughput gain curves for different values of κ are plotted for comparison. 45
3.3 The throughput gain of NC-BFSK within three different size duration sets. The value of κ is 200 for all the results. 49
3.4 The throughput gain of 4QAM for different values of κ. 49
3.5 The throughput gain of 16QAM for different values of κ. 50
3.6 The throughput gain of 64QAM for different values of κ. 50
3.7 The throughput gain of 4QAM, 16QAM and 64QAM. $\kappa = 1$ 51
3.8 The throughput gain of 4QAM, 16QAM and 64QAM. $\kappa = 10$ 51
3.9 The throughput gain of 4QAM, 16QAM and 64QAM. $\kappa = 100$ 52
3.10 The throughput gain of 4QAM, 16QAM and 64QAM. $\kappa = 1000$ 52
3.11 The throughput gain for NC-BFSK with different values of maximum Doppler shift f_D. 53
3.12 The channel gain correlation for different values of maximum Doppler shift f_D. 53

4.1 System diagram of the simulation to obtain the curve of $h_c(x)$, the BEP for constant receive SNR x over non-fading channel, for combinations of coding and modulation schemes. 59
4.2 System diagram of the simulation to obtain the curve of $\tilde{H}_c(x)$, the BEP for expected receive SNR x over Rayleigh fading channel, for combinations of coding and modulation schemes. 59
4.3 BEP curve $\tilde{H}_c(x)$ and $h_c(x)$. The coding scheme of the system is a 1/2 code rate convolutional code of constraint length 9 and hard-decision Viterbi decoding. The modulation scheme is QPSK. 60
4.4 The constellation plot of QPSK with $pi/4$ phase shift and Gray mapping. . . 65
4.5 Throughput gains of QPSK and convolutional codes (constraint length = 9) without interleaver for code rates of 1/2, 1/3 and 1/4. The decoding scheme is the soft-decision Viterbi algorithm. 65
4.6 Throughput Gain for convolutional code (constraint length = 9, code rate = 1/4) with MQAM. The decoding scheme is hard-decision Viterbi algorithm. . 67
4.7 Throughput Gain for convolutional code (constraint length = 9, code rate = 1/4) with MPSK. The decoding scheme is hard-decision Viterbi algorithm. . 67

4.8 Throughput Gain for convolutional code (constraint length = 9, code rate = 1/4) with NC-MFSK. The decoding scheme is hard-decision Viterbi algorithm. 68
4.9 Throughput Gain of 64QAM and convolutional code (constraint length = 9) for code rates of 1/2,1/3 and 1/4. The decoding scheme is hard-decision Viterbi algorithm. 68
4.10 Throughput Gain of BPSK and LDPC code (DVB S.2 code, code rate = 1/2) 69
4.11 Throughput Gains of BPSK and Hamming code (31, 26), BCH code (31,26) and Reed-Solomon code (31,27). 71
4.12 Throughput Gains of Hamming code (31, 26) with BPSK and MQAM. 71
4.13 System diagram of the simulation to obtain the curve of $\tilde{H}_c(x)$, the BEP for expected receive SNR x over interleaved Rayleigh fading channel. The coded sequence is interleaved before modulation and the demodulated signal is deinterleaved before fed to the decoder. 72
4.14 Throughput gains for QPSK with convolutional code (constraint length = 9, code rate = 1/4) and interleavers of the size of 768 (12×64), 3072 (48×64) and 18432 (48×384) bits. The decoding scheme is soft-decision Viterbi algorithm decoding. The throughput gain without interleaving and over uncorrelated Rayleigh fading channel is also plotted for the purpose of comparison. 73
4.15 Throughput gains for QPSK with convolutional code (constraint length = 9, code rate = 1/4) and interleavers of the size of 768 (12×64), 3072 (48×64) and 18432 (48×384) bits. The decoding scheme is hard-decision Viterbi algorithm decoding. The throughput gain without interleaving and over uncorrelated Rayleigh fading channel is also plotted for the purpose of comparison. 73
4.16 Throughput gains for QPSK with Hamming code (31, 26) and interleavers of the size of 768 (12 × 64), 3072 (48 × 64) bits. The throughput gains without interleaving are also plotted for the purpose of comparison. 75
4.17 Throughput gains for BPSK with LDPC (1/2 code rate DVB-S2 code) and interleavers of the size of 64800 (90 × 720), 648000 (90 × 7200) bits. The throughput gains without interleaving and over uncorrelated Rayleigh fading channel are also plotted for the purpose of comparison. 75

4.18 Throughput gains for QPSK and 1/2 code rate convolutional code of the constraint length of 9 over Rayleigh fading channels of maximum Doppler shift of 100, 200, 300 and 500 Hz. The decoding scheme is soft-decision Viterbi algorithm. 76

5.1 The throughput gain vs SEP required for BFSK with imperfect channel information. 85

Nomenclature

List of Abbreviations

3G or 3^{rd}G	the Third Generation
AWGN	Additive White Gaussian Noise
BEP	Bit Error Probability
BPSK	Binary Phase Shift Keying
CCK	Complementary Code Keying
CDMA	Code Division Multiple Access
CSI	Channel State Information
DCH	Dedicated Channel
DSGC	Dynamic Spreading Gain Control
DSSS	Direct Sequence Spread Spectrum
DVB-S2	Digital Video Broadcasting - Satellite - Second Generation
ERP	Extended Rate Physical
FBF	Frame By Frame
FBI	Feed Back Information
FEC	Forward Error Correction
FOSSIL	Forest for OVSF-Sequence-Set-Inducing Lineages
HSPA	High Speed Packet Access
LAN	Local Area Network
LDPC	Low Density Parity Check
MGF	Moment Generation Function
ML	maximum likelihood
MMSE	minimum mean square error
MRC	Maximal Ratio Combiner

NC-BFSK	Non-Coherent Binary Frequency Shift Keying
OFDM	Orthogonal Frequency-Division Multiplexing
OVSF	Orthogonal Varied Spreading Factor
PC	Personal Computer
pdf	probability density function
PN	Pseudo Noise
QAM	Quadrature Amplitude Modulation
QPSK	Quadrature Phase Shift Keying
RCPC	Rate Compatible Punctured Convolutional
RI	Rate Indicator
SBS	Symbol By Symbol
SEP	Symbol Error Probability
SG	Spreading Gain
SNR	Signal to Noise Ratio
USB	Universal Serial Bus
WCDMA	Wideband CDMA

List of Symbols

$\alpha[i]$	the power gain of the fading channel at time i
$\bar{L}_S$	the symbol duration in number of chips for SBS duration adaptation
$\bar{r}_S$	the average symbol rate achieved by SBS duration adaptation
η	denotes the value of $h_b^{-1}(\varepsilon_b)/\kappa$
Γ_X^j	a $L_j \times L_j$ positive definite matrix for X^j based on the channel correlation
γ	the signal to noise ratio per symbol
$\hat{a}(t+\tau)$	The prediction of the channel gain at time $t+\tau$
$\hat{p}_b$	the estimation of bit error probability
κ	the average SNR per chip
Λ	the discrete symbol duration set
$\mathcal{H}(\varepsilon_b)$	binary entropy function
$\mathcal{R}$	the throughput gain
Ω	the transmission mode set
Θ	the discrete symbol rate set
$\tilde{g}_i$	complex channel gain at chip time i
$\tilde{L}_F$	the symbol duration in number of chips for FBF duration adaptation within the discrete duration set Λ
$\tilde{Y}$	the random variable denotes normalized receive power
ε	the symbol error probability constraint
ε_b	the bit error probability constraint
ζ_i	the thresholds to divide the receive power range, $i = 1,\ 2,\ \ldots,\ N-1$
$a(t)$	the normalized complex channel gain
$a_{ES}(t)$	the channel gain estimation at time t
B	denotes the bandwidth
C	the OVSF code sequence set
C_n^i	the i^{th} code of the length of n bits in the FOSSIL
f_D	the maximum Doppler shift
$f_{\tilde{Y}}(\tilde{y})$	the probability density function of the normalized receive power $\tilde{Y}(t)$
g_i	normalized complex channel gain at chip time i
$h(\gamma)$	the symbol error probability function
$J_0(\mathrm{x})$	the zero-order Bessel function of the first kind
L	denotes the symbol duration or code sequence length in number of chips

L_F	the symbol duration in number of chips for FBF duration adaptation
N_0	the power spectral density of the additive white Gaussian noise
P	the average receive power
p_b	bit error probability
P_j	the probability of $h_b\left(\kappa\sum_{i=1}^{L_j}\left\|g_i\right\|^2\right)\leq\varepsilon_b$
P_T	the transmit power
P_{out}	the probability that the longest symbol duration in the duration set Λ cannot satisfy the bit error constraint ε_b
$Q(x)$	the Gaussian Q function
r	denotes the symbol rate
$r(\|a(t)\|)$	the rate adaptation policy based on $\|a(t)\|$
r_F	the symbol rate of FBF duration adaptation
SC_n^i	the i^{th} code of the length of n bits in the sibling FOSSIL
T_c	chip duration
T_s	the symbol duration
T_s	the symbol duration
X^j	random variable $\sum_{i=1}^{L_j}\left\|g_i\right\|^2$
$Y(t)$	the receive power
λ_i	the ith eigenvalue of matrix Γ_X^j
$\Phi_{\mathrm{FBI}}(j)$	the subset of FBI code set Ψ_{FBI} in which all codes have the spreading gain of $2^j p$
Ψ_{FBI}	FBI code set
Ψ_{RI}	RI code set
$\tilde{h}_c(\{r(y)\|y\})$	the BEP function for an SBS duration adaptation system with a coding scheme c
$\tilde{H}_c(\gamma)$	the BEP function for a non-adaptive system with a coding scheme c
$\tilde{a}(t)$	the complex channel gain
$a_v(t)$	the estimation error (noise) in $a_{ES}(t)$
$f_X^j(x)$	the probability density function of X^j
$r_p(\cdot)$	rate adaptation policy
$\|C\|$	the length of code C in number of chips
RS	Reed-Solomon (code)

Chapter 1

Introduction

The increasing demand to access the Internet from various locations is one of the main engine for the significant development in wireless communication. For example, WiFi (IEEE 802.11x) allows personal computers (PC) to be connected to local area networks (LAN) without wiring, providing great flexibility of Internet access. Nowadays, WiFi is widely available in public area (airports, libraries, universities, etc.) and private homes. In cellular systems, the focus of the business is shifting from voice service to Internet access and web applications. Mobile phones are rapidly turning from simple talking tools to sophisticated devices that have much of the capability of PCs and provide users accessibility to the Internet. Laptop users now can connect to the Internet through cellular networks (e.g., HSPA, the High Speed Packet Access standard) via tiny adapters like USB (Universal Serial Bus) modems. This kind of devices provide the laptop users the freedom to choose suitable location to access the Internet.

The increasing demand of voice, data and multimedia services continuously propels the need for higher capacity and data rates in wireless communication. However, radio spectrum is a limited resource and unable to provide an arbitrary amount of bandwidth. Thus, improving radio spectral efficiency is one of the most important issues in meeting the growing demand for communication services.

Wireless communication is greatly challenged by the multipath phenomena of wireless channels. In designing a communication system with fixed transmission parameters, the parameters, e.g., the transmit power, are chosen to give a sufficient margin to maintain the communication quality even with the worst channel conditions. In that way, the spectrum is not efficiently utilized and has much potential to be explored. The throughput, for a

specified bit/symbol error rate requirement, can be increased significantly if the system can adapt the transmission parameters to the channel conditions.

1.1 Adaptive transmission

The basic system model of an adaptive transmission is illustrated in Figure 1.1. The communication system is equipped with a feedback channel where the knowledge of the channel can be delivered from the receiver to the transmitter. The receiver performs channel estimation and symbol detection. The result of channel estimation, i.e., channel state information (CSI), is used to detect the received symbols, and is also fed back to the transmitter as reference for adjusting transmission parameters. The objective of the adaptive system could be optimizing the system spectral efficiency or maximizing the system throughput subject to a bit/symbol error probability (BEP/SEP) constraint.

Let N be the number of the transmission modes available in the communication system. Denote the set of transmission modes by $\Omega = \{\omega_1, \omega_2, \ldots, \omega_N\}$. These modes could be modulation constellation sizes, code rates, transmit power levels, etc, or some combination of them. The set Ω is known by both the transmitter and receiver. The transmitter assigns one of the modes in Ω to each group of incoming data bits on the basis of the available channel state information (CSI). The transmitter chooses the transmission mode in such a way that certain adaptation criteria can be achieved.

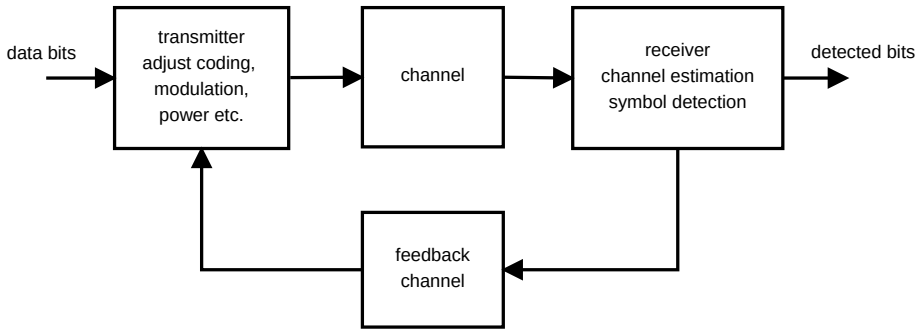

Figure 1.1: System model of adaptive transmission

In designing an adaptive transmission system, several requirements have to be considered. First, a feedback channel between the receiver and the transmitter is required. Second, channel estimation and prediction should provide reliable and timely channel information to

the transmitter. Finally, if the data rate is adjusted in response to the channel condition, the quality of the communication services subject to delay constraints (e.g., video applications) should not be compromised.

1.1.1 History of adaptive transmission

The idea of adaptive transmission can be traced back to the late sixties and early seventies of the last century. In the paper [3], the authors investigated transmit power adaptation over the Rayleigh fading channel. The result shows significant performance improvement brought by the adaptive feedback technique. In another paper [4], symbol rate adaptation was proposed where the system continuously adjusts its data rate (symbol duration) in response to signal strength variations in a Rayleigh fading channel. For the same typical value of symbol/bit error probability, rate adaptation provides tremendous saving on signal to noise ratio (SNR) relative to a fixed rate system.

Although the early research gave some good insight, the interest in adaptive transmission cooled down in the seventies. This is probably because: first, the hardware technology which can support the implementation of adaptive transmission were not available at that time; second, the required sophisticated channel estimation technique was also unavailable; lastly, mobile communication systems were scarce, so there was little improvement demand for spectral efficiency and throughput.

With the advances in technology, the idea of adaptive transmission revived in the nineties. Since then many adaptive transmission techniques have been proposed. These techniques fall into rate adaptation, power adaptation, or the combinations of them.

In [5] [6], the authors presented systematic analysis of the relation of adapting different parameters and channel capacity. The analyses indicate that the capacity of a flat-fading channel is maximized by adapting the rate and power [5], or adapting the power alone [6]. There is little capacity loss when adapting the data rate only [5]. In [7], the authors further considered adapting data rate, transmit power, instantaneous BEP to maximize spectral efficiency subject to an average power constraint and an average BEP constraint in adaptive modulation schemes. They concluded that adapting just one or two parameters could yield close to the maximal possible spectral efficiency achieved by adapting all parameters.

Power adaptation adjusts the transmission power in response to the changing channel condition. In [5] [6], the optimal power allocation policy that maximizes the channel capacity subject to an average power constraint is shown to be the “Water-filling” method

in time. Intuitively, the "Water-filling" method sends the data with more power when the channel condition is good, and less power when the channel degrades. A suboptimal policy, channel inversion, was also proposed in [7] [8], which compensates the receive power loss due to channel fading such that a constant receive signal-to-noise-ratio (SNR) is maintained. Channel inversion is a simple scheme and can be easily implemented with rate adaptation [8]. However, in a multiuser environment, increasing transmit power for one user will increase the interference to other users. The system needs centralized control and global knowledge of channel state information to implement the channel inversion technique such that the overall system capacity can be maintained.

There are many rate adaptation techniques that have been proposed during past two decades. Maintaining the symbol rate, adaptive modulation varies the modulation constellation size or modulation scheme to adjust the number of data bits carried by each modulation symbol such that the data rate over the channel is adjusted [8] [9] [10] [11]. Adaptive coding is the method to adjust the code rate to change the source data rate. For example, the Rate-Compatible Punctured Convolutional (RCPC) code [12] modifies the code rate by removing some of the code bits from the encoder output sequences according to a pre-designed pattern. This technique has been applied in some communication systems. Adaptive coded modulation [13] [14] jointly optimizes channel coding and modulation and brings superior performance.

In CDMA (Code Division Multiple Access) networks, rate adaptation can be realized by applying dynamic spreading gain control (DSGC) [15] [16] [17] where the symbol durations are adjusted by spreading the symbols with code sequences of different lengths. This technique is the basis of this thesis, and will be introduced in detail in section 1.2.

1.1.2 Current application of adaptive transmission

Some adaptive transmission techniques have been adopted in current communication systems, or have been included in some proposed standards. In the popular WiFi standard IEEE 802.11g [18] [19] [20], four physical layers are defined on the 2.4GHz band. Among these four, two are mandatory: ERP-DSSS/CCK (Extended Rate Physical layer-Direct-Sequence Spread Spectrum/Complementary Code Keying) and ERP-OFDM (Extended Rate Physical layer/Orthogonal Frequency-Division Multiplexing). ERP-DSSS/CCK supports data rates of 1, 2, 5.5, 11 Mb/s by selecting modulation/coding scheme among BPSK, QPSK and CCK. ERP-OFDM selects the modulation scheme among BPSK, QPSK,

16QAM, 64QAM and code rate of 1/2, 2/3 and 3/4 of the convolutional code ($K = 7$) such that the data rates of 6, 9, 12, 18, 24, 36, 48 and 54 Mb/s are supported. In the proposed wireless metropolitan area networks standard IEEE 802.16 (WiMAX) [21], adaptive transmission is implemented on both downlink and uplink by adjusting modulation constellation size among BPSK, QPSK, 16QAM, 64QAM and selecting the coding scheme among convolutional code, turbo code and LDPC code associated with several code rates. In WCDMA [22], dynamic spreading gain control is implemented by adjusting the spreading factor from 4 to 256 in order to vary the user data rate within the range of several kbps to 2.8 Mbps. In 3G CDMA2000 networks [23], the system is also able to change the spreading gain by assigning Walsh codes with different lengths to achieve data rate adaptation. Adjusting the code rate by puncturing the convolutional code is also implemented in addition to dynamic spreading gain control and adaptive modulation in WCDMA and CDMA2000.

1.2 Rapid Dynamic spreading gain control

1.2.1 Frame-by-frame dynamic spreading gain control

Dynamic spreading gain control is a method to adjust the symbol rate (duration), specially in DSSS/CDMA (Direct Sequence Spread Spectrum) systems. In DSSS/CDMA systems, the information data symbol is multiplied by a spreading code sequence with a bandwidth B (chip rate) larger than the information data rate r. The ratio of B/r is defined as the spreading gain (SG). In the CDMA systems of our interest, the chip rate and corresponding chip duration are fixed. Let us denote by T_c the chip duration , and denote by L the length in number of chips of the spreading code sequence, then the duration of the data symbol is LT_c, and its symbol rate is $1/(LT_c)$. If the spreading codes of different lengths are used to spread the data symbols, the resulting after-spread symbol durations are different. Thus the symbol rate can be adjusted by choosing a spreading code among a group of code sequences with different lengths.

The 3G WCDMA system is chosen to be the framework to illustrate the operation of the dynamic spreading gain control (DSGC). Figure 1.2 shows the spreading and modulation of the downlink dedicated physical data channel in the 3G WCDMA network [24]. The modulation scheme is QPSK (quaternary phase shift keying). The user's data bits alternately flow into two parallel branches (In-phase and Quadrature). Each pair of bits is spread by a channelization code and then scrambled by a pseudo-noise (PN) code. The channelization

code set assigned to a user consists of orthogonal varied spreading factor (OVSF) codes [25] which are cyclic orthogonal with one another and have different code lengths. By changing the spreading code from time to time, the symbol duration (rate) can be dynamically adjusted.

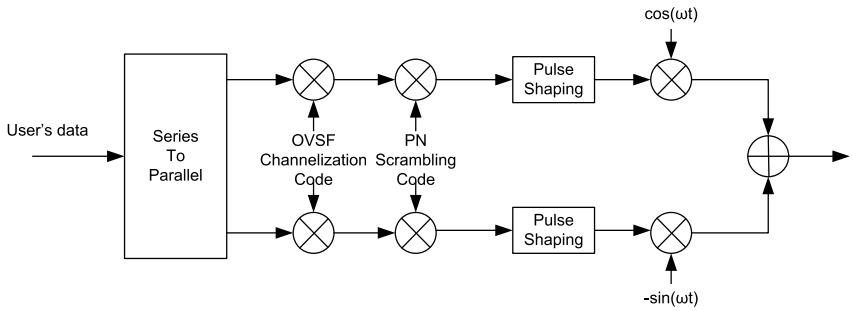

Figure 1.2: Spreading and modulation in a WCDMA downlink dedicated channel (DCH).

The primary purpose of using DSGC in 3G networks is to effectively integrate the data traffic with different rates in a multiple access environment. All types of data traffic can be spread onto the entire bandwidth by the concatenated OVSF/PN system [26]. In some of the WCDMA physical channels (e.g., uplink dedicated physical data channel), the symbol rate is adjusted at the beginning of each frame and remains constant during the frame. A message indicating the symbol rate can be delivered to the receiver in the frame to assist in choosing the right despreading code. A typical frame duration of 3G WCDMA system is 10 ms.

If the dynamic spreading gain control is applied to improve the channel spectrum efficiency in addition to integrating data traffic, the rate adjustment needs to be performed in response to channel variations. An example of time-varying channels is depicted in Figure 1.3. It is a Clarke's two-dimensional isotropic scattering model channel and is simulated by the Simulink^{TM} [1] Rayleigh fading channel simulator with the maximum Doppler shift $f_D = 100$Hz. The figure shows that the channel power gain fluctuates and forms a multi-peak multi-valley curve over time. The interval between two adjacent peaks or adjacent valleys is approximately $1/(2f_D)$. For the exemplary channel with $f_D = 100$Hz, the interval is about 5 ms. It is less than the typical frame duration of the 3G networks, which is 10ms. In this case, adjusting the rate frame by frame is not able to follow the channel fluctuation

[1] Simulink^{TM} is the trade mark of The MathWorks, Inc

and cannot improve the channel spectrum efficiency. The maximum Doppler shift of 100Hz

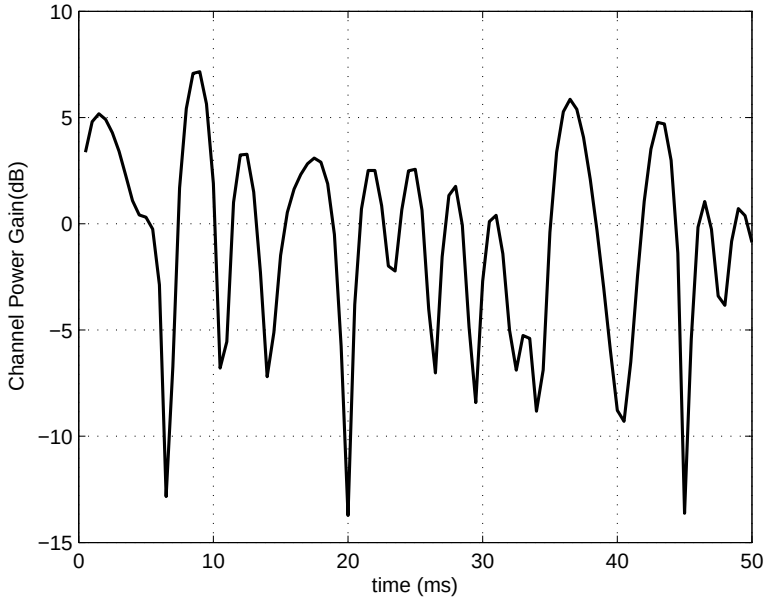

Figure 1.3: Channel power gain of a Rayleigh fading channel. The maximum Doppler shift of the channel is 100Hz.

is not a rare situation. Consider a wireless communication system with carrier frequency 1.8G Hz. If a mobile in the system is moving at a speed of 60km/h towards or away from its base station, the resulting maximum Doppler shift is 100Hz. Although the channel is still a slow fading channel in terms of comparing the coherence time to the symbol duration, the channel is fast time-varying relative to the frame duration, i.e., the rate adjustment interval of FBF DSGC. In order to explore the spectrum efficiency potential of this kind of fast time-varying channels, DSGC has to update the symbol rate/duration more frequently. The rapid DSGC, i.e., the symbol-by-symbol (SBS) duration adaptation was proposed to meet this need [1] [2].

1.2.2 Rapid spreading gain control

The main goal of symbol-by-symbol (SBS) duration adaptation is to improve the spectrum efficiency in wireless communication systems by adjusting the symbol rate in response to the channel condition while the communication quality is maintained. The communication

quality can be measured by average or instantaneous bit/symbol/package error probabilities. With the ability of adjusting the duration for each transmitted symbol in response to the instantaneous channel gain, the transmitter is able to effectively send symbols at a higher symbol rate when the channel gain is high, and give a symbol longer duration (lower symbol rate) when channel gain is low. To implement the SBS duration adaptation, the system need a very fast feedback mechanism and a message free detection scheme. The fast feedback mechanism provides the channel state information symbol by symbol for the transmitter. In frame-by-frame DSGC, a rate indicator (RI) can be inserted into each frame to assist in choosing the right despreading code. For SBS adaptation, if an RI message is needed for each symbol, that would be a huge burden and result in large overhead for transmission. So a message free detection (i.e., blind detection) is needed for SBS DSGC. The fast feedback and blind detection both can be realized by adopting OVSF FOSSIL (Forest for OVSF-Sequence-Set-Inducing Lineages) code sets [1] [2].

OVSF FOSSIL code

FOSSIL, the forest of binary code trees, consists of a group of OVSF binary code trees of which the root codes are orthogonal with one another half by half, i.e., the first halves of the root codes are orthogonal to one another and so are the second halves. An example of FOSSIL is shown in Figure 1.4. The codes in the FOSSIL are denoted by C_n^i where the subscript indicates the code length and the superscript indicates the index of the code among all the codes with length n across the whole FOSSIL. The length of code C is also denoted by $|C|$. All code sequences take the length of powers of 2, i.e., $|C| = 2^j$ for some integer j. The code C_n^i can be written as the concatenation of its first half ${}_1C_n^i$ and second half ${}_2C_n^i$, i.e., $C_n^i = [{}_1C_n^i,\ {}_2C_n^i]$. Each element of the code takes binary values $+1$ or -1, which are represented by $+$ and $-$, respectively. If a FOSSIL consists of I trees and the length of root codes is R, the I root codes $C_R^1, C_R^2, \ldots, C_R^I$ have the property that the first halves are orthogonal to one another and so are the second halves; i.e., ${}_1C_R^i *_1 C_R^j = 0$ and ${}_2C_R^i *_2 C_R^j = 0$ for $i, j = 1, 2, \ldots, I$ and $i \neq j$, where $*$ denotes the binary inner product. The binary inner product of two binary sequences U and V of length L is defined as

$$U * V = \sum_{k=1}^{L} U[k]\, V[k] \tag{1.1}$$

Each code $C_n^i = [{}_1C_n^i,\ {}_2C_n^i]$ begets two children $C_{2n}^{2i-1} = [{}_1C_n^i,\ {}_2C_n^i,\ {}_1C_n^i,\ {}_2C_n^i]$ and $C_{2n}^{2i} = [{}_1C_n^i,\ -{}_2C_n^i,\ -{}_1C_n^i,\ {}_2C_n^i]$. The child code $C_{2n}^{2i} = [{}_1C_n^i,\ -{}_2C_n^i,\ -{}_1C_n^i,\ {}_2C_n^i]$ is referred as the "first-born" child of $C_n^i = [{}_1C_n^i,\ {}_2C_n^i]$. The "first-born lineage" is defined as the set of codes with distinctive lengths such that the code of length $2n$ is the first-born child of the code of length n. The exemplary FOSSIL in Figure 1.4 consists of two code trees. The two root codes are $C_4^1 = [A,\ a]$ and $C_4^2 = [B,\ b]$, where $A = {}_1C_4^1$, $a = {}_2C_4^1$, $B = {}_1C_4^2$ and $b = {}_2C_4^2$. It can be observed that $A * B = a * b = 0$. $\{C_4^1, C_8^2, C_{16}^4, \ldots\}$ and $\{C_4^2, C_8^4, C_{16}^8, \ldots\}$ are first-born lineages.

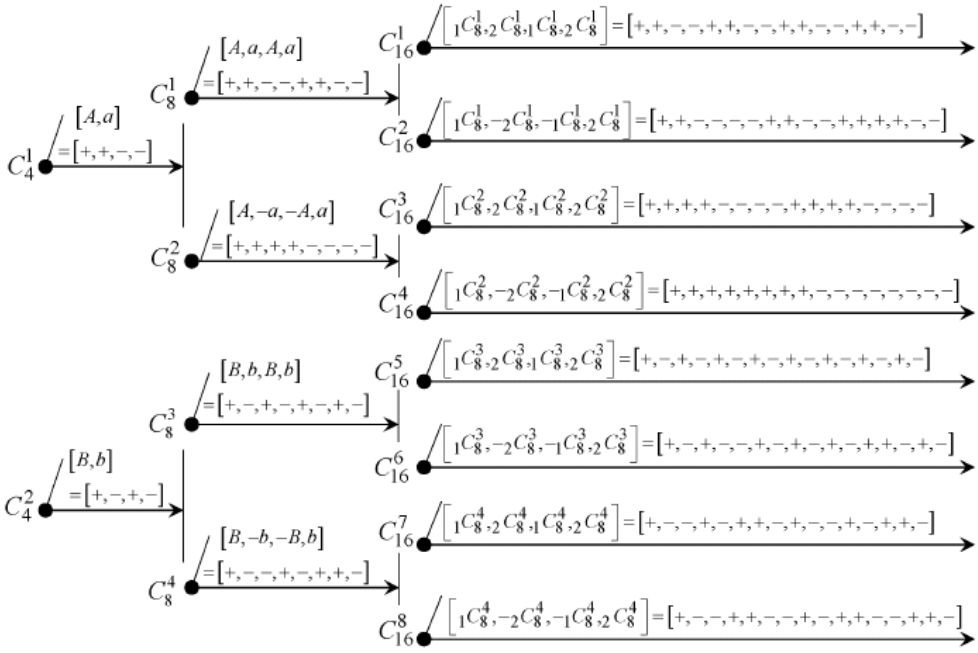

Figure 1.4: Example of FOSSIL.

If a FOSSIL is generated by some root codes $[A,\ a]$, $[B,\ b]$, $[C,\ c]$, ..., the codes $\pm[A,\ -a]$, $\pm[B,\ -b]$, $\pm[C,\ -c]$, ... can be used to be root codes to generate other FOSSILs. The FOSSILs generated from $\pm[A,\ -a]$, $\pm[B,\ -b]$, $\pm[C,\ -c]$, etc, are referred as sibling FOSSILs [2] or conjugate FOSSILs [27]. The example of a sibling FOSSIL of the FOSSIL shown in Figure 1.4 is illustrated in Figure 1.5, where the root codes are $SC_4^1 = [A,\ -a]$ and $SC_4^2 = [B,\ -b]$. The codes in sibling FOSSIL is denoted by SC_n^i. The first-born child of SC_n^i is denoted by SC_{2n}^{2i-1} and the second-born is denoted by SC_{2n}^{2i}. The first-born lineages

in the sibling FOSSIL are $\left\{SC_4^1, SC_8^1, SC_{16}^1, \ldots\right\}$ and $\left\{SC_4^2, SC_8^3, SC_{16}^5, \ldots\right\}$.

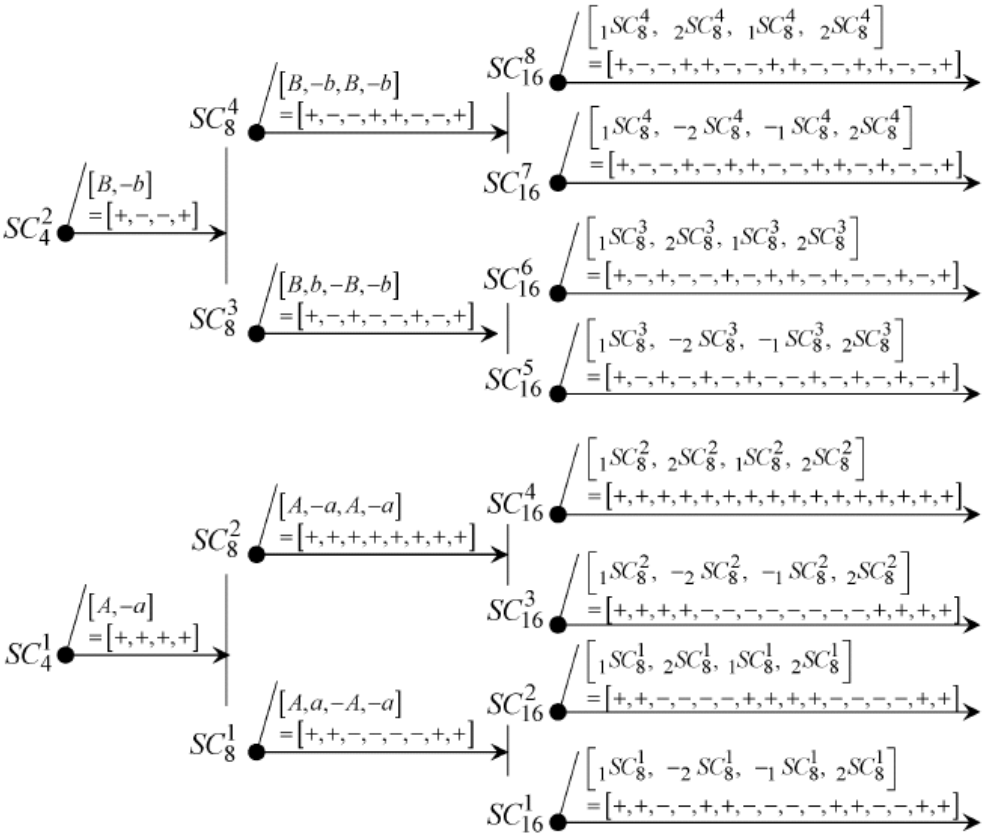

Figure 1.5: Example of sibling (conjugate) FOSSIL.

The FOSSIL and Sibling FOSSIL have two important properties:

1. OVSF property: any pair of codes C_n^i and C_m^j are cyclic orthogonal with one another, with the unit length $\min(\mathrm{n}, \mathrm{m})$, as long as one is not a descendant of the other.

2. IOVSF property: two codes C_n^i and C_m^j in the same first-born lineage are cyclic orthogonal to each other, with the unit length $\min(\mathrm{n}, \mathrm{m})$.

The cyclic orthogonality (i.e., shift orthogonality) of the sequences U of length L and the sequence V of length ML with unit length L is defined as

$$\sum_{k=1}^{L} U\left[k\right] V\left[k + mL\right] = 0, \quad \text{for } \mathrm{m} = 0, 1, 2, \ldots, \mathrm{M} - 1 \tag{1.2}$$

SBS DSGC loop

The symbol-by-symbol DSGC operates in a full duplex communication system and allows the transmitters on both sides to adjust the spreading gain for each symbol. A channel in the full duplex system also acts as the feedback channel for the opposite channel. The transmission power is assumed to be constant on both transmitters, i.e., the system does not adopt the transmission power adaptation. In a multi-access environment like the 3G system, increasing power for one user brings more interference to others. Optimizing the power allocation for all users needs centralized control and global knowledge of all channels. On the other hand, symbol-by-symbol spreading gain control can be performed locally in a full duplex communication link.

In order to implement fast feedback and blind detection, two different kinds of spreading code set are constructed by the OVSF FOSSIL codes, the rate information (RI) code set and the feedback information (FBI) code set. If a symbol is spread by a spreading code from the RI code set (RI code), the symbol is called an RI symbol. Similarly, the symbol is called an FBI symbol if it is spread by a code from FBI code set (FBI code). The basic idea is transmitting an FBI symbol right after an RI symbol. The RI symbol implicitly carries the rate information for its own and the following FBI symbol. The FBI symbol has the same spreading gain as the previous RI symbol and implicitly carries the channel state information (CSI) of the opposite channel to the peer transmitter.

A RI code set consists of codes from the same first-born lineage. The codes in a RI code set have different lengths and cyclic orthogonal with one another. The dynamic range of the spreading gain of the RI code set satisfies the rate requirement to serve the users. When an RI symbol is sent to the receiver, the receiver correlates the received symbol with all the codes in the RI code set. In the absence of noise and distortion, only the correlation to the code spreading the symbol is not zero because of the orthogonality among the RI codes. By doing so, the receiver can despread the received symbol without explicit rate information from the transmitter. In the presence of noise and distortion, decision rules based on the correlations can be set such that blind detection is still in effect. One possible rule could be maximum-likelihood detection which chooses the RI code yielding the maximum correlation.

The FBI code set associated with a RI code set covers all spreading gains except the smallest one. In an FBI code set, there are multiple codes with the same spreading gain

and they form a subset of the FBI code set. Denote the RI code set by

$$\Psi_{\mathrm{RI}} = \left\{ C_{2^j p}^{2^j \alpha} | j = 0, 1, \ldots, L-1 \right\} \tag{1.3}$$

where α is the index of the code tree among the FOSSIL. The spreading gain of the RI code set Ψ_{RI} ranges from p to $2^{L-1}p$. The associated FBI code set Ψ_{FBI} has the spreading gain range from $2p$ to $2^{L-1}p$. Denote by $\Phi_{\mathrm{FBI}}(j)$ a subset of Ψ_{FBI} and all codes in $\Phi_{\mathrm{FBI}}(j)$ have the spreading gain of $2^j p$, where $j = 1, 2, \ldots, L-1$. The subset $\Phi_{\mathrm{FBI}}(j)$ has $2^{j+1} - 1$ codes: $SC_{2^j p}^{2^j(\alpha-1)+1}$, $SC_{2^j p}^{2^j(\alpha-1)+2}$, $\ldots$, $SC_{2^j p}^{2^j \alpha - 1}$, $C_{2^j p}^{2^j \alpha}$, $C_{2^j p}^{2^j \alpha - 1}$, $\ldots$, $C_{2^j p}^{2^j(\alpha-1)+1}$. We further define $\Phi_{\mathrm{FBI}}(0)$ as the FBI subset which is equal to $\Phi_{\mathrm{FBI}}(1)$. Note there are 3 codes in $\Phi_{\mathrm{FBI}}(0)$ and all codes have the spreading gain $2p$. Then the FBI set can be written as $\Psi_{\mathrm{FBI}} = \Phi_{\mathrm{FBI}}(0) \bigcup \Phi_{\mathrm{FBI}}(1) \bigcup \ldots \bigcup \Phi_{\mathrm{FBI}}(L-1)$. An illustration of the code assignment is shown in Figure 1.6. Note that the codes within the same subset $\Phi_{\mathrm{FBI}}(j)$ are orthogonal

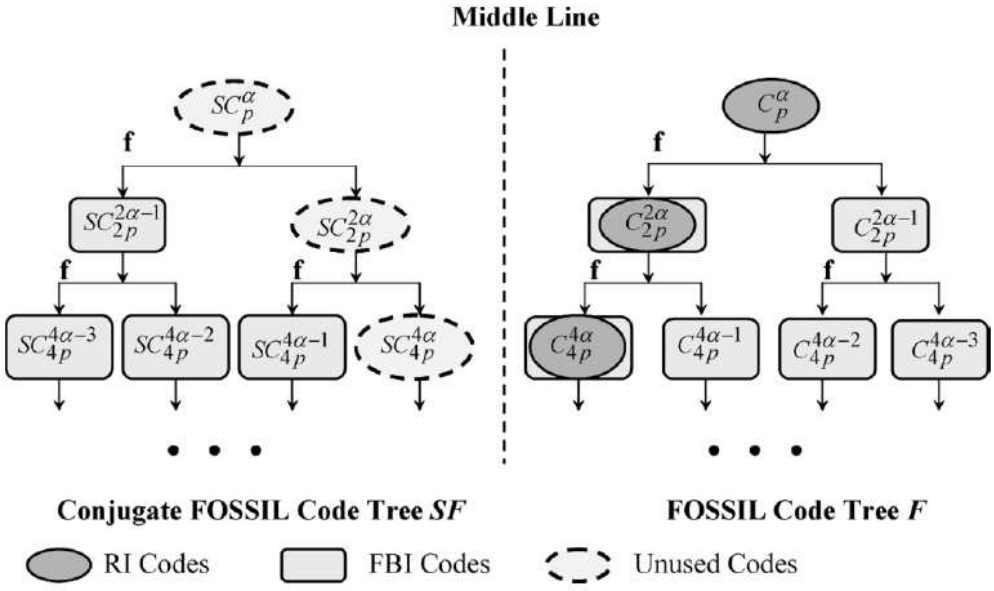

Figure 1.6: RI and FBI code sets.

with one another. But two codes from different subsets are not necessarily orthogonal or cyclic orthogonal. An FBI symbol has to be sent after an RI symbol and has the same spreading gain as the RI symbol. The spreading code for the FBI symbol is chosen from the FBI subset corresponding to the spread gain of the RI symbol it follows. Within the FBI subset $\Phi_{\mathrm{FBI}}(j)$, there are $2^{j+1} - 1$ codes to be chosen ($\Phi_{\mathrm{FBI}}(0)$ has 3 codes). Then

there are $2^{j+1}-1$ different feedback messages available to represent the channel condition of the opposite channel. The rule of mapping channel state information (CSI) to the feedback message is a system design issue. One exemplary rule [2] is that the code choices represent different requests of spreading gain increment relative to the previous feedback message.

The zero correlation between orthogonal codes is the key to blind detection of the receive symbols. When two orthogonal code sequences miss the alignment, the result of correlation is not zero. The misalignment could happen when a symbol is spread by a code which is shorter than the code was used to spread the previous symbol, or at the forward channel, where the base station simultaneously transmits to different mobiles, when the symbols to different mobiles lose synchronization among themselves [27]. In order to avoid the non-zero correlation caused by the misalignment, a modulo-counter Y is maintained by the transmitter. Starting from zero, Y increases by one whenever a one-chip duration of the data symbols elapses. The counter Y is reset to zero when it reaches the value of longest symbol length 2^{L-1}. A symbol can be spread by a code C only when $(Y \ mod \ |C| = 0)$. At the receiver side, a modulo-counter is also maintained and synchronized to the transmitter's modulo-counter [27]. The receiver modulo counter assists in the code detection.

The transmission protocol of symbol-by-symbol DGSC is summarized as the following:

1. After sending an FBI symbol, the transmitter must send an RI symbol.
2. After sending an RI symbol, the transmitter can
   - send an FBI symbol with the same spreading gain as the RI symbol just sent;
   - or send an RI symbol with spreading gain longer than the RI symbol just sent.
3. After sending an RI symbol with the smallest spreading gain p, send another RI symbol with spreading gain p. Then send an FBI symbol spread by a code from $\Phi_{\mathrm{FBI}}(0)$.

The detection strategy at receiver side is summarized as the following:

1. After detecting an FBI symbol, the next symbol can only be an RI symbol;
2. After detecting an RI symbol with the spreading gain $2^{L-1}p$, the next symbol can only be a FBI symbol spread by a code from $\Phi_{\mathrm{FBI}}(L-1)$.
3. After detecting an RI symbol with the spreading gain $2^{j}p$, and $(Y \ mod \ 2^{j+1}p \neq 0)$, the next symbol can only be an FBI symbol spread by a code from $\Phi_{\mathrm{FBI}}(j)$.

4. After detecting an RI symbol with the spreading gain $2^j p$, and (Y *mod* $2^{j+1}p = 0$), the next symbol can be either an FBI symbol spread by a code from $\Phi_{\mathrm{FBI}}(j)$ or an RI symbol with a larger spreading gain $2^{j+l}p$ and (Y mod $2^{j+l}p = 0$).

5. After detecting an RI symbol with spreading gain p, the next symbol is another RI symbol with spreading gain p and then followed by an FBI symbol spread by a code from $\Phi_{\mathrm{FBI}}(0)$.

The protocols and architecture of rapid dynamic spreading gain control are just briefly introduced here. Reference [2] [27] give full details of the protocols and the code set constructions.

1.2.3 Throughput gain of symbol-by-symbol DGSC

In order to evaluate the performance of rapid DGSC, the data rate achieved by symbol-by-symbol (SBS) duration adaptation system is compared to the data rate of frame-by-frame (FBF) duration adaptation system where both systems give the same symbol/bit error probability. Reference [28] [29] have given good theoretical analysis on the throughput improvement brought by SBS duration adaptation in uncoded systems. In this section, the analysis results are briefly reviewed.

In a symbol-by-symbol rate adaptation system, the duration (rate) of each symbol is able to be adjusted in response to the channel condition. Let us denote by $\tilde{a}(t)$ the complex fading channel gain at time t and by P_T the transmit power. Then the receive power is given by $P_T|\tilde{a}(t)|^2$ and the average receive power is $P = P_T E[|\tilde{a}(t)|^2]$. Let $a(t)$ be the normalized fading channel gain, i.e., $a(t) = \tilde{a}(t) / \sqrt{E\left(|\tilde{a}(t)|^2\right)}$. Then the receive power can be written as $P|a(t)|^2$. Under the assumption that the receive power stays constant during each symbol duration, the instantaneous signal to noise ratio (SNR) per symbol is given by

$$\gamma = P|a(t)|^2 T_s / N_0 \tag{1.4}$$

where T_s is the symbol duration and N_0 the power spectral density of the additive white noise. Denote the rate adaptation policy by $r(|a(t)|)$, i.e., the instantaneous symbol rate is a function of the magnitude of instantaneous channel gain $|a(t)|$. Let $f_{|a|}(\alpha)$ be the probability density function (pdf) of the random variable $|a(t)|$. Then the average symbol rate achieved by SBS duration adaptation is given by

$$\bar{r}_S = \int_0^\infty r(\alpha) f_{|a|}(\alpha)\, d\alpha \tag{1.5}$$

Denote by $h(\gamma)$ the symbol error probability (SEP) which is a function of instantaneous symbol SNR γ. Different modulation schemes have different SEP function $h(\gamma)$. In the rate adaptation system, if a symbol is sent with rate $r(|a(t)|)$, its symbol SNR is $\frac{P|a(t)|^2}{N_0 r(|a(t)|)}$ and the probability that the symbol is in error is $h(\frac{P|a(t)|^2}{N_0 r(|a(t)|)})$. Then the number of symbols in error per second is $r(|a(t)|)h(\frac{P|a(t)|^2}{N_0 r(|a(t)|)})$. The overall average symbol error probability is given by

$$\begin{aligned}\bar{P}e &= \frac{E\left[\text{number of symbol errors in a unit time}\right]}{E\left[\text{number of symbols transmitted in a unit time}\right]} \\ &= \frac{\int_0^\infty r\left(\alpha\right) h\left(\frac{P\alpha^2}{N_0 r(\alpha)}\right) f_{|a|}\left(\alpha\right) d\alpha}{\int_0^\infty r\left(\alpha\right) f_{|a|}\left(\alpha\right) d\alpha}\end{aligned} \tag{1.6}$$

The rate adaptation policy should maximize the throughput, the average symbol rate $\bar{r}_S$, while a target overall SEP is maintained. The maximum-throughput adaptation policy is derived through the following maximization

$$\begin{aligned}&\max_{r(\alpha)} \quad \int_0^\infty r\left(\alpha\right) f_{|a|}\left(\alpha\right) d\alpha \\ &\text{subject to} \quad \frac{\int_0^\infty r\left(\alpha\right) h\left(\frac{P\alpha^2}{N_0 r(\alpha)}\right) f_{|a|}\left(\alpha\right) d\alpha}{\int_0^\infty r\left(\alpha\right) f_{|a|}\left(\alpha\right) d\alpha} \leq \varepsilon\end{aligned} \tag{1.7}$$

where ε is the SEP constraint. In [28], the maximization (1.7) is solved by applying Lagrangian. The optimal rate adaptation policy was shown to be

$$r(|a(t)|) = \frac{P|a(t)|^2}{N_0 h^{-1}(\varepsilon)} \tag{1.8}$$

where $h^{-1}(\varepsilon)$ is the inverse function of $h(\gamma)$. The resulting throughput, i.e., the average symbol rate is

$$\bar{r}_S = \frac{P}{N_0 h^{-1}(\varepsilon)} \tag{1.9}$$

Now consider the maximal average symbol rate for frame-by-frame duration adaptation. It has been explained that if the channel is fast time-varying relative to the frame duration, FBF adaptation cannot track the channel variation. Over a fast time-varying channel, a data frame suffers one or more fluctuations. When the channel is highly fluctuating, the empirical distribution of the fading channel gain in each frame can be approximated by the ensemble distribution of the channel gain. Each frame's symbol error probability associated with a particular symbol rate r can be approximated by the SEP when the symbol rate is fixed at r

at all the time [28]. It means that the FBF duration adaptation is approximately equivalent to non-adaptation when the channel is fast time-varying. The maximal throughput is the maximal rate which satisfies the SEP constraint, i.e.,

$$\begin{aligned} &\max r_F \\ &\text{subject to } \int_0^\infty h\left(\frac{P\alpha^2}{N_0 r_F}\right) f_{|a|}(\alpha) d\alpha \leq \varepsilon \end{aligned} \tag{1.10}$$

Define a function

$$H(z) \equiv \int_0^\infty h(z\xi) f_{|a|^2}(\xi)\, d\xi \tag{1.11}$$

where $f_{|a|^2}(\xi)$ is probability density function of $|a(t)|^2$, the normalized channel power gain. Then maximal symbol rate for FBF adaptation is solved as

$$r_F = \frac{P}{N_0 H^{-1}(\varepsilon)} \tag{1.12}$$

In order to compare the throughput between SBS adaptation and FBF adaptation, the throughput gain is defined as the ratio $\mathcal{R} \equiv \bar{r}_S / r_F$. Then, from (1.9) and (1.12), we have

$$\mathcal{R} \equiv \frac{\bar{r}_S}{r_F} = \frac{H^{-1}(\varepsilon)}{h^{-1}(\varepsilon)} \tag{1.13}$$

Figure 1.7 and 1.8 show the throughput gains for non-coherent Binary Frequency Shift Keying (NC-BFSK) modulation and M-ary Quadrature Amplitude Modulation (MQAM) over Rayleigh fading channel. It is observed that the throughput gain $\mathcal{R}$ is larger for the smaller SEP requirement ε. $\log \mathcal{R}$ is more or less proportional to $\log \varepsilon$. Thus, $\mathcal{R}$ and ε have a power-law relation. More importantly, the results show that symbol-by-symbol adaptation can achieve a throughput gain by orders of magnitude in a wide range of modulation schemes and SEP requirements [28].

1.3 Outline of this thesis

The throughput gain achieved by rapid dynamic spreading gain control shown in Figure 1.7 and 1.8 and also in [28] is significant. These results are obtained based on some ideal assumptions. First, the symbol rate is assumed to be able to take any real positive value in solving the symbol rate for SBS and FBF duration adaptation (1.7) (1.8). In fact, the spreading gain control is performed by spreading the data symbols with OVSF codes of

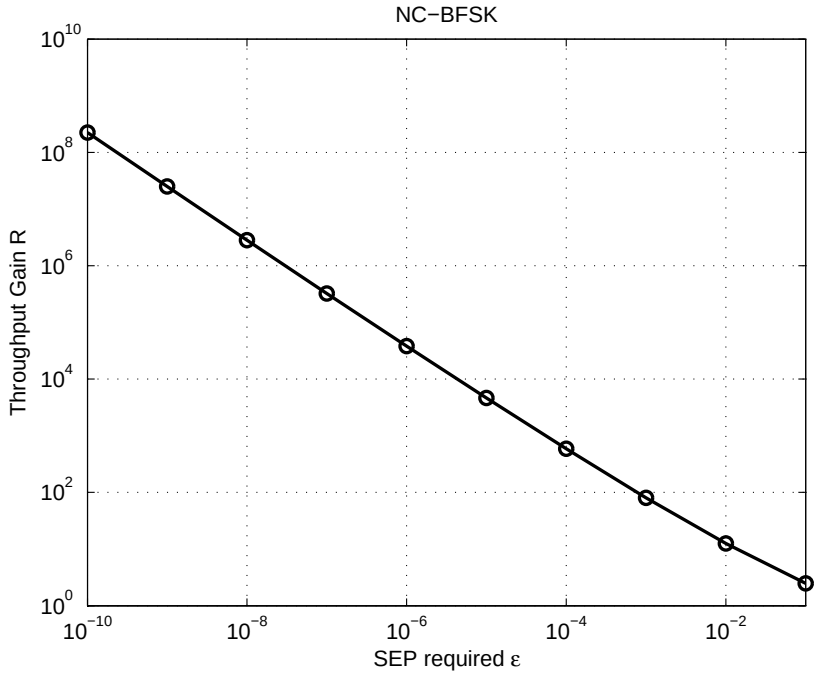

Figure 1.7: Throughput gain for NC-BFSK over Rayleigh fading channel.

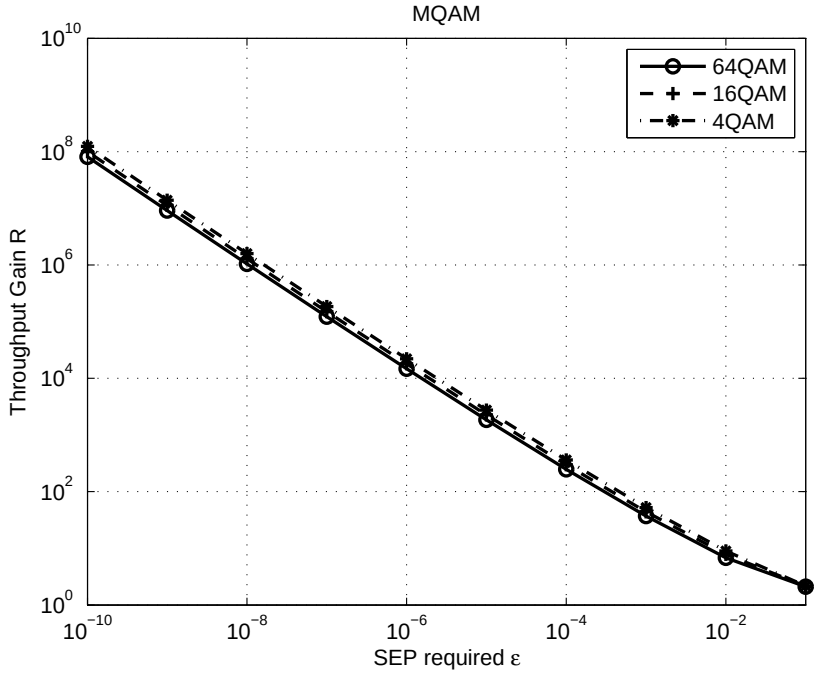

Figure 1.8: Throughput gain for MQAM over Rayleigh fading channel.

which the code lengths take on some discrete values. The symbol durations (rates) form a discrete and finite set. Second, the channel gain is assumed to stay constant in each symbol duration. When a large dynamic range of spreading gain control is considered, the symbol duration may be long and the assumption is difficult to hold. Third, the rate adaptation policy is based on the true instantaneous channel gain, and perfect channel estimation and ideal feedback are assumed. When estimation error and feedback delay are considered, the throughput gain is expected to be less.

This thesis presents an extended study on the throughput gain achieved by SBS duration adaptation over FBF adaptation in fast time-varying fading channels. In chapter 2, we assume that the spreading gain control can only choose the symbol duration from a finite set of durations. This is the case that the system adopts OVSF codes to adjust the symbol duration. The channel gain is assumed to remain constant during each symbol duration but vary from symbol to symbol. The throughput gain within a discrete duration set for uncoded systems is analyzed and the numerical results show that within a discrete duration set, SBS adaptation may achieve the throughput gain similar to the gain achieved with the continuous duration. The maximal achievable throughput gain is limited by the dynamic range of the discrete duration set. In chapter 3, the assumption that the channel gain remains constant for each symbol duration is avoided. The channel gain is only assumed to stay unchanged during each chip duration. Under this much more realistic assumption, the numerical analysis shows that the throughput gain within discrete duration sets is still large for uncoded systems. Chapter 4 studies the throughput gain of the duration adaptation system employing forward error-control (FEC) codes. The simulation results indicate that the throughput gain in a coded system depends on its coding scheme and interleaving scenario. For some common used FEC codes and non-ideal interleaved fading channel, SBS duration adaptation may further boost the error-constrained throughput. However, if the system adopts a superior forward error correction code, e.g., DVB-S2 LDPC codes, or if the system employs a large size interleaver to make the channel much less time correlated, there will be little benefit to apply SBS duration adaptation to increase the throughput. Chapter 5 introduces the preliminary study on the throughput gain with outdated and imperfect channel information in the uncoded system. The numerical study shows that the throughput gain achieved by SBS duration adaptation in uncoded system is promising but the throughput improvement relies on the estimation/prediction accuracy and timeliness. Finally, chapter 6 gives further discussions on performance and implementation of the rapid

spreading gain control and concludes the whole thesis.

Chapter 2

Throughput Gain within Discrete Duration Set

This chapter presents the quantitative analysis on the gain in error-constrained bit throughput achieved by the rapid symbol duration adaptation. The analysis is focused on the adaptive system that can choose for each symbol a symbol duration only from a discrete set of symbol durations. The results show that the rapid adaptation with a discrete duration set can often achieve a throughput gain similar to that achieved with a continuous set of durations.

2.1 System model

The symbol by symbol duration adaptation can be performed by applying OVSF code sequences in a set to spread the data sequence. Let us denote the OVSF code sequence set as $C = \{C_1, C_2, ..., C_N\}$, and also denote L_i as the length of the code sequence C_i. In the CDMA system considered in this chapter (and also in [27]), L_i takes the values of power of 2 such that $L_{i+1} = 2L_i$. The symbol duration is L_iT_c when the code C_i is used to spread the data symbol, where T_c is the chip duration. Each symbol duration L_iT_c also corresponds to instantaneous symbol rate $r_i = 1/(L_iT_c)$. Therefore, it can be construed that each symbol is transmitted with an instantaneous symbol rate in a set of discrete symbol rates $\Theta = \{r_1, r_2, \ldots, r_N\}$, where $r_i = 1/(L_iT_c)$ and $r_{i+1} = r_i/2$. We also denote by $\Lambda = \{L_1, L_2, \ldots, L_N\}$ the code length set of C.

The transmission power of the system is assumed to be fixed over time. The channel is assumed to remain constant during each symbol duration, which is a common assumption for such studies as this [5]. Thus, with constant transmission power, the receive power also remains constant for each symbol. The transmission rate is adjusted in accordance with the receive power $Y(t)$. In the transmission rate (or equivalently, symbol duration) adaptation policy, the range of $Y(t)$ is divided to N regions with $N-1$ thresholds $\{\zeta_1, \zeta_2, \cdots, \zeta_{N-1}\}$, as shown in Figure 2.1. A symbol is spread by sequence C_i when the receive power is in interval $[\zeta_i,\ \zeta_{i-1})$, then the symbol has L_i chips, the symbol rate is r_i . The SNR per symbol is

$$\frac{Y(t)\,T_s}{N_0} = \frac{L_i T_c Y(t)}{N_0} \tag{2.1}$$

where T_s is the symbol duration, and N_0 is the additive white noise power density.

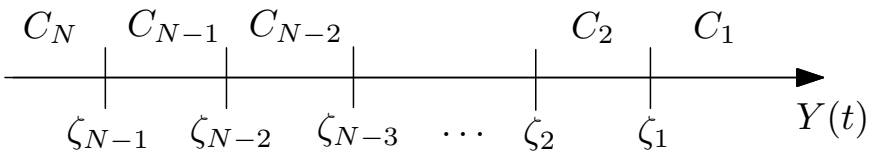

Figure 2.1: Receive power thresholds for symbol rate adaptation

The probability that a symbol is sent with rate r_i is

$$\Pr(r_i) = \Pr(\zeta_i \le Y(t) < \zeta_{i-1}) = \int_{\zeta_i}^{\zeta_{i-1}} f_Y(y)\,dy \tag{2.2}$$

where $f_Y(y)$ is the probability distribution function of $Y(t)$, and $\zeta_0 = \infty$, $\zeta_N = 0$.

The average symbol rate is

$$\bar{r}_S = \sum_{i=1}^{N} r_i \Pr(\zeta_i \le Y(t) < \zeta_{i-1}) = \sum_{i=1}^{N} \frac{1}{L_i T_c} \int_{\zeta_i}^{\zeta_{i-1}} f_Y(y)\,dy \tag{2.3}$$

where $\zeta_0 = \infty$, $\zeta_N = 0$. When the transmit symbol is one of M-ary modulations symbols, each symbol carries $\log_2 M$ bits. The average bit rate is hence $\bar{r}_s \log_2 M$.

Denote by $h_b(\gamma)$ the bit error probability (BEP) function, where γ is the signal-to-noise ratio per symbol. When the receive power is $Y(t)$ and the transmit symbol has the length of L_i in chips, the bit rate is $r_i(\log_2 M))$ and the bit error probability is $P_b(e|Y(t)) = h_b(L_i T_c Y(t)/N_0)$. The average number of bits in error per second is $(r_i \log_2 M) P_b(e|Y(t))$.

The overall average bit error probability is given by:

$$\begin{aligned}\bar{P}_b &= \frac{E\left[\text{number of bit errors in a unit time}\right]}{E\left[\text{number of bits transmitted in a unit time}\right]} \\ &= \frac{\sum_{i=1}^{N} r_i \int_{\zeta_i}^{\zeta_{i-1}} P_b\left(e|y\right) f_Y\left(y\right) dy}{\sum_{i=1}^{N} r_i \int_{\zeta_i}^{\zeta_{i-1}} f_Y\left(y\right) dy} \\ &= \frac{\sum_{i=1}^{N} \frac{1}{L_i T_c} \int_{\zeta_i}^{\zeta_{i-1}} h_b\left(\frac{L_i T_c y}{N_0}\right) f_Y\left(y\right) dy}{\sum_{i=1}^{N} \frac{1}{L_i T_c} \int_{\zeta_i}^{\zeta_{i-1}} f_Y\left(y\right) dy} \\ &= \frac{\sum_{i=1}^{N} \frac{1}{L_i} \int_{\zeta_i}^{\zeta_{i-1}} h_b\left(\frac{L_i T_c y}{N_0}\right) f_Y\left(y\right) dy}{\sum_{i=1}^{N} \frac{1}{L_i} \int_{\zeta_i}^{\zeta_{i-1}} f_Y\left(y\right) dy}\end{aligned} \tag{2.4}$$

The optimal adaptation policy $\{\zeta_{N-1}\ ,\ \zeta_{N-2}\ ,\ \ldots,\ \zeta_1\}$ maximizes the throughput (the average bit rate) $\bar{r}_s \log_2 M$ while satisfying the bit error probability requirements. With a discrete duration set, the maximum average bit rate can be found through the following optimization:

$$\begin{aligned}&\max\nolimits_{\{\zeta_1,\zeta_2,\cdots,\zeta_{N-1}\}} \bar{r}_s \log_2 M \\ &\text{subject to } \bar{P}_b \le \varepsilon_b\end{aligned} \tag{2.5}$$

i.e.,

$$\begin{aligned}&\max\nolimits_{\{\zeta_1,\zeta_2,\cdots,\zeta_{N-1}\}} \sum_{i=1}^{N} \frac{\log_2 M}{L_i T_c} \int_{\zeta_i}^{\zeta_{i-1}} f_Y\left(y\right) dy \\ &\text{subject to } \frac{\sum_{i=1}^{N} \frac{1}{L_i} \int_{\zeta_i}^{\zeta_{i-1}} h_b\left(\frac{L_i T_c y}{N_0}\right) f_Y(y) dy}{\sum_{i=1}^{N} \frac{1}{L_i} \int_{\zeta_i}^{\zeta_{i-1}} f_Y(y) dy} \le \varepsilon_b\end{aligned} \tag{2.6}$$

where ε_b is the bit error probability constraint (fidelity requirement), and $\zeta_0 = \infty$, $\zeta_N = 0$. Define $\tilde{Y} = Y/E[Y]$ as the normalized receive power and denote by $\kappa = T_c E(Y)/N_0$ the average signal to noise ratio (SNR) per chip. Then, the optimization above is reformulated as

$$\begin{aligned}&\max\nolimits_{\{\zeta_1',\zeta_2',\cdots,\zeta_{N-1}'\}} \sum_{i=1}^{N} \frac{\log_2 M}{L_i T_c} \int_{\zeta_i'}^{\zeta_{i-1}'} f_{\tilde{Y}}\left(\tilde{y}\right) d\tilde{y} \\ &\text{subject to } \frac{\sum_{i=1}^{N} \frac{1}{L_i} \int_{\zeta_i'}^{\zeta_{i-1}'} h_b(L_i \kappa \tilde{y}) f_{\tilde{Y}}(\tilde{y}) d\tilde{y}}{\sum_{i=1}^{N} \frac{1}{L_i} \int_{\zeta_i'}^{\zeta_{i-1}'} f_{\tilde{Y}}(\tilde{y}) d\tilde{y}} \le \varepsilon_b\end{aligned} \tag{2.7}$$

where $\zeta_i{}' = \zeta_i / E[Y]$, and $\zeta_0{}' = \infty$, $\zeta_N{}' = 0$.

As introduced in Section 1.2.3, in the case of fast time-varying channels, the frame-by-frame duration (FBF) adaptation is more or less equivalent to non-adaptation as long as the frame length is long relative to the time-varying dynamics of the channel fluctuation. The symbol rate r_F is fixed and each symbol carries $\log_2 M$ bits. The maximal bit rate for FBF adaptation can be obtained through following optimization:

$$\begin{array}{l} \max_{r_F \in \{r_1, r_2, \ldots, r_N\}} r_F \log_2 M \\ \text{subject to } \int_0^\infty h_b\left(\frac{y}{r_F N_0}\right) f_Y(y)\, dy \le \varepsilon_b \end{array} \tag{2.8}$$

Denote by $L_F = 1/(r_F T_c)$, which is the symbol length in chips for FBF duration adaptation. In order to facilitate the comparison with optimization (2.7), the formulation of (2.8) is rewritten as

$$\begin{array}{l} \max_{L_F \in \{L_1, L_2, \ldots, L_N\}} \frac{\log_2 M}{L_F T_c} \\ \text{subject to } \int_0^\infty h_b\left(L_F \kappa \tilde{y}\right) f_{\tilde{Y}}(\tilde{y})\, d\tilde{y} \le \varepsilon_b \end{array} \tag{2.9}$$

Because of the monotonicity of error probability function $h_b(x)$, the integral in the constraint inequality decreases as L_F increases. Hence the optimization (2.9) seeks in $\{L_1, L_2, \ldots, L_N\}$ the smallest number L_F that satisfied

$$\int_0^\infty h_b\left(L_F \kappa \tilde{y}\right) f_{\tilde{Y}}(\tilde{y})\, d\tilde{y} \le \varepsilon_b \tag{2.10}$$

Defining function

$$H_b(x) \equiv \int_0^\infty h_b(x\tilde{y})\, f_{\tilde{Y}}(\tilde{y})\, d\tilde{y} \tag{2.11}$$

which is a decreasing function of x, the solution to optimization (2.9) can be expressed as

$$\tilde{L}_F = \left\lceil H^{-1}(\varepsilon_b)/\kappa \right\rceil_\Lambda \tag{2.12}$$

where $\tilde{L}_F = \lceil x \rceil_\Lambda$ denotes the smallest number greater than or equal to x in the set $\Lambda \equiv \{L_1, L_2, \ldots, L_N\}$.

The throughput gain is defined as

$$\mathcal{R} = \frac{\bar{r}_S \log_2 M}{\tilde{r}_F \log_2 M} = \frac{1}{\bar{L}_s T_c} \Big/ \frac{1}{\tilde{L}_F T_c} = \frac{\tilde{L}_F}{\bar{L}_S} \tag{2.13}$$

where $\bar{L}_S = 1/\bar{r}_s T_c$.

2.2 Numerical study of throughput gain

In this section, the throughput gain (2.13) for several modulation schemes is numerically studied. The channel is assumed to be Rayleigh fading channel. Thus the normalized receive power has the pdf

$$f_{\tilde{Y}}(\tilde{y}) = \exp(-\tilde{y}), \quad \tilde{y} \geq 0 \tag{2.14}$$

2.2.1 Non-coherent BFSK

Non-coherent BFSK (Binary Frequency Shift Keying) has the bit error probability function

$$h(\gamma) = \frac{1}{2}\exp\left(-\frac{\gamma}{2}\right) \tag{2.15}$$

With (2.14) and (2.15) , the optimal L_F is obtained by solving (2.9), so we have

$$\tilde{L}_F = \left\lceil \frac{1-2\varepsilon_b}{\kappa\varepsilon_b} \right\rceil_\Lambda \tag{2.16}$$

Also substituting (2.14) and (2.15) into (2.7), the optimization to solve the maximum bit rate achieved by SBS adaptation becomes

$$\begin{aligned} &\max_{\{\zeta_1', \zeta_2', \cdots, \zeta_{N-1}'\}} \frac{1}{L_N} + \sum_{i=1}^{N-1} \left(\frac{1}{L_i} - \frac{1}{L_{i+1}}\right)\exp\left(-\zeta_i'\right) \\ &\text{subject to } \frac{1}{L_N(L_N\kappa+2)} - \frac{\varepsilon}{L_N} \\ &\quad + \sum_{i=1}^{N-1} \left\{ \begin{array}{l} \frac{1}{L_i(L_i\kappa+2)}\exp\left(-\left(\frac{1}{2}L_i\kappa+1\right)\zeta_i'\right) \\ -\frac{1}{L_{i+1}(L_{i+1}\kappa+2)}\exp\left(-\left(\frac{1}{2}L_i\kappa+1\right)\zeta_i'\right) \\ -\varepsilon_b \sum_{i=1}^{N-1}\left(\frac{1}{L_i} - \frac{1}{L_{i+1}}\right)\exp\left(-\zeta_i'\right) \end{array} \right\} \leq 0 \\ &\text{and} \qquad \zeta_1' \geq \zeta_2' \geq \ldots \geq \zeta_{N-1}' \geq 0 \end{aligned} \tag{2.17}$$

The optimization (2.17) is solved numerically. In the numerical study, we consider an OVSF code set that has totally 32 code sequences, and the sequences in the code set have 2 chips to 2^{32} chips in length, i.e., $L_1 = 2$, $L_2 = 4$, ..., $L_{32} = 2^{32}$. The throughput gain is analyzed for different error constraints ε_b (10^{-1} to 10^{-9}). The result is shown in Figure 2.2, in which the throughput gain is plotted against error constraint ε_b with both discrete rate set and continuous rate. The throughput gain of continuous rate is originally published in [29] and was also introduced in Section 1.2.3 (Equation (1.10) to (1.13) and Figure 1.7). Compared with the result of the continuous rate, the discrete rate set shows more or less

the same throughput gains as the case of the continuous unlimited range of symbol rates (durations). At some points the throughput gains associated with the discrete rate set are higher than those with the continuous rate set. That is mainly because the symbol length for FBF adaptation, $\tilde{L}_F$, can only take the discrete values in the code length set Λ in the case discrete set. Due to the approximation (2.12), $\tilde{L}_F$ might be quite larger than $H^{-1}(\epsilon_b)/\kappa$. Note that the average symbol rate resulting from using only a discrete set of rates is lower than that resulting from using the set of all symbol rate in a continuum in both SBS and FBF cases. However, it is observed that using only a discrete set of rates can occasionally result in slightly higher throughput gain (2.13). Figure 2.3 shows how the expected SNR per chip κ affects the throughput gains. Figure 2.3 shows the limited choice of symbol rates (durations) makes the throughput gain different from the case of unlimited choice in symbol durations in a continuum. The constant κ reflects the average receive power. When the average receive power is sufficiently high, the FBF duration adaptation (non-adaptation) can achieve the required BEP (the fidelity requirement) even with the highest symbol rate r_1 (equivalently, the smallest number, L_1, of chips in a symbol duration) in the discrete rate set Θ. With the same average receive power, the average symbol rate that SBS adaptation achieves is also r_1. Thus the throughput gain is 1 if κ is sufficiently high. That is why the curves for $\kappa = 10^7, 10^5$ and 10^3 remain 1 from low to moderate BEP fidelity. On the other hand, when the average receive power is too low, the FBF adaptation cannot achieve the given BEP requirement even with the lowest symbol rate r_N (equivalently, the largest number, L_N, of chips in a symbol duration). In this case, the solution of $\tilde{L}_F$ and the throughput gain do not exist. That is why throughput gain curves for $\kappa = 10^{-7}, 10^{-6}$ and 10^{-5} only span in the low BEP fidelity region in Figure 2.3.

In practical systems, the spreading gain control may not have the long dynamic range from 2 to 2^{32}. Figure 2.4 plots the throughput gains where the OVSF code sets have 10, 16, and 20 code sequences. The code lengths are from 2 to 2^{10}, 2 to 2^{16}, and 2 to 2^{20}, respectively. It is again observed that the throughput gain increases as the BEP fidelity goes higher. After some points, the throughput gains do not increase but remain more or less constant. Within the OVSF code set in which code lengths are from 2 to 2^{10}, the smallest value of the average code length for SBS cannot be less than 2 ($\bar{L}_S \geq 2$). And the largest value of the code length for FBF cannot be more than 2^{10} ($\tilde{L}_F \leq 2^{10}$). From (2.13), the throughput gain cannot exceed $2^{10}/2 = 2^9$ ($2^9 = 512$). Similarly, the throughput gain can not be more than 2^{15} with the 16-code OVSF set, and not more than 2^{19} with the

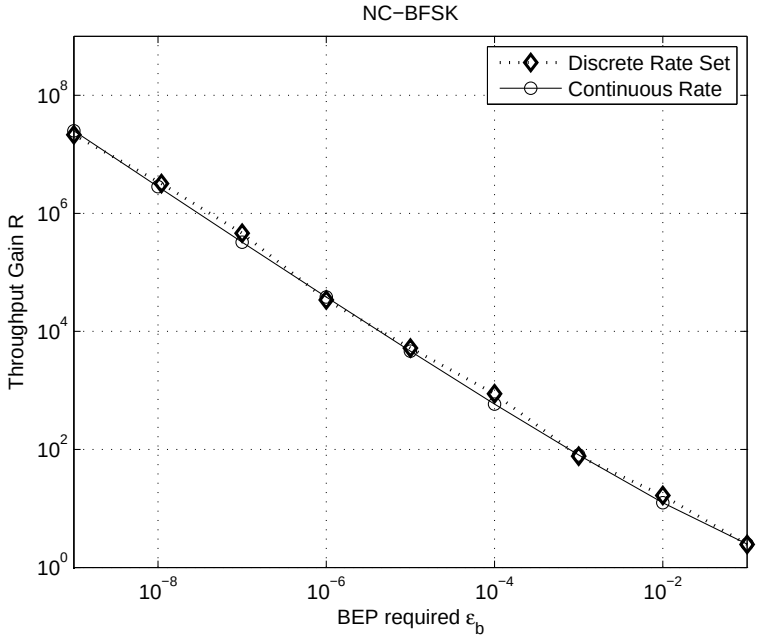

Figure 2.2: The throughput gain achieved by SBS with non-coherent BFSK and the 32-code set, $\kappa = 1$

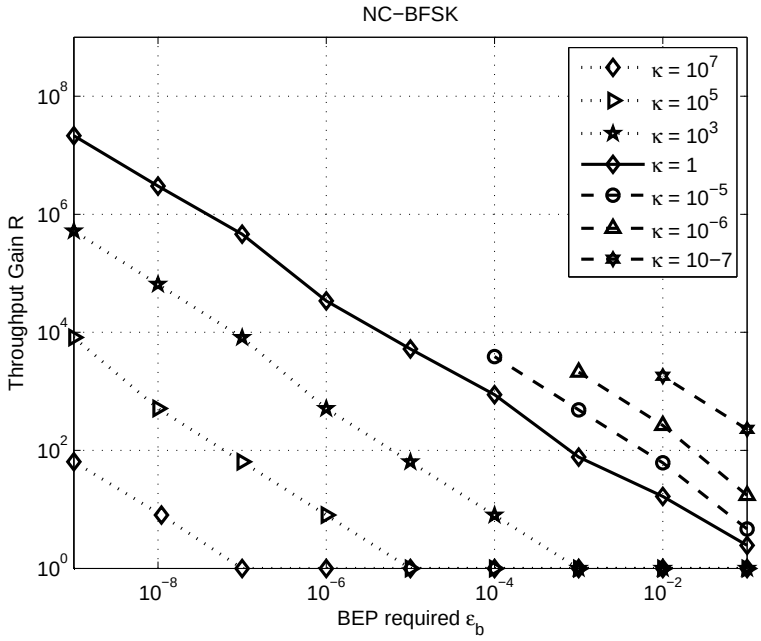

Figure 2.3: Throughput gain for NC-BFSK with different values of κ

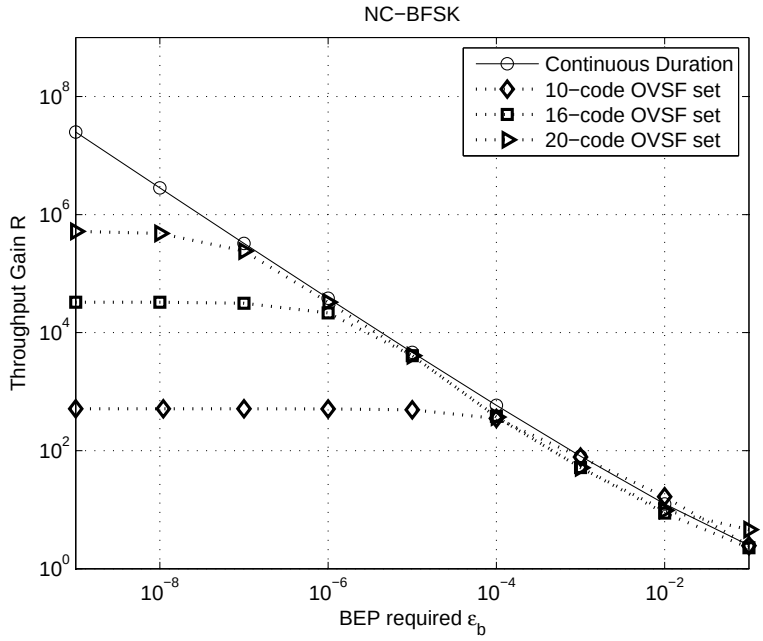

Figure 2.4: Throughput gains for NC-BFSK with the code length only spanning from 2 to 2^{10}, 2 to 2^{16}, 2 to 2^{20}

20-code set. Note that in Figure 2.4, on each throughput gain curve, different values of κ were chosen for different fidelity requirements ε_b. As shown in Figure 2.3, given a single value of κ and a rate set Θ, FBF adaptation may not achieve all BEP requirements. Hence for each BEP fidelity requirement ε_b, κ was chosen so that the FBF adaptation system can barely achieve the BEP requirement with constant symbol rate r_N, which corresponds to the longest symbol duration allowed. Table 2.1 lists the values of κ associated with the throughput gains shown in Figure 2.4.

2.2.2 M-QAM

The bit error probability function of Gray mapped MQAM (M-ary quadrature amplitude modulation) can be generally written in the form of [30]

$$h_b(\gamma) = \sum_{i=1}^{m_1} \Lambda_i Q\left(\sqrt{\alpha_i \gamma}\right) - \sum_{j=1}^{m_2} \Upsilon_j Q\left(\sqrt{\beta_j \gamma}\right) \tag{2.18}$$

where the values of Λ, Υ, α and β are tabulated in table 2.2 according to [31, 32].

Table 2.1: The values of κ for Fig. 2.3

ϵ_b	10-code set	16-code set	20-code set
10^{-1}	7.813×10^{-3}	1.221×10^{-4}	7.629×10^{-6}
10^{-2}	9.570×10^{-2}	1.495×10^{-3}	9.346×10^{-5}
10^{-3}	9.746×10^{-1}	1.523×10^{-2}	9.518×10^{-4}
10^{-4}	9.764	1.526×10^{-1}	9.535×10^{-3}
10^{-5}	9.765×10^{1}	1.526	9.537×10^{-2}
10^{-6}	9.766×10^{2}	1.526×10^{1}	9.537×10^{-1}
10^{-7}	9.766×10^{3}	1.526×10^{2}	9.537
10^{-8}	9.766×10^{4}	1.526×10^{3}	9.537×10^{1}
10^{-9}	9.766×10^{5}	1.526×10^{4}	9.537×10^{2}

Table 2.2: The values of Λ, Υ, α and β for (2.18)

Constellation	Λ_i and α_i	Υ_j and β_j
4-QAM	$(1, 1)$	—
16-QAM	$(\frac{3}{4}, \frac{1}{5})$, $(\frac{2}{4}, \frac{5}{5})$	$(\frac{1}{4}, \frac{25}{5})$
64-QAM	$(\frac{7}{12}, \frac{1}{21})$, $(\frac{6}{12}, \frac{9}{21})$, $(\frac{1}{12}, \frac{81}{21})$	$(\frac{1}{12}, \frac{25}{21})$, $(\frac{1}{12}, \frac{169}{21})$

Substituting (2.18) and (2.14) into (2.10) and referring to [33, eqn 5.6], (2.10) becomes

$$H_b(\gamma) = \sum_{i=1}^{m_1} \frac{\Lambda_i}{2} \left(1 - \sqrt{\frac{\alpha_i \gamma \kappa}{2 + \alpha_i \gamma \kappa}}\right) - \sum_{j=1}^{m_2} \frac{\Upsilon_j}{2} \left(1 - \sqrt{\frac{\beta_j \gamma \kappa}{2 + \beta_j \gamma \kappa}}\right) \tag{2.19}$$

The optimal symbol length in chips of FBF duration adaptation is given by $\tilde{L}_F = \lceil x \rceil_\Lambda$, where x is obtained by solving

$$\sum_{i=1}^{m_1} \frac{\Lambda_i}{2} \left(1 - \sqrt{\frac{\alpha_i x \kappa}{2 + \alpha_i x \kappa}}\right) - \sum_{j=1}^{m_2} \frac{\Upsilon_j}{2} \left(1 - \sqrt{\frac{\beta_j x \kappa}{2 + \beta_j x \kappa}}\right) = \varepsilon_b \tag{2.20}$$

For SBS duration adaptation, (2.7) should be solved by using $h_b(\gamma)$ in (2.18). Since $h_b(\gamma)$ includes one or more Q functions, the non-linear constraint inequality in (2.7) then involves a summation of double integrations. In order to simplify numerical computation of the optimization, we applied the following tight bounds [34] of the exact BEP functions:

$$h_b(\gamma) \leq c_1 \exp\left(\frac{-c_2 \gamma}{M - 1}\right) \tag{2.21}$$

Reference [34] suggests $c_1 = 0.2$, $c_2 = 1.5$ for MQAM for moderate to high SNR, $c_1 = 2$, $c_2 = 1.5$ for low SNR. The bound with $c_1 = 2$, $c_2 = 1.5$ are too loose in low SNR region, so the values were modified. For 4QAM, c_1 and c_2 were set to be 0.35 and 2 for symbol SNR $\leq$ 6.23 dB. For 16QAM, c_1 and c_2 were set to be 0.4 and 3.5 for symbol SNR $\leq$ 7.38 dB. For 64QAM, c_1 and c_2 were chosen to be 0.4 and 6 for symbol SNR $\leq$ 9.97 dB. These bounds are plotted with the exact BEP functions in Figure 2.5.

With (2.21) and (2.14), the optimization (2.7) becomes

$$\begin{aligned} &\max_{\{\zeta_1',\zeta_2',\cdots,\zeta_{N-1}'\}} \frac{1}{L_N} + \sum_{i=1}^{N-1} \left(\frac{1}{L_i} - \frac{1}{L_{i+1}}\right) e^{-\zeta_i'} \\ &\text{subject to } \frac{V_N}{L_N} - \frac{\varepsilon_b}{L_N} + \sum_{k=1}^{N-1} \begin{bmatrix} \frac{V_k}{L_k} \exp\left(-W_k \zeta_k'\right) \\ -\frac{V_{k+1}}{L_{k+1}} \exp\left(-W_{k+1}\zeta_k'\right) \\ -\varepsilon_b \left(\frac{1}{L_k} - \frac{1}{L_{k+1}}\right) \exp\left(-\zeta_k'\right) \end{bmatrix} \leq 0 \end{aligned} \tag{2.22}$$

where $V_i = \frac{c_1(M-1)}{c_2 L_i \kappa + M - 1}$, $W_i = \frac{c_2 L_i \kappa}{M-1} + 1$.

The numerical results of throughput gains for 4QAM, 16QAM and 64QAM are shown in Figure 2.6, 2.7 and 2.8. The throughput gains with the continuous rate [29] (also shown in Figure 1.8) are also plotted in the figures for comparison. The plots show that SBS duration adaptation with the discrete rate set can achieve the similar throughput gain as that with the continuous rate. Hence the discrete rate set does not degrade the throughput gain for MQAM either. The throughput gain also increases more or less linearly as the BEP fidelity increases in log-log scale.

The thresholds $\{\zeta_{N-1}', \zeta_{N-2}', \ldots, \zeta_1'\}$ obtained by the optimization (2.22) is employed to implement the rapid duration adaptation. Since upper bounds instead of the exact BEP functions were applied to numerically perform the optimization, the SBS adaptation throughput obtained by solving (2.22) is pessimistic. Furthermore, the FBF throughput is solved with exact BEP functions (2.20), so the throughput gains shown in Figure 2.6 to 2.8 are also pessimistic.

2.3 Chapter conclusion

In this paper, the throughput gain of symbol-by-symbol duration adaptation over frame-by-frame duration adaptation with discrete duration sets is formulated and numerically analyzed. The results show that, for NC-BFSK and MQAM, the rapid dynamic spreading

gain adaptation within a discrete duration set can often achieve a throughput gain similar to that achieved with a continuous set of durations.

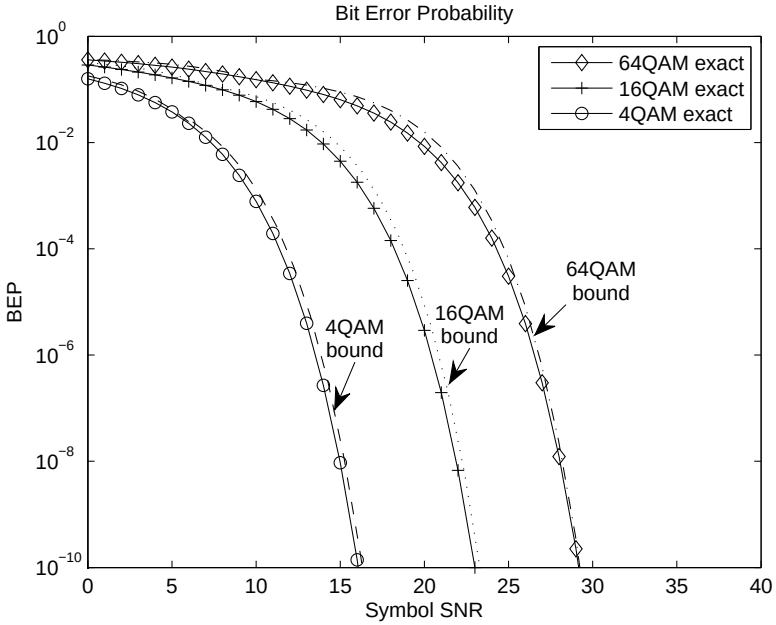

Figure 2.5: The BEP bounds for MQAM

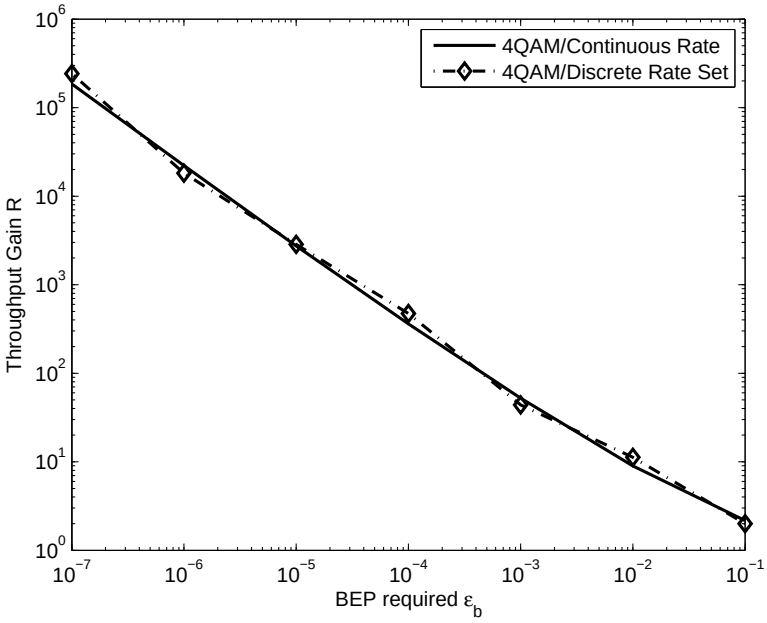

Figure 2.6: The throughput gain for 4QAM within the 28-code set and $\kappa = 1$

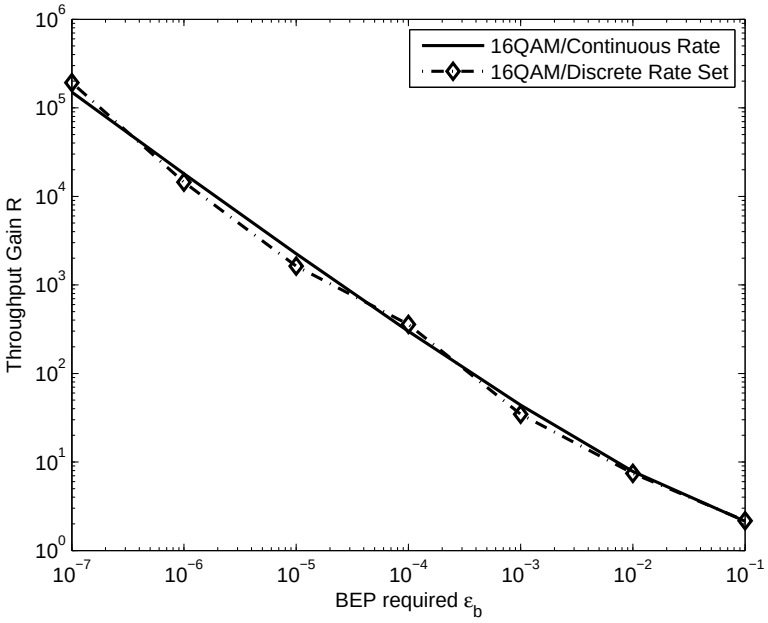

Figure 2.7: The throughput gain for 16QAM within the 28-code set and $\kappa = 1$

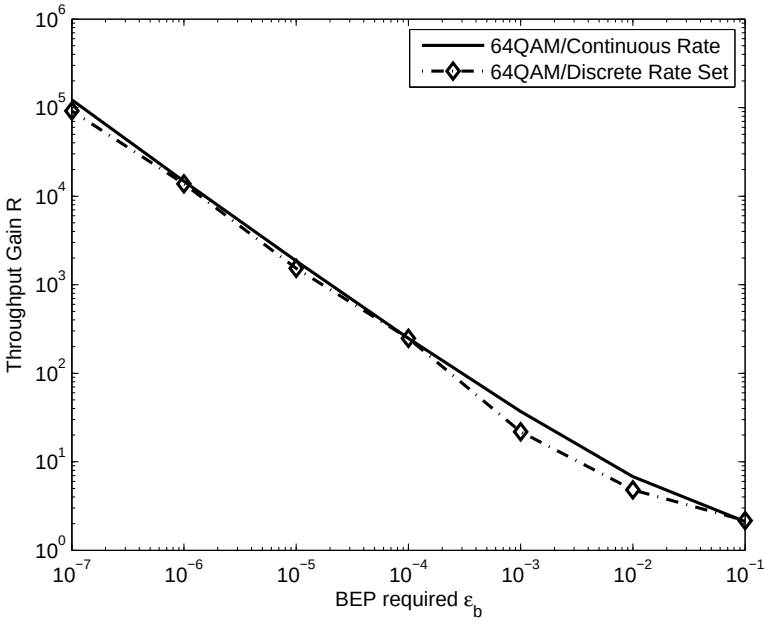

Figure 2.8: The throughput gain for 64QAM within the 28-code set and $\kappa = 1$

Chapter 3

Throughput Gain within Discrete Duration Set over Channels Varying in A Symbol Duration

In the throughput gain analysis of Chapter 2, we consider the duration adaptation system that can only choose a symbol duration from a finite discrete set. The numerical results show that within a finite duration set, the symbol-by-symbol duration adaptation can achieve the throughput gain similar to that for the case that the duration set is a continuum. The analysis was under the assumption that the channel gain remains unchanged during each symbol duration. For a long dynamic range of the spreading gain control, this assumption is not realistic. In this chapter, the throughput gain study is extended to the case that the channel gain can vary within each symbol time. The channel gain is merely assumed to remain constant for each chip duration.

3.1 System model

Let us denote the OVSF code sequence set by $C = \{C_1, C_2, \ldots, C_N\}$, and also denote by L_j the the length of the sequence C_j. The lengths of the code sequences take the values of power of 2 such that $L_{j+1} = 2L_j$. The symbol duration is $L_j T_c$ when the code C_j is used to spread the data symbol, where T_c is the chip duration. Furthermore, denote by $\Lambda = \{L_1, L_2, \ldots, L_N\}$ the code length set of C. Each symbol duration $L_i T_c$ also corresponds

to an instantaneous symbol rate $r_i = 1/(L_i T_c)$. Therefore, it can be construed that each symbol is transmitted with an instantaneous symbol rate in a set of discrete rates $\Theta = \{r_1, r_2, \ldots, r_N\}$, where $r_i = 1/(L_i T_c)$ and $r_{i+1} = r_i/2$.

The transmission power is assumed to be fixed over time. The channel is assumed to remain constant during each chip duration. Thus, the received power remains unchanged in a each chip duration, but varies from chip to chip. It is also assumed that the system can perfectly predict the channel gain for the near future. The prediction range is large enough for the system to determine the next symbol duration, i.e., the range is larger than the longest possible symbol duration ($L_N T_c$) plus the processing and feedback delays associated with channel prediction. Let $t = 0$ be the beginning time of the next symbol and let $\tilde{g}_1, \tilde{g}_2, \ldots, \tilde{g}_i, \ldots$ be the complex channel gains for chip time $1, 2, \ldots, i, \ldots$ after $t = 0$. We assume that $\tilde{g}_1, \tilde{g}_2, \ldots, \tilde{g}_i, \ldots$ is an ergodic stationary random process. If the next symbol is spread by C_j, the symbol has the length of L_j chips. The received symbol signal to noise ratio (SNR) at the output of the maximal ratio combiner (MRC) is

$$\gamma = \frac{P_T T_c}{N_0} \sum_{i=1}^{L_j} |\tilde{g}_i|^2 \tag{3.1}$$

where P_T is the transmit power, N_0 is power spectral density of the additive white Gaussian noise (AWGN). Let g_i be the normalized complex channel gain, i.e., $g_i = \tilde{g}_i / \sqrt{E(|\tilde{g}_i|^2)}$. Denote by $\kappa = P_T T_c E(|\tilde{g}_i|^2)/N_0$ the average SNR per chip. Also denote by $h_b(\gamma)$ the bit error probability (BEP) function, where γ is the symbol SNR. The bit error probability of the next symbol is

$$h_b(\gamma) = h_b\left(\frac{P_T T_c}{N_0} \sum_{i=1}^{L_j} |\tilde{g}_i|^2\right) = h_b\left(\kappa \sum_{i=1}^{L_j} |g_i|^2\right) \tag{3.2}$$

We consider the duration adaptation policy that chooses the minimum symbol length (maximum symbol rate) while satisfying an instantaneous bit error probability constraint, i.e.,

$$\begin{aligned} &\min_{L \in \{L_1, L_2, \ldots, L_N\}} L \\ &\text{subject to} \quad h_b\left(\kappa \sum_{i=1}^{L} |g_i|^2\right) \le \varepsilon_b \end{aligned} \tag{3.3}$$

where ε_b is the BEP constraint.

3.1.1 Throughput of symbol-by-symbol duration adaptation

In accordance with (3.3), the next symbol length for SBS adaptation, L_S, is determined by choosing the least one among those within $\Lambda = \{L_1,\ L_2, \ldots, L_N\}$ that satisfy

$$h_b\left(\kappa \sum\nolimits_{i=1}^{L_S} |g_i|^2\right) \leq \varepsilon_b$$

Let $\eta \equiv h_b^{-1}(\varepsilon_b)/\kappa$, where $h_b^{-1}(x)$ is the inverse function of $h_b(\gamma)$. Then

$$h_b\left(\kappa \sum\nolimits_{i=1}^{L_j} |g_i|^2\right) \leq \varepsilon_b \Leftrightarrow \sum\nolimits_{i=1}^{L_j} |g_i|^2 \geq \eta$$

Define random variables $X^j \equiv \sum_{i=1}^{L_j} |g_i|^2$, $j = 1, 2, \ldots, N$.

Now we consider the average symbol duration in the number of chips achieved by symbol-by-symbol (SBS) duration adaptation. Define P_j as the probability that $h_b\left(\kappa \sum_{i=1}^{L_j} |g_i|^2\right) \leq \varepsilon_b$, i.e.,

$$P_j = \Pr\left(h_b\left(\kappa \sum\nolimits_{i=1}^{L_j} |g_i|^2\right) \leq \varepsilon_b\right) = \Pr\left(\sum\nolimits_{i=1}^{L_j} |g_i|^2 \geq \eta\right) = \int_{\eta}^{\infty} f_X^j(x)dx \tag{3.4}$$

where $f_X^j(x)$ the probability density function of the random variable X^j. The symbol length is chosen to be L_j when L_j can satisfy the bit error requirement ε_b but L_{j-1} cannot, i.e., $h_b\left(\kappa \sum_{i=1}^{L_j} |g_i|^2\right) \leq \varepsilon_b$ and $h_b\left(\kappa \sum_{i=1}^{L_{j-1}} |g_i|^2\right) > \varepsilon_b$. Let $\Pr(L_j)$ be the probability that L_j is chosen, i.e.,

$$\begin{aligned}\Pr(L_j) &= \Pr\left(h_b\left(\kappa \sum\nolimits_{i=1}^{L_j} |g_i|^2\right) \leq \varepsilon_b \ \text{ and } \ h_b\left(\kappa \sum\nolimits_{i=1}^{L_{j-1}} |g_i|^2\right) > \varepsilon_b\right) \\ &= \Pr\left(\sum_{i=1}^{L_j} |g_i|^2 \geq \eta \ \text{ and } \ \sum_{i=1}^{L_{j-1}} |g_i|^2 < \eta\right)\end{aligned}$$

We know the probability P_j is

$$\begin{aligned}P_j &= \Pr\left(\sum_{i=1}^{L_j} |g_i|^2 \geq \eta\right) \\ &= \Pr\left(\sum_{i=1}^{L_j} |g_i|^2 \geq \eta \ \text{ and } \ \sum_{i=1}^{L_{j-1}} |g_i|^2 \geq \eta\right) + \Pr\left(\sum_{i=1}^{L_j} |g_i|^2 \geq \eta \ \text{ and } \ \sum_{i=1}^{L_{j-1}} |g_i|^2 < \eta\right) \\ &= \Pr\left(\sum_{i=1}^{L_{j-1}} |g_i|^2 \geq \eta\right) + \Pr\left(\sum_{i=1}^{L_j} |g_i|^2 \geq \eta \ \text{ and } \ \sum_{i=1}^{L_{j-1}} |g_i|^2 < \eta\right) \\ &= P_{j-1} + \Pr(L_j)\end{aligned}$$

Therefore, the probability that L_j is chosen is

$$\Pr(L_j) = P_j - P_{j-1} \tag{3.5}$$

Then the average symbol length in chips is given by

$$\bar{L}_S = \sum_{j=1}^{N} L_j \Pr(L_j) = \sum_{j=1}^{N} L_j (P_j - P_{j-1}) \tag{3.6}$$

where $P_0 = 0$. Denote by $L^{(k)}$ the duration of the k^{th} symbol in the number of chips. Then the throughput, i.e., the average symbol rate achieved by SBS duration adaptation, is

$$\begin{aligned} \bar{r}_S &= \lim_{k\to\infty} \frac{k}{L^{(1)}T_c + L^{(2)}T_c + \cdots + L^{(k)}T_c} \\ &= \frac{1}{\lim\limits_{k\to\infty} \frac{L^{(1)}+L^{(2)}+\cdots+L^{(k)}}{k} T_c} \\ &= \frac{1}{\bar{L}_S T_c} \end{aligned} \tag{3.7}$$

with probability 1.

Note that there is an outage probability $P_{out} = 1 - P_N$ when even the longest symbol length L_N cannot satisfy the bit error constraint ε_b, i.e., $h_b\left(\kappa \sum_{i=1}^{L_N} |g_i|^2\right) > \varepsilon_b$. In this case, the transmitter cannot sent any data at beginning of the next symbol time, $t = 0$. The outage probability is given by

$$P_{out} = \Pr\left(h_b\left(\kappa \sum\nolimits_{i=1}^{L_N} |g_i|^2\right) \geq \varepsilon_b\right) = \Pr\left(\sum\nolimits_{i=1}^{L_N} |g_i|^2 \leq \eta\right) = \int_0^{\eta} f_X^N(x)dx \tag{3.8}$$

3.1.2 Throughput of frame-by-frame adaptation

As it has been explained in [27] and also in chapter 1, for fast time-varying channel, we assumed that frame-by-frame duration adaptation is equivalent to a non-adaptive scheme. We make the same assumption for the case that the channel varies chip by chip. Over a fast time-varying channel, the frame length is relative long compared to the interval between adjacent deep fades of the channel, which is approximately $1/(2f_D)$. The empirical distribution of the channel gain in each frame can be approximated by the ensemble distribution of the channel gain. Thus, with a particular fixed symbol length L, the bit error probability of each frame can be approximated by the bit error probability average over the entire time horizon.

Therefore, the adaptation policy for FBF duration adaptation is given by

$$\begin{array}{l} \min_{L_F \in \{L_1,\, L_2, \ldots, L_N\}} L_F \\ \text{subject to} \quad E\left[h_b\left(\kappa \sum_{i=1}^{L_F} |g_i|^2\right)\right] \leq \varepsilon_b \end{array} \tag{3.9}$$

Because of the monotonicity of the error probability function $h_b(\gamma)$, the expectation in the constraint inequality decreases as L_F increases. Hence the optimization (3.9) seeks in $\Lambda = \{L_1, L_2, \ldots, L_N\}$ the smallest number L_j that satisfies $E\left[h_b\left(\kappa \sum_{i=1}^{L_j} |g_i|^2\right)\right] \leq \varepsilon_b$. Also let $X^j \equiv \sum_{i=1}^{L_j} |g_i|^2$, $j = 1, 2, \ldots, N$. Then

$$E\left[h_b\left(\kappa \sum_{i=1}^{L_j} |g_i|^2\right)\right] = \int_0^\infty h_b(\kappa x)\, f_X^j(x) dx \tag{3.10}$$

where $f_X^j(x)$ is the pdf of X^j.

Given an bit error fidelity ε_b, to find L_F, we should compute

$$\begin{array}{l} \int_0^\infty h_b(\kappa x)\, f_X^1(x) dx, \\ \int_0^\infty h_b(\kappa x)\, f_X^2(x) dx, \\ \ldots \\ \int_0^\infty h_b(\kappa x)\, f_X^j(x) dx, \end{array}$$

until finding the length L_j that satisfies the bit error constraint, i.e., $\int_0^\infty h_b(\kappa x)\, f_X^j(x) dx \leq \varepsilon_b$. Then the symbol length for the next frame, L_F, is chosen to be L_j. The throughput, i.e., the symbol rate achieved by FBF adaptation, is

$$r_F = \frac{1}{L_F T c} \tag{3.11}$$

3.1.3 Throughput gain

In order to compare the SBS duration adaptation with FBF adaptation, the throughput gain is defined as

$$\mathcal{R} = \frac{\bar{r}_S}{r_F} = \frac{L_F}{\bar{L}_S} \tag{3.12}$$

The average bit error probability achieved by SBS adaptation is lower than the instantaneous BEP fidelity requirement ε_b because for most of the time, a symbol length chosen from the finite set Λ to satisfy ε_b leads to the bit error probability of that symbol being strictly less than ε_b.

3.2 Numerical method

In order to compute the average symbol length in chips of SBS duration adaptation (3.6) and FBF adaptation (3.9), numerical methods are needed to compute the integrals in (3.4) and (3.10). Both integrals involve the pdf $f_X^j(x)$ of the random variable $X^j \equiv \sum_{i=1}^{L_j} |g_i|^2$. We assume that the channel gain is a zero-mean complex Gaussian variable. Then X^j is a chi-square random variable with $2L_j$ degrees of freedom. Furthermore, the channel gain has time correlation in many fading environments of interest. It is difficult to work with the pdf $f_X^j(x)$ directly to compute the integrals. An alternative approach is to compute these integrals by using the moment generating function (MGF) [33] [35] [36] [37]. This method facilitates analyzing the performance of systems with complex channel models and sophisticated diversity techniques [33].

In this chapter, we assume the channel is the Clarke's two-dimensional isotropic scattering model. Then, the normalized channel gains $g_1, g_2, \ldots, g_j, \ldots$ are zero-mean complex Gaussian random variables with the autocorrelation [38]

$$E\left[g_i g_j^*\right] = J_0\left(2\pi f_D (j-i) T_c\right) \tag{3.13}$$

where $J_0(\,)$ is the zero-order Bessel function of the first kind, and f_D is the maximum Doppler shift.

3.2.1 MGF of received SNR at MRC output

In accordance with Equation (3.1), the random variable X^j and the MRC output SNR differs only by a coefficient κ. Thus, X^j is equivalent to the scaled received symbol SNR at the output of an L_j-branch ideal maximal ratio combiner.

For the correlated Rayleigh fading channel with normalized channel gains $g_1, g_2, \ldots, g_{L_j}$ (i.e., $E\{|g_1|^2\} = E\{|g_2|^2\} = \ldots = E\{|g_{L_j}|^2\} = 1$), the moment generating function of the SNR resulting from MRC is given by [36][37] [1]

[1] For a correlated Nakagami-m fading channel, the MGF of the SNR at the L_j-branch MRC output [36] is

$$M_X^j(s) = \det\left(I + \frac{s}{m} D_G \Gamma_X^j\right)^{-m}$$

where D_G is the diagonal matrix diag$\{E\{|g_1|^2\}, E\{|g_1|^2\}, \ldots, E\{|g_{Lj}|^2\}\}$. Here we consider the correlated Rayleigh fading channel (i.e., $m = 1$) with normalized channel gains (i.e., $E\{|g_1|^2\} = E\{|g_2|^2\} = \ldots = E\{|g_{L_j}|^2\} = 1$). Then the MGF is given by (3.14)

$$M_X^j(s) = \det\left(I + s\Gamma_X^j\right)^{-1} = \prod_{i=1}^{L_j} \frac{1}{1+s\lambda_i} \tag{3.14}$$

where Γ_X^j is an $L_j \times L_j$ positive definite matrix based on the channel correlation, and λ_i is the ith eigenvalue of matrix Γ_X^j. The (i,j) entry of Γ_X^j is [36]

$$\Gamma_X^j(i,j) = \sqrt{\rho\left(|g_i|^2, |g_j|^2\right)} \tag{3.15}$$

where

$$\rho\left(|g_i|^2, |g_j|^2\right) = \frac{E\left[|g_i|^2|g_j|^2\right] - E\left[|g_i|^2\right]E\left[|g_j|^2\right]}{\sqrt{E\left[\left(|g_i|^2\right)^2\right] - \left(E\left[|g_i|^2\right]\right)^2} \times \sqrt{E\left[\left(|g_j|^2\right)^2\right] - \left(E\left[|g_j|^2\right]\right)^2}} \tag{3.16}$$

For the case that the channel gain has the autocorrelation of (3.13), we have [38]

$$\begin{aligned} E\left[|g_i|^2|g_j|^2\right] &= 1 + J_0^2\left(2\pi f_D(j-i)T_c\right) \\ E\left[|g_i|^2\right] &= E\left[|g_j|^2\right] = 1 \\ E\left[\left(|g_i|^2\right)^2\right] &= 2 \end{aligned} \tag{3.17}$$

The derivation of the first equation of (3.17) is shown is Appendix A. The second and the third equation are immediately derived from (3.13) and the first equation of (3.17) by letting $i = j$. By substituting (3.17) into (3.16), the (i,j) entry of Γ_X^j is given by

$$\Gamma_X^j(i,j) = \left|J_0\left(2\pi f_D(j-i)T_c\right)\right| \tag{3.18}$$

3.2.2 Expectation of BEP for NC-BFSK

Non-coherent BFSK modulation has the BEP function of(the same as (2.15))

$$h_b(\gamma) = \frac{1}{2}\exp\left(-\frac{\gamma}{2}\right) \tag{3.19}$$

where γ is the SNR per symbol.

Substituting (3.19) into (3.10), we have the expectation of BEP when the symbol length is chosen to be L_j

$$\begin{aligned}
&\int_0^\infty h_b(\kappa x) f_X^j(x)\,dx \\
=&\int_0^\infty \frac{1}{2}\exp\left(-\frac{\kappa x}{2}\right) f_X^j(x)\,dx \\
=&\frac{1}{2}\int_0^\infty \exp(sz) f_X^j(x)\,dx\Big|_{s=-\frac{\kappa}{2}} \\
=&\frac{M_X^j(s)}{2}\Big|_{s=-\frac{\kappa}{2}}
\end{aligned} \tag{3.20}$$

In accordance with Section 3.1.2, the throughput of FBF adaptation is determined by calculating $\frac{M_X^1(s)}{2}\Big|_{s=-\frac{\kappa}{2}}$, $\frac{M_X^2(s)}{2}\Big|_{s=-\frac{\kappa}{2}}$, ..., until j where $\frac{M_X^j(s)}{2}\Big|_{s=-\frac{\kappa}{2}} \leq \varepsilon_b$ is satisfied. Then the symbol length L_F is chosen to be L_j.

3.2.3 Expectation of BEP for MQAM

The BEP function of MQAM is the same as that in Equation (2.18). It is reprinted here:

$$h_b(\gamma) = \sum_{i=1}^{m_1} \Lambda_i Q\left(\sqrt{\alpha_i \gamma}\right) - \sum_{j=1}^{m_2} \Upsilon_j Q\left(\sqrt{\beta_j \gamma}\right) \tag{3.21}$$

where the values of Λ, Υ, α and β are also re-tabulated here (They are the same as in table 2.2).

Table 3.1: The values of Λ, Υ, α and β for (3.21)

Constellation	Λ_i and α_i	Υ_j and β_j
4-QAM	$(1, 1)$	—
16-QAM	$(\frac{3}{4}, \frac{1}{5})$, $(\frac{2}{4}, \frac{5}{5})$	$(\frac{1}{4}, \frac{25}{5})$
64-QAM	$(\frac{7}{12}, \frac{1}{21})$, $(\frac{6}{12}, \frac{9}{21})$, $(\frac{1}{12}, \frac{81}{21})$	$(\frac{1}{12}, \frac{25}{21})$, $(\frac{1}{12}, \frac{169}{21})$

Instead of the canonical definition of Q function

$$Q(x) = \int_x^\infty \frac{1}{\sqrt{2\pi}} \exp\left(-\frac{y^2}{2}\right) dy$$

Q function could also be expressed as [33]

$$Q(x) = \frac{1}{\pi}\int_0^{\pi/2} \exp\left(-\frac{x^2}{2\sin^2\theta}\right) d\theta \tag{3.22}$$

By applying (3.21) with (3.10), also using the alternative form of Q function (3.22), the expected BEP of MQAM is given by

$$\begin{aligned}
&\int_0^\infty h_b(\kappa z) f_X^j(z)\, dz \\
&= \sum_{i=1}^{m_1} \Lambda_i \int_0^\infty Q\left(\sqrt{\alpha_i \kappa z}\right) f_X^j(z)\, dz - \sum_{j=1}^{m_2} \Upsilon_j \int_0^\infty Q\left(\sqrt{\beta_j \kappa z}\right) f_X^j(z)\, dz \\
&= \sum_{i=1}^{m_1} \Lambda_i \int_0^\infty \left[\frac{1}{\pi}\int_0^{\pi/2} \exp\left(-\frac{\alpha_i \kappa z}{2\sin^2\theta}\right) d\theta\right] f_X^j(z)\, dz \\
&\quad - \sum_{j=1}^{m_2} \Upsilon_j \int_0^\infty \left[\frac{1}{\pi}\int_0^{\pi/2} \exp\left(-\frac{\beta_j \kappa z}{2\sin^2\theta}\right) d\theta\right] f_X^j(z)\, dz \\
&= \sum_{i=1}^{m_1} \frac{\Lambda_i}{\pi}\int_0^{\pi/2} M_X^j(s)\Big|_{s=-\frac{\alpha_i\kappa}{2\sin^2\theta}} d\theta - \sum_{j=1}^{m_2} \frac{\Upsilon_j}{\pi}\int_0^{\pi/2} M_X^j(s)\Big|_{s=-\frac{\beta_j\kappa}{2\sin^2\theta}} d\theta
\end{aligned} \tag{3.23}$$

In (3.20) and (3.23), calculating the expected BEP for both NC-BFSK and MQAM involves evaluating the moment generating function (MGF). This method is called *MGF-based approach* in [33].

3.2.4 Computing P_j with MGF

In accordance with Equation (3.4), the probability of $h_b\left(\kappa \sum_{i=1}^{L_j} |g_i|^2\right) \le \varepsilon_b$ is given by

$$P_j = \int_\eta^\infty f_X^j(x) dx \tag{3.24}$$

The complementary probability of P_j

$$\bar{P}_j = \int_0^\eta f_X^j(x) dx \tag{3.25}$$

is in fact the probability that the bit error probability exceeds the BEP requirement ε_b when symbol length is fixed to L_j. Because the Laplace transform of $\int_0^\eta f_X^j(x) dx$ is $\frac{M_X^j(-s)}{s}$, $\bar{P}_j$ can be computed by inverse Laplace transform of $\frac{M_X^j(-s)}{s}$ [33, eqn (1.6)], i.e.,

$$\bar{P}_j = \int_0^\eta f_X^j(x)\, dx = \frac{1}{2\pi j}\int_{\sigma-j\infty}^{\sigma+j\infty} \frac{M_X^j(-s)}{s} e^{s\eta} ds \tag{3.26}$$

where σ is chosen in the region of convergence of the integral in complex s plane. A numerical method to evaluate the above integral is also introduced in appendix 9B of [33].

Let $\hat{f}(s) \equiv \frac{M_X^j(-s)}{s}$, and $f(\eta) \equiv \frac{1}{2\pi j}\int_{\sigma-j\infty}^{\sigma+j\infty} \frac{M_X^j(-s)}{s} e^{s\eta} ds$. Then we have

$$f(\eta) = \frac{1}{2\pi j}\int_{\sigma-j\infty}^{\sigma+j\infty} \hat{f}(s)\, e^{s\eta} ds \tag{3.27}$$

By changing the variable $s = a + ju$, we have

$$\begin{aligned} f(\eta) &= \frac{1}{2\pi j}\int_{\sigma-j\infty}^{\sigma+j\infty} \hat{f}(s)\, e^{s\eta} ds \\ &= \frac{1}{2\pi}\int_{-\infty}^{\infty} \hat{f}(a+ju)\, e^{(a+ju)\eta} du \\ &= \frac{e^{a\eta}}{2\pi}\int_{-\infty}^{\infty} \hat{f}(a+ju)\left[\cos(u\eta) + j\sin(u\eta)\right] du \\ &= \frac{e^{a\eta}}{2\pi}\int_{-\infty}^{\infty} \left\{ \mathrm{Re}\left[\hat{f}(a+ju)\right]\cos(u\eta) - \mathrm{Im}\left[\hat{f}(a+ju)\right]\sin(u\eta)\right\} du \end{aligned}$$

We know the random variable X^j is positive. For $\eta \geq 0$, $f(-\eta) = \int_{-\eta}^{0} f_X^j(x)dx = 0$. Hence,

$$f(-\eta) = \frac{e^{-a\eta}}{2\pi}\int_{-\infty}^{\infty} \left\{ \mathrm{Re}\left[\hat{f}(a+ju)\right]\cos(u\eta) + \mathrm{Im}\left[\hat{f}(a+ju)\right]\sin(u\eta)\right\} du = 0$$

Thus,

$$\int_{-\infty}^{\infty} \mathrm{Re}\left[\hat{f}(a+ju)\right]\cos(u\eta)\, du = -\int_{-\infty}^{\infty} \mathrm{Im}\left[\hat{f}(a+ju)\right]\sin(u\eta) du$$

Then we have

$$f(\eta) = \frac{2e^{a\eta}}{\pi}\int_{0}^{\infty} \mathrm{Re}\left[\hat{f}(a+ju)\right]\cos(u\eta)\, du \tag{3.28}$$

Applying the trapezoidal rule with the step size $h = \frac{\pi}{2\eta}$, and defining $a = \frac{A}{2\eta}$, we get

$$f(\eta) = \frac{e^{A/2}}{\eta}\sum_{n=0}^{\infty} \frac{(-1)^n}{\alpha_n} \mathrm{Re}\left[\hat{f}\left(\frac{A+2\pi jn}{2\eta}\right)\right] \tag{3.29}$$

where

$$\alpha_n = \begin{cases} 2 & n = 0 \\ 1 & n = 1,\ 2,\ \ldots \end{cases}$$

Truncate the infinite summation, and accelerate the convergence by the Euler summation technique. (3.29) becomes

$$f(\eta) = \frac{e^{A/2}}{\eta}\sum_{k=0}^{K} 2^{-K} \binom{K}{k} \left\{ \sum_{n=0}^{N+k} \frac{(-1)^n}{\alpha_n} \mathrm{Re}\left[\hat{f}\left(\frac{A+2\pi jn}{2\eta}\right)\right]\right\} \tag{3.30}$$

The discretization error, i.e., the error caused by the value of A, is bounded by

$$|E(A)| \leq e^{-A} \tag{3.31}$$

We consider that the target accuracy of the numerical analysis is 10^{-12}. Then the value of A is chosen to be 28.

The truncation error, i.e., the error caused by the values of N and K, can be estimated by

$$E(N,K) \simeq \frac{e^{A/2}}{\eta} \sum_{k=0}^{K} 2^{-K}(-1)^{N+1+k} \begin{pmatrix} K \\ k \end{pmatrix} \mathrm{Re}\left[\hat{f}\left(\frac{A + 2\pi j\,(N+k+1)}{2\eta}\right)\right] \tag{3.32}$$

The choice of N and K depends on the target accuracy, modulation scheme related BEP function $h_b(\gamma)$, BEP fidelity requirement ε_b, and the average SNR per chip κ. By experiments, it is found that the larger values of N and K are required for a higher BEP fidelity ε_b and a lower chip SNR κ. The chip duration T_c and the maximum Doppler shift f_D also have impact on the choice of N and K. For the target accuracy of 10^{-12} and NC-BFSK modulation, one exemplary choice of N and K is tabulated in table 3.2. These values were obtained by using $T_c = 1/(1.2288 \times 10^6)$ seconds and $f_D = 100$, 200, 300, 500 Hz to specify the matrix Γ_X^j and setting $\varepsilon_b = 10^{-6}$ and $\kappa = 0.01$ which are the highest BEP fidelity and lowest average SNR per chip considered in this chapter. For MQAM, only $f_D = 100$ Hz is considered and $\kappa = 0.1$ is used to evaluate N, K. One choice of N and K for MQAM is shown in table 3.3. From table 3.2 and 3.3, there is no significant difference in the value choices of N and K for those situations. To simplify the programs, we simply choose the largest values $N = 10$ and $K = 52$ in both tables for the numerical analysis, which produces the results in section 3.3.

When $\bar{P}_j$ is known, P_j is determined. Then the average symbol length $\bar{L}_S$ and the throughput $\bar{r}_S$ of SBS adaptation can be computed with Equation (3.6) and (3.7).

3.3 Numerical results

The numerical methods described in previous section are applied to obtain the throughput of SBS (3.7) and FBF (3.11) duration adaptation and the throughput gain (3.12). The channel is assumed to be the Clarke's two-dimensional isotropic scattering model; the autocorrelation of channel complex gain has the form of Equation (3.13). In the numerical analysis, the

Table 3.2: the values of N and K for NC-BFSK

j	L	N	$K/f_d = 100$	$K/f_d = 200$	$K/f_d = 300$	$K/f_d = 500$
1	2	10	52	52	52	52
2	4	10	52	52	52	52
3	8	10	52	52	52	52
4	16	10	52	52	52	52
5	32	10	52	52	52	52
6	64	10	50	52	52	52
7	128	10	50	50	50	52
8	256	10	50	50	50	52
9	512	10	48	48	48	46
10	1024	10	46	42	44	44
11	2048	10	42	42	38	30
12	4096	10	40	26	24	22

Table 3.3: the values of N and K for MQAM

j	L	N	K/4QAM	K/16QAM	K/64QAM
1	2	10	52	52	52
2	4	10	52	52	52
3	8	10	50	52	52
4	16	10	50	52	52
5	32	10	48	50	52
6	64	10	48	50	52
7	128	10	46	50	50
8	256	10	46	48	50
9	512	10	44	48	50
10	1024	10	38	44	48
11	2048	10	36	40	42
12	4096	10	32	38	42

maximum Doppler shift is set to be 100Hz, and the CDMA chip rate is chosen to be 1.2288×10^6 chips per second(the chip duration T_c is the reciprocal of 1.2288×10^6 second). The throughput gain for the systems equipped with NC-BFSK and MQAM modulation are investigated.

NC-BFSK modulation has the BEP function of (3.19). We consider that the duration adaptation is performed within an OVSF code set with 12 code sequences ($N = 12$).

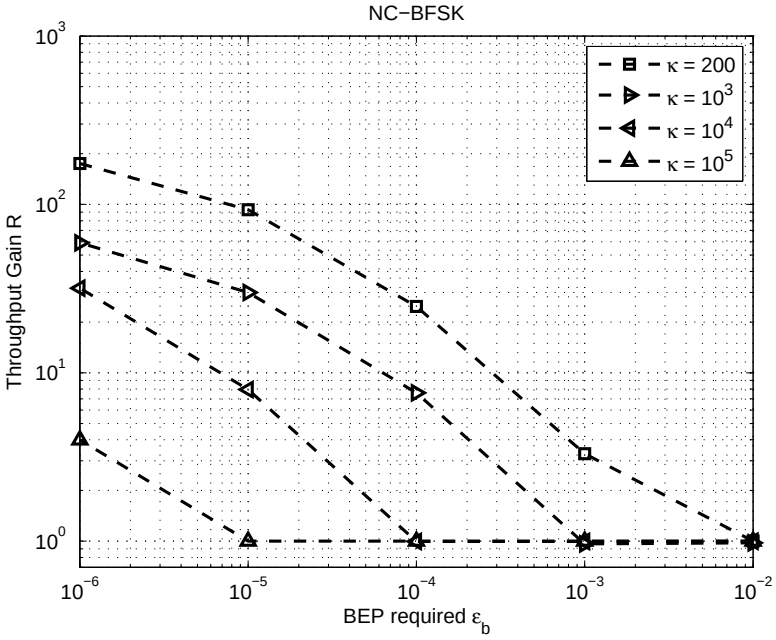

Figure 3.1: The throughput gain achieved by SBS duration adaptation with 12-code duration set ($N = 12$) for NC-BFSK modulation. The throughput gain curves for different values of κ are plotted for comparison.

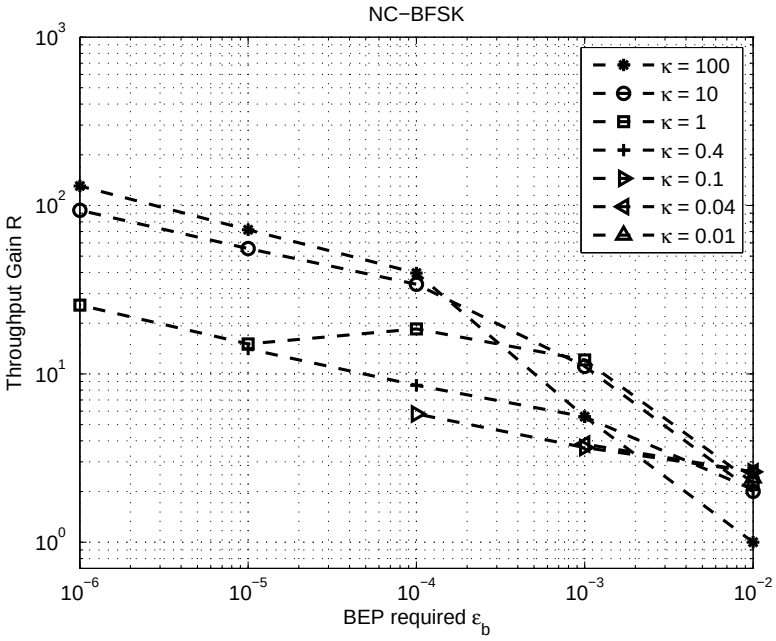

Figure 3.2: The throughput gain achieved by SBS duration adaptation with 12-code duration set ($N = 12$) for NC-BFSK modulation. The throughput gain curves for different values of κ are plotted for comparison.

The code sequences have 2 chips to 2^{12} chips in length. Then the duration set is $\Lambda = \{2, 4, \ldots, 2^{12}\}$. The throughput gain is analyzed for different bit error constraints ε_b (10^{-2} to 10^{-6}). The numerical results of throughput gain are shown in Figure 3.1 and 3.2. In both figures, we observe that the throughput gain increases as the BEP fidelity becomes higher. However, it does not increase linearly in log-log scale. The curves are more or less concave. In other words, in low fidelity region, the gains increase faster than in high fidelity region. This is a different phenomenon from what we have seen in Chapter 1 and 2 where the channel was assumed to remain constant during each symbol and the throughput gain increases almost linearly in log-log scale as BEP constraint becomes smaller. Figure 3.1 and 3.2 also show the impact of the average SNR per chip, $\kappa = P_T T_c E(|\tilde{g}_i|^2)/N_0$, on the throughput gain. Figure 3.1 shows that for $\kappa = 200, 1000, 10^4$ and 10^5, the throughput gain decreases as κ increases. As κ increases, the throughput gain curves collapse to the horizontal axis of $\mathcal{R} = 1$ from $\varepsilon_b = 10^{-2}$ to some higher BEP fidelities. It is a phenomenon similar to the one shown in Figure 2.3. The average chip SNR κ reflects the average receive power. As the average receive power increases, the throughput of both FBF and SBS adaptation increases. Within the finite discrete duration set Λ, the maximum throughput can be achieved is $1/(L_1 T_c)$ and the symbol length has a lower limit L_1. As κ increases, the throughput of SBS approaches $1/(L_1 T_c)$ but cannot exceed that. Meanwhile, the throughput of FBF adaptation also increases as κ increases. That is the reason why the throughput gain decreases as κ increases. When the average receive power is sufficiently high, FBF adaptation can also choose L_1, the shortest symbol length, to satisfy the BEP requirement. In this case, both L_F and $\bar{L}_S$ are L_1, and the throughput gain collapses to 1. Figure 3.2 shows the throughput gain for some small κ values. Some phenomena different from Figure 3.1 can be observed. First, some throughput gain curves only appear over a part of the horizontal axis. It is because, when the average receive power is too low, FBF adaptation cannot achieve some high BEP fidelities even with the longest symbol length L_N among Λ. In these cases, the solution of the FBF symbol length (3.9) does not exist. Second, the throughput gain decreases as κ decreases in the high BEP fidelity region. However, in the low fidelity region, the throughput gain does not simply decrease or increase with κ. There are some crossovers between the curves. Third, for small κ values like 1, 0.4, 0.1, 0.04 and 0.01, the curves are not as steep as those of large κ values. In other words, the throughput gain increases slower as the required BEP decreases than in the case of higher κ values shown in Figure 3.1. One interesting fact is that, on the curve of $\kappa = 1$, the gain for

$\varepsilon_b = 10^{-5}$ is less than that for $\varepsilon_b = 10^{-4}$. The gain decreases as the BEP fidelity increases from 10^{-4} to 10^{-5}. This exception is caused by the discretization of the symbol duration. The symbol length chosen by FBF adaptation, L_F, for both $\varepsilon_b = 10^{-4}$ and $\varepsilon_b = 10^{-5}$ are 2^{11} (2048). The average symbol length for SBS adaptation, $\bar{L}_S$, for $\varepsilon_b = 10^{-5}$ is surely larger than that for $\varepsilon_b = 10^{-4}$. Thus the throughput gain, the ratio of L_F to $\bar{L}_S$, decreases as ε_b goes from 10^{-4} to 10^{-5}.

Figure 3.3 compares the throughput gains for NC-BFSK modulation among three duration sets of different sizes. We considered three OVSF code sets which have 8, 10 and 12 code sequences. The code lengths are from 2 to 2^8 ($N = 8$), 2 to 2^{10} ($N = 10$)and 2 to 2^{12} ($N = 12$), respectively. In the numerical analysis, the average SNR per chip κ is set to be 200. In the figure, it can be observed that the throughput gain curves for $N = 12$, 10 and 8 well overlap except the curve for $N = 8$ does not appear over the region of $\varepsilon = 10^{-5}$ to 10^{-6}. Within the duration set of $N = 8$, FBF adaptation cannot satisfy BEP requirement $\varepsilon_b = 10^{-6}$ even with the longest symbol length 2^8 of the set. Thus the solution of FBF symbol length decision (Equation (3.9)) do not exist for $\varepsilon_b = 10^{-6}$. Except that, the throughput gain for the three different duration set are almost the same. Within different duration sets, for a given ε_b, the symbol durations chosen by FBF adaptation, L_F, are the same. The throughput gain difference comes from the difference of $\bar{L}_S$, the average symbol durations achieved by SBS adaptation. The numberical results show that, with κ of 200, the probability $\Pr(L_j)$ decreases as j increases. The Probabilities $\Pr(L_9)$, $\Pr(L_{10})$, $\Pr(L_{11})$ and $\Pr(L_{12})$ are close to zero, and the resultant values of $\bar{L}_S$ are very close with one another for $N = 8,$, 10 and 12. The throughput gain are hence almost the same.

In the throughput gain analysis of MQAM modulation, we also consider the 12-code OVSF code set ($N = 12$) and numerically obtain the throughput gains for different κ values. The throughput gains for 4QAM, 16QAM and 64QAM associated with different values of κ are plotted in Figure 3.4, 3.5 and 3.6. In general, the throughput gain increases as the BEP fidelity increases. However, there are some exceptions, e.g., the point of $\varepsilon_b = 10^{-5}$ and $\kappa = 10$ on the 16QAM plot where the throughput gain is less than that for $\varepsilon_b = 10^{-4}$. The reason is the same as that for the case of NC-BFSK. The throughput gain does not monotonically decrease or increase as κ. For large κ values, the gain decreases as κ increases, and the curve gradually collapses to one; for small κ values, the gain increases as κ increases in the high BEP fidelity region. The curves for large κ values are steeper than those for small κ values. There are crossovers between some curves, e.g., the curves of $\kappa = 10$ and

$\kappa = 100$ have a crossover at $\varepsilon_b \approx 10^{-4}$ in Figure 3.4.

Figure 3.7 to 3.10 illustrate the throughput gain comparison between the three constellation sizes of MQAM. Each figure plots the throughput gains for 4QAM, 16QAM and 64QAM for the same κ value. We observe crossovers between the curves. There is no clear relation between the constellation size and the throughput gain for $\kappa = 1,\ 10,\ 100$. However, for $\kappa = 1000$, the gain increases as the constellation size becomes larger.

All the results above are obtained with the maximum Doppler shift $f_D = 100$Hz. The impact of the value of f_D on the throughput gain is also investigated. If the carrier frequency is 1.8G Hz, when a mobile is moving with a speed of $60km/h$, $120km/h$, $180km/h$ or $300km/h$ towards or away from the base station, the maximum Doppler shift f_D is 100Hz, 200Hz, 300Hz and 500Hz, respectively. Figure 3.11 plots the throughput gains for NC-BFSK with these values of f_D. The 12-code OVSF code set is considered ($N = 12$) and κ is set to be 200 for these results. In general, the throughput gains decrease as f_D increases. However, the curves of $f_D = 200$ and $f_D = 300$ overlap. Figure 3.12 plots the channel gain autocorrelation of Equation (3.13) versus the chip index difference $j - i$. Within the discrete duration set of $\Lambda = \{2, 4, \ldots, 2^{12}\}$, the index difference is from 0 to 4096. The curve of $f_D = 100$ is monotonically decreasing over this index range, while the other curves experience one or more fluctuations.

3.4 Chapter conclusion

In this chapter, a more realistic channel model is considered in the throughput gain analysis. The channel is assumed to vary from chip to chip and remain constant during each chip duration. The rate adaptation is performed by choosing the spreading code from an OVSF code set, so the symbol durations form a discrete duration set. The moment generation function based approach is applied to numerically analyze the throughput of symbol-by-symbol and frame-by-frame duration adaptation within the discrete duration set. The numerical results show that, within a fairly small duration set (e.g., $N = 12$), the throughput gain is still promising (from tens to more than one hundred) for NC-BFSK and MQAM.

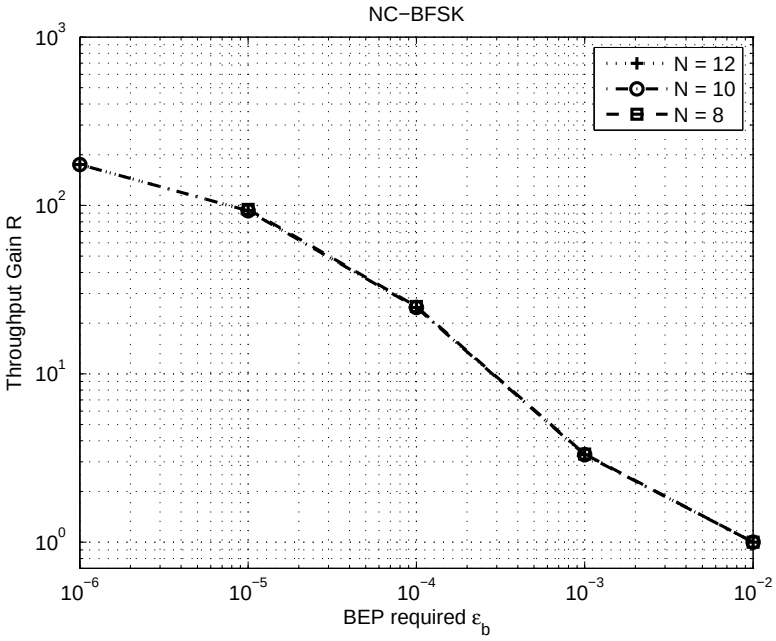

Figure 3.3: The throughput gain of NC-BFSK within three different size duration sets. The value of κ is 200 for all the results.

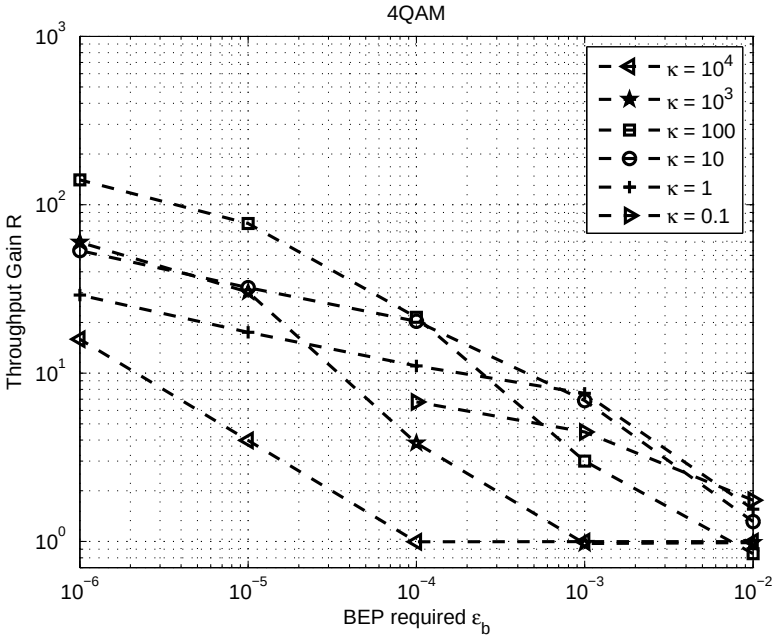

Figure 3.4: The throughput gain of 4QAM for different values of κ.

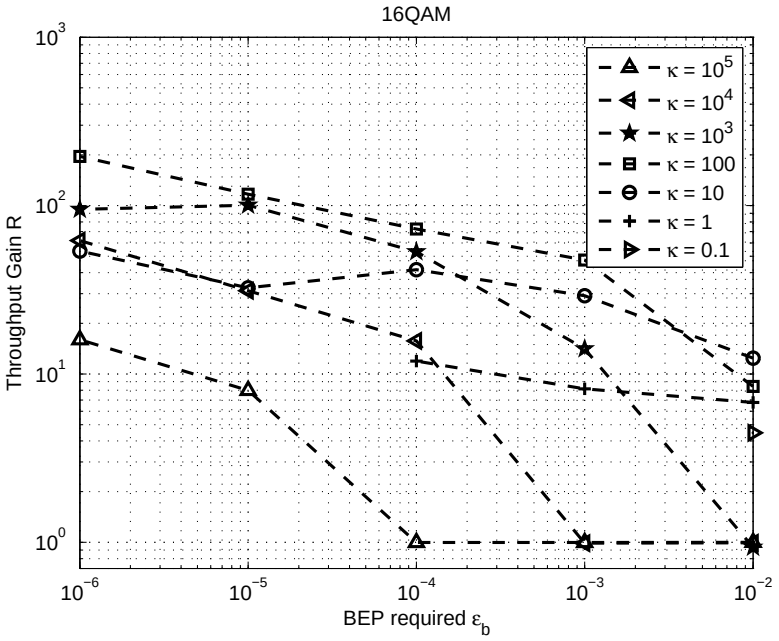

Figure 3.5: The throughput gain of 16QAM for different values of κ.

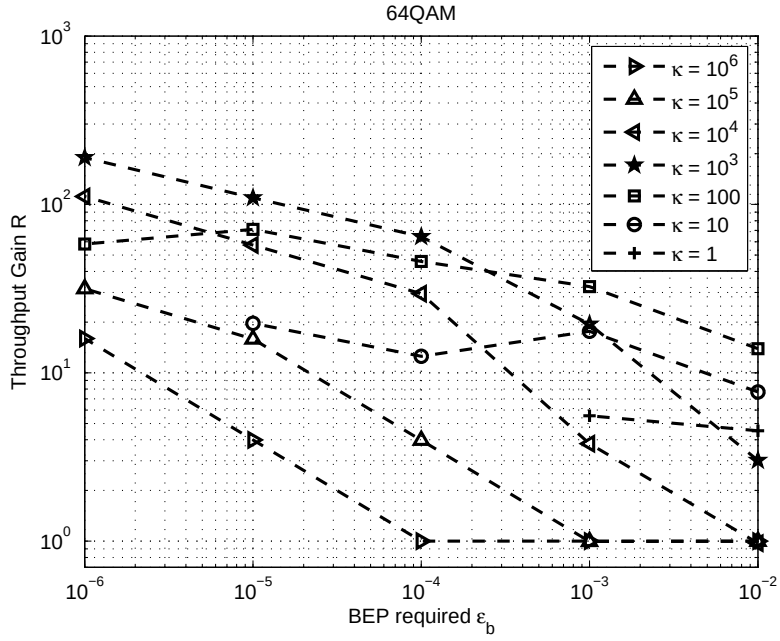

Figure 3.6: The throughput gain of 64QAM for different values of κ.

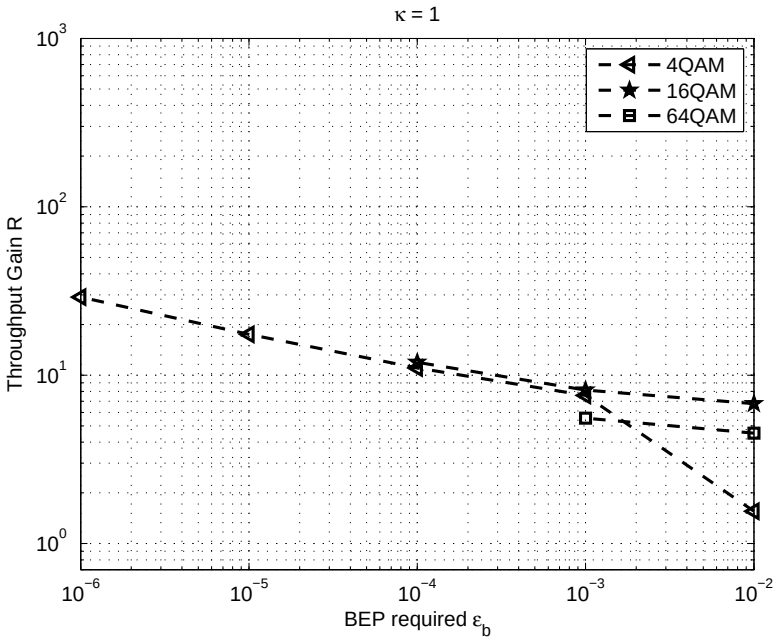

Figure 3.7: The throughput gain of 4QAM, 16QAM and 64QAM. $\kappa = 1$

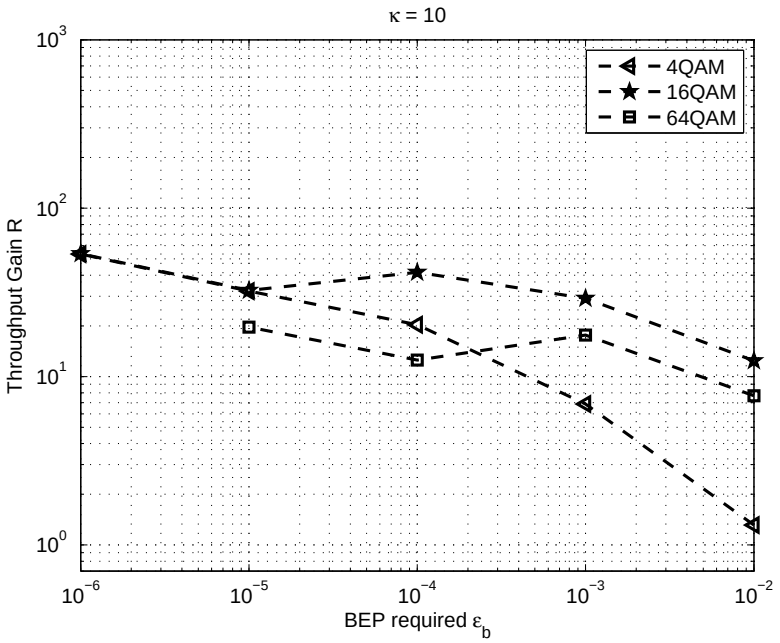

Figure 3.8: The throughput gain of 4QAM, 16QAM and 64QAM. $\kappa = 10$

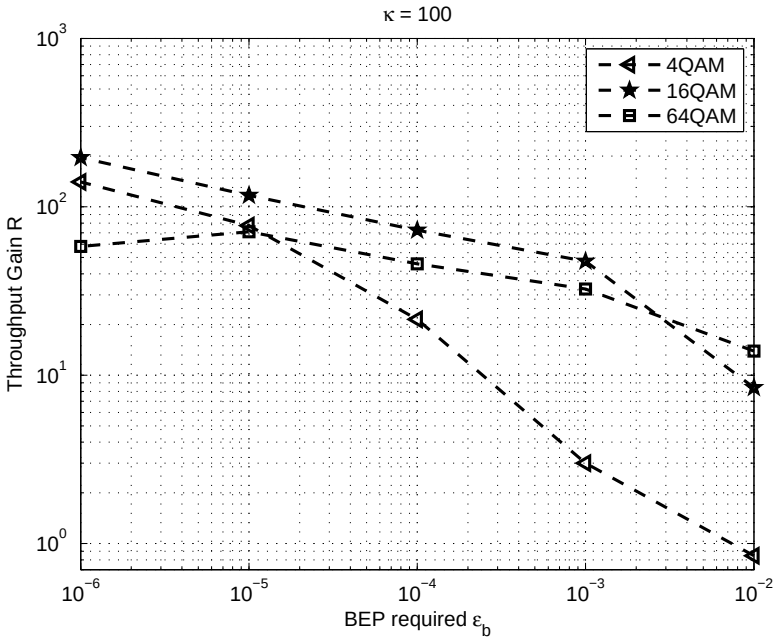

Figure 3.9: The throughput gain of 4QAM, 16QAM and 64QAM. $\kappa = 100$

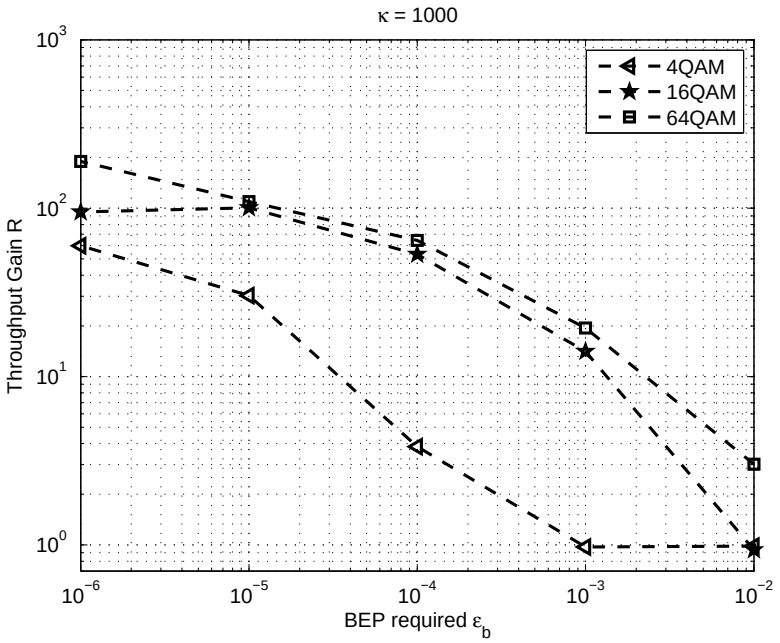

Figure 3.10: The throughput gain of 4QAM, 16QAM and 64QAM. $\kappa = 1000$

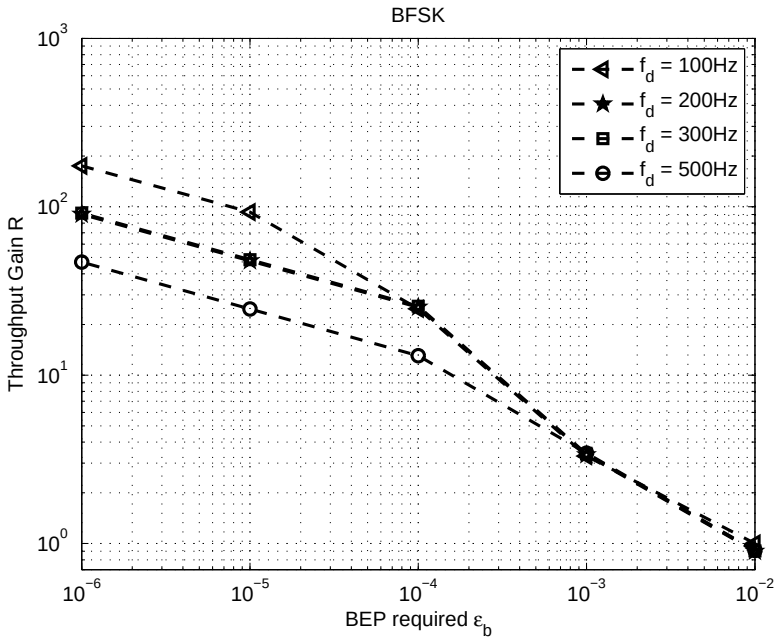

Figure 3.11: The throughput gain for NC-BFSK with different values of maximum Doppler shift f_D.

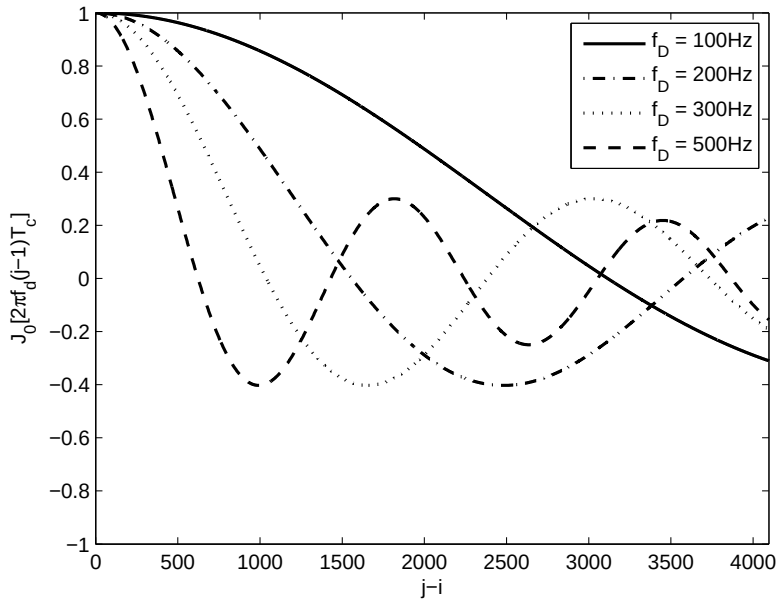

Figure 3.12: The channel gain correlation for different values of maximum Doppler shift f_D.

Chapter 4

Throughput Gain Achieved In Coded Systems

In modern communication systems, forward error control (FEC) coding is extensively implemented to improve the quality of service. Thereby the performance of SBS duration adaptation in coded systems is of interest. In this chapter, the throughput gain achieved in coded systems is investigated. The analysis and numerical results were first presented in [39].

4.1 System model

4.1.1 Capacity analysis

This section analyzes the fundamental aspects of the throughput gain from rapid symbol duration adaptation in coded systems. The rapid duration adaptation can be implemented in a direct sequence spread spectrum (DSSS) system [1] [27], so the analysis will focus on the channel capacity of a DSSS system. Consider a system with chip rate B in which each transmitter's signal is separated by its own pseudo noise (PN) sequence and every transmitter is transmitting with a constant power. An individual transmitter-receiver pair practices symbol duration (spreading factor) adaptation without power adaptation. For this transmitter-receiver pair, the communication system can be represented by a discrete-time model:

$$y[i] = \sqrt{\alpha[i]}x[i] + n[i] \tag{4.1}$$

where $y[i]$ is the i^{th} sample (chip) of the received signal; $\alpha[i]$ is the channel power gain at time i; $n[i]$ is an i.i.d. sequence representing both noise and interference from other users; sequence $x[i]$ represents chips of symbols from coded message. The time-varying fading channel gain is assumed to be a stationary and ergodic random process. It is hypothetically assumed that the transmitter and receiver have perfect channel side information (CSI) $\sqrt{\alpha[i]}$. In accordance with [5] [6], the channel capacity of this communication system is

$$C_1 = BE\left[\log\left(1+\frac{P^T\alpha}{N_0B}\right)\right] = B\int_0^\infty \log\left(1+\frac{P^T\alpha}{N_0B}\right) f_\alpha(\alpha)dg \tag{4.2}$$

where α is the channel power gain; $f_\alpha(\alpha)$ is the probability distribution of the channel power gain; N_0 is the noise density associated with $n[i]$. Note that this system does not have transmission power adaptation.

The capacity of (4.2) gives the ultimate data rate limit for the error probability arbitrarily close to zero. If an error probability ε_b can be tolerated, by Shannon's rate distortion theory , a larger rate limit is achievable

$$r \le \frac{C_1}{1-\mathcal{H}(\varepsilon_b)}, \quad \text{for } \varepsilon_b < \frac{1}{2} \tag{4.3}$$

where

$$\mathcal{H}(\varepsilon_b) \equiv -\varepsilon_b \log_2\varepsilon_b - (1-\varepsilon_b)\log_2(1-\varepsilon_b)$$

is the binary entropy function [40].

A rapid symbol duration adaptation realized by adapting the spreading factor can be viewed as an adaptive coding scheme. For example, a longer symbol duration symbol means more redundancy or having a time-repetition coding with more repetitions. Therefore, the composite system of an error correction code over the spreading gain adaptation can be viewed as an adaptive coding scheme, and this composite system cannot yield an asymptotic error-constrained throughput higher than the capacity achieved by the Gaussian codebook. If the capacity-achieving Gaussian codebook can be implemented, adapting symbol duration in addition to an error correction code does not have any merit in terms of improving error-constrained throughput. However, capacity-achieving code is difficult to implement. In fact, many commonly used codes perform far from the channel capacity. The gap provides the potential for rapid symbol duration adaptation to increase the throughput. In this chapter, the throughput gain for different coding schemes are investigated.

4.1.2 Throughput gain in coded systems

Channel coding adds redundancy to the information sequences in a controlled manner to combat the distortion caused by the channel which the signals carrying the information sequences travel through. In order to show the throughput gain achieved by rapid duration adaptation in a coded system, the error constrained throughput of FBF and SBS adaptation will be analyzed in this section.

In the analysis of [27] and previous chapters, it has been assumed that, for the fast time-varying channel (i.e., the frame duration is relatively long compared to $1/(2f_d)$.), the frame-by-frame (FBF) duration adaptation is equivalent to non-adaptation. To analyze the throughput gain for coded systems, the throughput achieved by SBS duration adaptation is also compared with the throughput achieved by FBF adaptation, which is basically the throughput of non-adaptation when the channel is fast time-varying.

For a non-adaptive system, denote by r the transmission rate of the symbols and thus the duration of the transmitted symbols is $1/r$. Also, denote the receive power as a random variable Y. The receive power is assumed to be constant during each symbol time through this chapter. Then the received signal to noise ratio (SNR) per symbol can be written as a random variable $Y/(rN_0)$, where N_0 is the additive white noise power density. The realizations of the variable $Y/(rN_o)$ for different symbols $Y_1/(rN_o)$, $Y_2/(rN_o)$, ..., $Y_i/(rN_o)$, ... can be viewed as a random process. Given a coding scheme c, the bit error probability of the information bits can be written as a function of the expected signal-to-noise-ratio per symbol $\gamma = E(Y)/(rN_o)$. Let us denote this function by $\tilde{H}_c(\gamma)$. This function takes into account the coding/decoding and modulation/demodulations schemes and the statistics of the random process formed by the realizations of random variable $Y/(rN_0)$. Note that $\tilde{H}_c(\gamma)$ depends on the statistics (e.g., correlation) of random process $Y_1/(rN_o)$, $Y_2/(rN_o)$, ..., $Y_i/(rN_o)$, ... because of the error correction code across time. In short, the BEP of the coded system without duration adaptation is written as $\tilde{H}_c(E(Y)/(rN_0))$. Therefore, the maximal symbol rate for non-adaptive system can be written as

$$r = \frac{E(Y)}{\tilde{H}_c^{-1}(\varepsilon_b) N_0} \tag{4.4}$$

where $\tilde{H}_c^{-1}(x)$ is the inverse function of $\tilde{H}_c(\gamma)$.

The BEP of a coded system with rapid symbol duration adaptation will depend on the error correction coding-decoding scheme, the modulation-demodulation scenario, the

symbol duration adaptation policy, and the statistical nature of the received signal power. Let us denote by $\tilde{h}_c\left(\{r\left(y\right)|y\}\right)$ the average BEP of the duration-adaptive coded system for a particular coding-decoding scheme c, duration adaptation policy $\{r\left(y\right)|y\}$ where y is the receive power, and the statistics of the random process representing the received power y. Then, in a particular coded system the maximum-throughput policy is derived through the following maximization:

$$\begin{array}{l} \max_{r(y)} \int r\left(y\right) f_Y\left(y\right) dy \\ \text{subject to } \tilde{h}_c(\{r(y)|y\}) \leq \varepsilon_b \end{array} \tag{4.5}$$

where $f_Y\left(y\right)$ is the probability density function of the receive power Y. It is assumed that the received power at different times is modeled as a stationary ergodic process. Because the expression $\tilde{h}_c(\{r(y)|y\})$ is not available, the above optimization of the duration adaptation policy is difficult. Instead, a suboptimal duration adaptation policy is considered. Let $h_c(\chi)$ be the BEP of a coded system with particular code c as a function of constant received signal-to-noise ratio per symbol χ. Consider a suboptimal duration adaptation policy $\{r_c^*\left(y\right) = q_c^* y\}$, where q_c^* is a constant that satisfies $h_c\left(1/N_0 q_c^*\right) = \varepsilon_b$, or equivalently,

$$q_c^* = \frac{1}{N_0 h_c^{-1}\left(\varepsilon_b\right)} \tag{4.6}$$

This policy keeps the received signal to noise ratio per symbol $Y/(N_0 r(Y)) = Y/(N_0 q_c^* Y) = 1/(N_0 q_c^*)$ constant, and the resulting BEP of the system is given by

$$h_c\left(\frac{1}{N_0 q_c^*}\right) = \varepsilon_b \tag{4.7}$$

The symbol throughput of this SBS duration-adaptive coded system is given by

$$\begin{array}{l} \bar{r}_s = \int r\left(y\right) f_Y\left(y\right) dy \\ = \int q_c^* y f_Y\left(y\right) dy \\ = q_c^* E\left(Y\right) \\ = \frac{E(Y)}{N_0 h_c^{-1}(\varepsilon_b)} \end{array} \tag{4.8}$$

Therefore, from (4.4) and (4.8) the throughput gain is

$$\mathcal{R} = \frac{\bar{r}_s}{r} = \frac{E\left[Y\right]}{N_0 h_c^{-1}(\varepsilon_b)} \Big/ \frac{E(Y)}{N_0 \tilde{H}_c^{-1}(\varepsilon_b)} = \frac{\tilde{H}_c^{-1}(\varepsilon_b)}{h_c^{-1}(\varepsilon_b)} \tag{4.9}$$

Because the adaptation policy considered here is suboptimal, Equation (4.9) serves as a lower bound of throughput gain for the rapid symbol duration adaptation.

4.1.3 Simulation systems

In this subsection, the numerical values of throughput gain (4.9) are examined. To obtain the throughput gain (4.9) achieved by rapid duration adaptation, the two curves $\tilde{H}_c(x)$ vs. x and $h_c(x)$ vs. x are constructed through random simulations and the throughput gain is then computed. Function $h_c(x)$ evaluates the BEP for constant receive SNR x for the coded system. To obtain the $h_c(x)$ curve, the simulation system illustrated in Figure 4.1 is used in simulation. The data sequence is generated by the Bernoulli binary sequence generator, and is passed to the channel encoder. The coded sequence is then modulated, and the output signal is sent to the receiver. The additive white Gaussian noise is added to the signal. The received signal is demodulated and then decoded to reconstruct the data sequence. The error rate calculation block compares the reconstructed data sequence to the original data sequence to compute the bit error probability (BEP). With a specified noise power density N_0, the receive SNR is constant. By running simulation with different values of noise power density, we obtain the curve of $h_c(x)$.

To obtain the $\tilde{H}_c(x)$ curve, the simulation system shown in Figure 4.2 is employed. In addition to all the components in Figure 4.1, the system in Figure 4.2 also includes a Rayleigh fading channel and a matched filter. With the receiver's knowledge of channel state information (CSI), i.e., the fading channel gain here, the matched filter is able to correct the phase distortion and maximize the output SNR. With constant transmit power, the receive SNR has the same statistics as the channel power gain. The channel realizations provide the realizations of the randomly varying SNR $Y/(rN_0)$. The bit error probability is obtained by averaging over a sufficient number of channel realizations.

The simulation systems shown in Figure 4.1 and 4.2 were simulated in Simulink™ [1]. Simulink™ provides many common communication components such as encoder/decoder, modulator/demodulator and fading channels, so a variety of coding and modulation combinations can be easily experimented. All numerical results presented in this section are obtained by simulating the systems in Simulink™.

The exemplary curves of $\tilde{H}_c(x)$ and $h_c(x)$ are shown in Figure 4.3. The coding scheme of the system for Figure 4.3 is a 1/2 code rate convolutional code of constraint length 9 and hard-decision Viterbi decoding. The modulation scheme is QPSK. For a specified value of ε_b, e.g., 10^{-4}, $\tilde{H}_c^{-1}(\varepsilon_b)$ and $h_c^{-1}(\varepsilon_b)$ are read from the curves by interpolation. Then the

[1] Simulink™ is the trade mark of The MathWorks, Inc

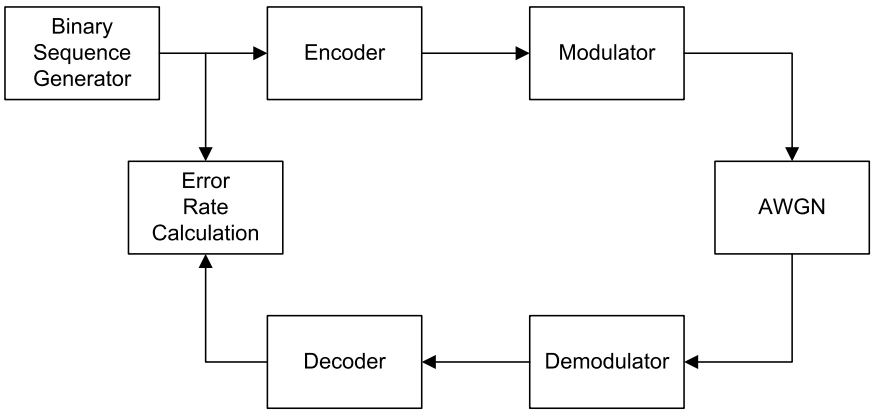

Figure 4.1: System diagram of the simulation to obtain the curve of $h_c(x)$, the BEP for constant receive SNR x over non-fading channel, for combinations of coding and modulation schemes.

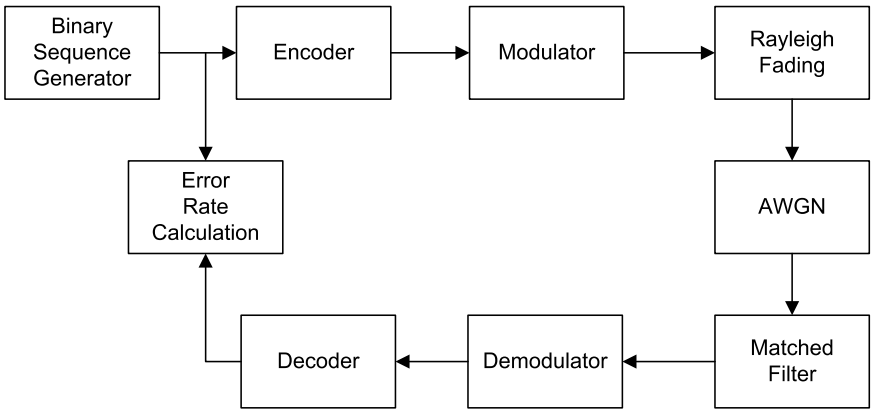

Figure 4.2: System diagram of the simulation to obtain the curve of $\tilde{H}_c(x)$, the BEP for expected receive SNR x over Rayleigh fading channel, for combinations of coding and modulation schemes.

throughput gain is computed according to (4.9).

4.1.4 Sample size and confidence interval

In order to obtain reliable curves of BEP functions $\tilde{H}_c(x)$ and $h_c(x)$, a sufficient number of samples have to be experimented. For each BEP fidelity ε_b, how many information bits should be sent through the system in simulation needs to be decided in designing the simulation experiment. The idea of a confidence interval for a population proportion [41] is exercised to determine the sample size of the simulation.

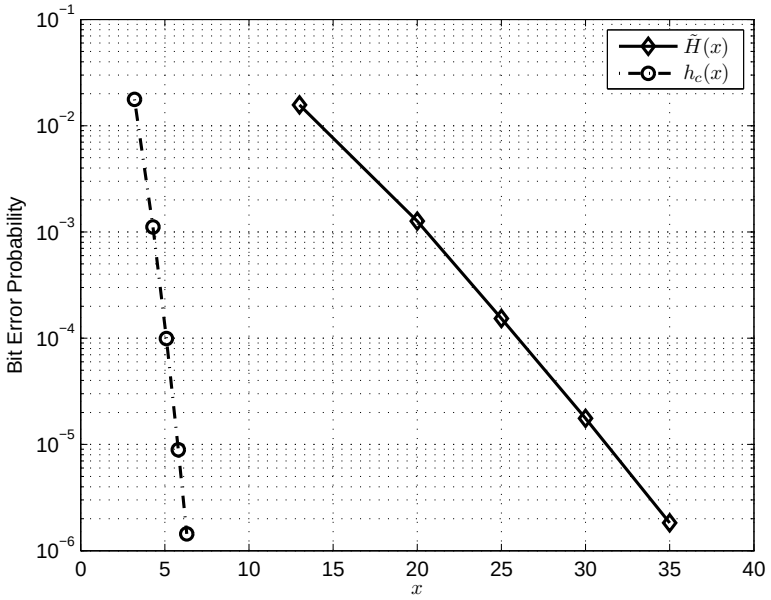

Figure 4.3: BEP curve $\tilde{H}_c(x)$ and $h_c(x)$. The coding scheme of the system is a 1/2 code rate convolutional code of constraint length 9 and hard-decision Viterbi decoding. The modulation scheme is QPSK.

Let p_b denote the bit error probability of a communication system. To estimate p_b by simulation, randomly generated n information bits are sent through the system. Let us denote by X the number of bits in error at output of the system. The nature estimator of p_b is $\hat{p}_b = X/n$, the sample fraction of errors. When n is large (e.g., $np_b \geq 10$ and $n(1-p_b) \geq 10$), $\hat{p}_b$ has approximately a Gaussian distribution with mean $E(\hat{p}_b) = p_b$ and variance $\sigma^2_{\hat{p}_b} = p_b(1-p_b)/n$. $\hat{p}_b$ is an unbiased estimator of p_b and $(\hat{p}_b - p_b)/\sigma_{\hat{p}_b}$ has approximately a standard Gaussian distribution. For a confidence level of $100(1-\alpha)\%$ (e.g., $\alpha = 5$), we denote by $z_{\alpha/2}$ the critical value which provides the tail probability of a standard Gaussian variable Z is equal to $\alpha/2$, i.e., $\Pr(Z > z_{\alpha/2}) = \alpha/2$. Then we have

$$\Pr\left\{-z_{\alpha/2} < \frac{\hat{p}_b - p_b}{\hat{\sigma}_{\hat{p}_b}} < z_{\alpha/2}\right\} \approx 1 - \alpha \tag{4.10}$$

i.e.,

$$\Pr\left\{-z_{\alpha/2} < \frac{\hat{p}_b - p_b}{\sqrt{p_b(1-p_b)/n}} < z_{\alpha/2}\right\} \approx 1 - \alpha \tag{4.11}$$

Then by solving (4.11) as a quadratic inequality for p_b, we have the confidence interval for

p_b with confidence level approximately $100(1-\alpha)\%$

$$\left(\frac{\hat{p}_b + \frac{z^2_{\alpha/2}}{2n} - z_{\alpha/2}\sqrt{\frac{\hat{p}_b(1-\hat{p}_b)}{n} + \frac{z^2_{\alpha/2}}{4n^2}}}{1+\frac{z^2_{\alpha/2}}{n}}, \frac{\hat{p}_b + \frac{z^2_{\alpha/2}}{2n} + z_{\alpha/2}\sqrt{\frac{\hat{p}_b(1-\hat{p}_b)}{n} + \frac{z^2_{\alpha/2}}{4n^2}}}{1+\frac{z^2_{\alpha/2}}{n}} \right) \tag{4.12}$$

The width of the interval is given by [2]

$$w = \frac{2z_{\alpha/2}\sqrt{\frac{\hat{p}_b(1-\hat{p}_b)}{n} + \frac{z^2_{\alpha/2}}{4n^2}}}{1+\frac{z^2_{\alpha/2}}{n}} \tag{4.13}$$

The width of the interval w shows the estimation precision of p_b, and the confidence level $100(1-\alpha)\%$ indicates how surely the true value of p_b lies within the interval. Given a width of the interval w and the confidence level $100(1-\alpha)\%$, the sample size can be determined from (4.13) [3]

$$n = \frac{2z^2_{\alpha/2}\hat{p}_b\left(1-\hat{p}_b\right) - z^2_{\alpha/2}w^2 + z^2_{\alpha/2}\sqrt{4\hat{p}_b^2(1-\hat{p}_b)^2 - 4w^2\hat{p}_b\left(1-\hat{p}_b\right) + w^2}}{w^2} \tag{4.14}$$

In our simulations, the target confidence level is set to $100(1-\alpha)\% = 99\%$ and the confidence interval width is chosen to be $w = 0.1\hat{p}_b$. The critical value $z_{\alpha/2}$ is equal to 2.575 for 99% confidence level. For the bit error probabilities requirement ε_b of 10^{-2} to 10^{-6}, the sample sizes are determined and tabulated in Table 4.1.

We note that the bit errors caused by deep fades of a fading channel in a coded system are bursty and not statistically independent. This will challenge the validity of the preceding

[2] If the sample size is quite large, the term $z^2/(2n)$, $z^2/(4n^2)$ in Equations (4.12) and (4.13) are negligible. Then, the confidence interval in (4.12) can be approximated as

$$\left(\hat{p}_b - z_{\alpha/2}\sqrt{\frac{\hat{p}_b(1-\hat{p}_b)}{n}},\ \hat{p}_b + z_{\alpha/2}\sqrt{\frac{\hat{p}_b(1-\hat{p}_b)}{n}} \right)$$

The width of the confidence interval is approximately

$$2z_{\alpha/2}\sqrt{\frac{\hat{p}_b(1-\hat{p}_b)}{n}}$$

[3] By neglecting the terms involving w^2 in the numerator, Equation (4.14) can be approximated as

$$n \approx \frac{4z^2_{\alpha/2}\hat{p}_b(1-\hat{p}_b)}{w^2}$$

Table 4.1: The simulation sample size to obtain bit error probability curves for coded systems. The confidence level is set to 99% and the width of the confidence interval is set to be $0.1\varepsilon_b$.

ε_b	sample size
10^{-2}	2.652×10^5
10^{-3}	2.652×10^6
10^{-4}	2.652×10^7
10^{-5}	2.652×10^8
10^{-6}	2.652×10^9

confidence interval analysis. Nevertheless, the channel we consider is fast time-varying with large maximum Doppler shift f_d. The associated level crossing rate is high (which is proportional to f_d), and the average fade duration is small (which is proportional to $1/f_d$). In other words, the deep fades of the channel appear frequently and the average duration of deep fades is short. In this case, the sample sizes derived from the preceding analysis still provides good guidelines for our simulation.

4.2 Numerical results

4.2.1 Convolutional codes

Convolutional codes are widely used in current communication systems. For example, in CDMA2000 standard, convoluatioal codes of constraint length 9 with different code rates are used in both downlink and uplink channels. Hence, the throughput gains for convolutional coded system are specially of interest.

In decoding of a convolutional code for a memoryless channel, Hamming distance or Euclidean distance is computed, resulting in hard-decision decoding or soft-decision decoding, respectively. The throughput gain for both soft-decision and hard-decision decoding systems are presented in this section.

Soft decision decoding

To implement soft-decision on the output of the fading channel, the branch metric with CSI needs to be derived. Let the information sequence be $\bar{b} = [b_1, b_2, \ldots, b_i, \ldots]$, and coded sequence be $\bar{c} = [c_1, c_2, \ldots, c_m, \ldots]$. The coded sequence is modulated as sequence $\bar{x} =$

$[x_1,\ x_2,\ \ldots,\ x_k,\ \ldots]$ and transmitted to the channel. The receive signal from a memoryless channel is denoted by $\bar{y} = [y_1,\ y_2,\ \ldots,\ y_k,\ \ldots]$. The maximum-likelihood (ML) sequence detection rule is to maximize the the joint probability of the receive sequence conditioned on the transmit sequence

$$\begin{aligned} &\arg\max_{b_1,b_2,\ldots} p\left(y_1,\ y_2,\ \ldots | b_1,\ b_2,\ \ldots\right) \\ &= \arg\max_{b_1,b_2,\ldots} p\left(y_1,\ y_2,\ \ldots | c_1,\ c_2,\ \ldots\right) \end{aligned} \tag{4.15}$$

Now let us consider a flat fading channel:

$$y_i = g_i x_i + n_i \tag{4.16}$$

where g_i is the complex channel gain. The channel gain g_i is assumed to be known by the receiver. Then the output of the matched filter can be written as

$$\tilde{y}_i = \frac{y_i}{g_i} = x_i + \frac{n_i}{g_i} = x_i + \tilde{n}_i \tag{4.17}$$

where $\tilde{n}_i$ is complex white Gaussian noise with variance $\sigma^2/|g_i|^2$.

If the modulation scheme is QPSK with $\pi/4$ phase shift and Gray mapping, the constellation is shown as Figure 4.4. Each modulated symbol x_i carries two coded bits $c_{i,1}c_{i,2}$. By observing the constellation plot, we note that the real part of x_i carries $c_{i,2}$ and the imaginary part of x_i carries $c_{i,1}$. The output of matched filter (4.17) can be written as

$$\begin{aligned} \tilde{y}_i^R &= x_i^R + \tilde{n}_i^R = \frac{1}{\sqrt{2}}\left(1 - 2c_{i,2}\right) + \tilde{n}_i^R \\ \tilde{y}_i^I &= x_i^I + \tilde{n}_i^I = \frac{1}{\sqrt{2}}\left(1 - 2c_{i,1}\right) + \tilde{n}_i^I \end{aligned} \tag{4.18}$$

where $\tilde{n}_i^R$ and $\tilde{n}_i^I$ are real Gaussian noise with variance $\sigma^2/(2|g_i|^2)$. The ML decoding rule then becomes

$$\begin{aligned} &\arg \max_{b_1,b_2,\ldots} p\left(y_1,\ y_2,\ \ldots | c_1,\ c_2,\ \ldots\right) \\ &= \arg \max_{b_1,\ b_2,\ \ldots} \prod_{all\ i} p\left(\tilde{y}_i | c_{i,1}, c_{i,2}\right) \\ &= \arg \max_{b_1,\ b_2,\ \ldots} \prod_{all\ i} p\left(\tilde{y}_i^R | c_{i,2}\right) p\left(\tilde{y}_i^I | c_{i,1}\right) \\ &= \arg \max_{b_1,\ b_2,\ \ldots} \sum_{all\ i} \left\{\ln p\left(\tilde{y}_i^R | c_{i,2}\right) + \ln p\left(\tilde{y}_i^I | c_{i,1}\right)\right\} \end{aligned}$$

$$
\begin{aligned}
&= \arg \max_{b_1,\, b_2,\, \ldots} \sum_{all\ i} \ln \left\{ \frac{1}{\sqrt{\pi}\tilde{\sigma}_i} \exp \left[- \frac{\left(y_i^R - (1 - 2c_{i,2}) \right)^2}{\tilde{\sigma}_i^2} \right] \right\} \\
&\qquad + \sum_{all\ i} \ln \left\{ \frac{1}{\sqrt{\pi}\tilde{\sigma}_i} \exp \left[- \frac{\left(y_i^I - (1 - 2c_{i,1}) \right)^2}{\tilde{\sigma}_i^2} \right] \right\} \\
&= \arg \max_{b_1,\, b_2,\, \ldots} \sum_{all\ i} \left\{ 2 \ln \frac{1}{\sqrt{\pi}\tilde{\sigma}_i} - \frac{1}{\tilde{\sigma}_i^2} \left[y_i^R - (1 - 2c_{i,2}) \right]^2 - \frac{1}{\tilde{\sigma}_i^2} \left[y_i^I - (1 - 2c_{i,1}) \right]^2 \right\} \\
&= \arg \min_{b_1,\, b_2,\, \ldots} \sum_{all\ i} \left\{ 2 \ln \sqrt{\pi}\tilde{\sigma}_i + \frac{1}{\tilde{\sigma}_i^2} \left[y_i^R - (1 - 2c_{i,2}) \right]^2 + \frac{1}{\tilde{\sigma}_i^2} \left[y_i^I - (1 - 2c_{i,1}) \right]^2 \right\} \qquad (4.19)
\end{aligned}
$$

The demodulator should be able to output the metric (4.20) for each received symbol y_i to the Viterbi decoder. The Viterbi decoder performs the Viterbi algorithm to find the shortest path through the trellis to decode the receive sequence.

$$
2 \ln \sqrt{\pi}\tilde{\sigma}_i + \frac{1}{\tilde{\sigma}_i^2} \left[y_i^R - (1 - 2c_{i,2}) \right]^2 + \frac{1}{\tilde{\sigma}_i^2} \left[y_i^I - (1 - 2c_{i,1}) \right]^2 \qquad (4.20)
$$

Figure 4.5 shows the throughput gain achieved due to rapid adaptation policy (4.6) in systems equipped with QPSK modulation and convolutional coding with the constraint length of 9 and soft-decision decoding. In this simulation, the maximum Doppler shift was set to be 100Hz, and the bit rate was set to 14400 bps. Three code rates 1/2, 1/3 and 1/4 were experimented. The plot shows that the throughput gain $\mathcal{R}$ is also larger for the smaller BER requirement ε_b in coded systems, and $\log\mathcal{R}$ is more or less proportional to $\log\varepsilon_b$ as in the case of the uncoded systems. In comparison with the results of the uncoded QPSK (4QAM) system shown in Figure 1.8, SBS duration adaptation policy achieves less throughput gain in the coded systems, but the gain for convolutional codes is still significant. By comparing the results of three code rates with one another, it is also observed that the throughput gains are very similar for different code rates. Note that in either the SBS adaptive system or the non-adaptive system, the bit error probabilities for different code rates are different. However, for different code rates, the differences between the SNRs achieving a given BEP constraint ε_b in the SBS adaptive system and the non-adaptive system are very close to one another. Therefore, the throughput gains are similar.

Hard decision decoding

In hard-decision decoding scheme, the demodulator makes hard-decision on the matched filter output $\tilde{y}_1$, $\tilde{y}_2$, ... and outputs an estimated sequence of the coded sequence $\hat{c}$, i.e.,

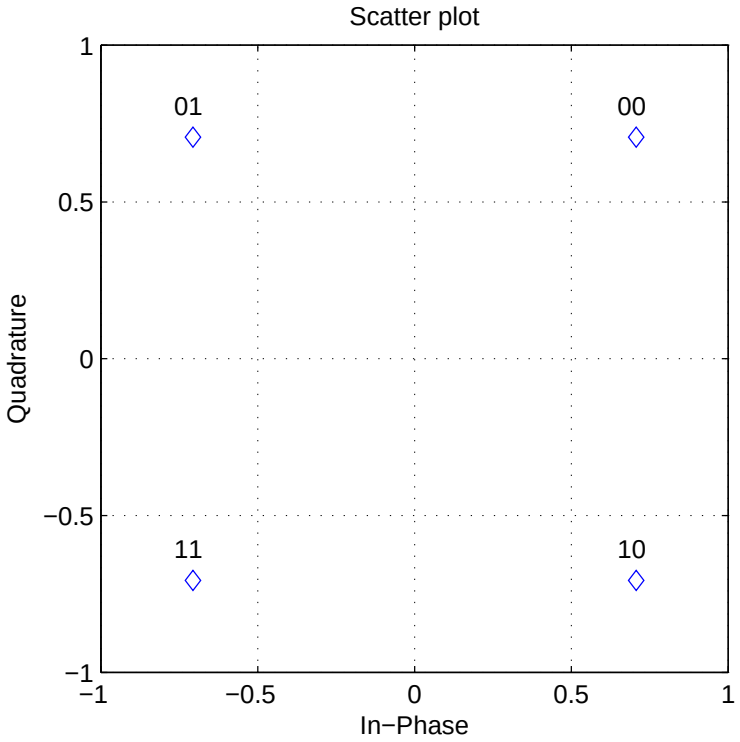

Figure 4.4: The constellation plot of QPSK with $pi/4$ phase shift and Gray mapping.

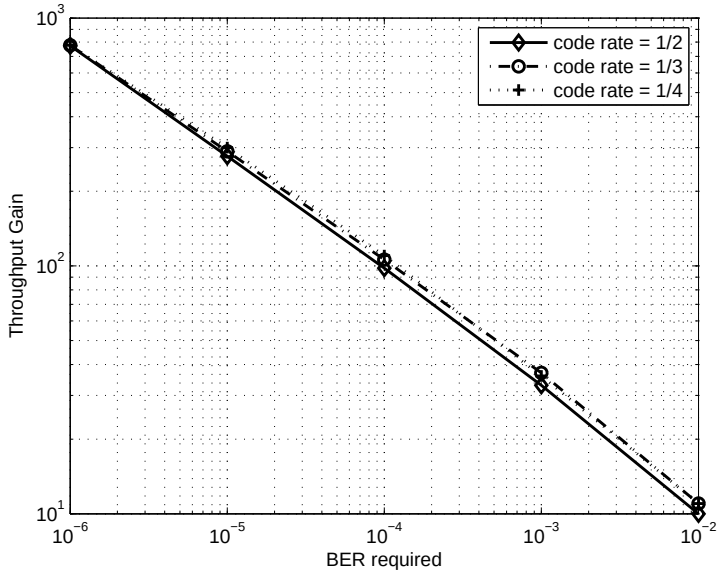

Figure 4.5: Throughput gains of QPSK and convolutional codes (constraint length = 9) without interleaver for code rates of 1/2, 1/3 and 1/4. The decoding scheme is the soft-decision Viterbi algorithm.

$\hat{c}_1$, $\hat{c}_2$, ... The estimated sequence is fed to the Viterbi decoder. The Viterbi decoder goes through the code trellis and finds the shortest path which has the minimum Hamming distance to the estimated coded sequence $\hat{c}_1$, $\hat{c}_2$, ... The information sequence associated with the shortest path is the decoding result.

Figure 4.6, 4.7 and 4.8 plot the throughput gains for convolutional coding (constraint length of 9) combined with MQAM, MPSK and non-coherent MFSK modulations. In simulation, we also set the maximum Doppler shift to be 100Hz, and the bit rate to be 14400 bps. The simulation results show that in coded systems associated with different modulation schemes, the throughput gain $\mathcal{R}$ also increases when BEP requirement ε_b becomes smaller. Compared with the results shown in Figure 1.7, 1.8 and presented in [39], the throughput gains in the coded systems are less than those in uncoded systems, but the gains are still large. We observe that the throughput gains vary slightly as the modulation constellation size changes.

Figure 4.9 shows the throughput gains of 64QAM and the convolutional code (constraint length of 9) for code rates of 1/2, 1/3 and 1/4. For different code rates, the throughput gain increases slightly as the code rate decreases. We note that as the code rate decreases, the bit error probability in both the SBS adaptive system and the non-adaptive system decreases. For different code rates, the difference between the SNRs achieving a given BEP constraint ε_b in the SBS adaptive system and the non-adaptive system also varies. The variation depends on the error performance of the combination of coding and modulation scheme. For 64QAM and the convolutional code of constraint length 9, the variation results in a throughput gain increase as the code rate decreases. For QPSK and the convolutional code of constraint length 9 (Figure 4.5), the variation is not obvious, and thus the throughput gains similar for different code rates. In fact, a very small amount of increase in throughput gain can also be observed in Figure 4.5 as the code rate decreases.

The numerical results for convolutional codes show that a large throughput gain could be achieved by applying SBS duration adaptation. This is because the Viterbi decoder is fairly sensitive to burst errors [42]. If the convolutional code is used in the correlated fading channel, the deep fades corrupt the signal and bring burst errors. The burst errors result in a large decoding bit error probability. Therefore, there is a large gap between curves of $\tilde{H}_c(x)$ and $h_c(x)$ for convolutional codes. In accordance with (4.9), this gap explains why there is a significant throughput gain from rapid symbol duration adaptation.

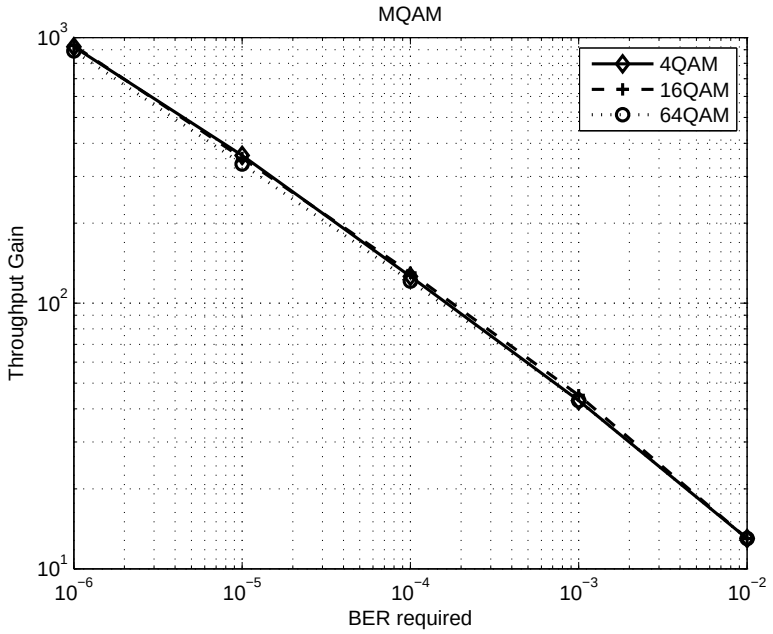

Figure 4.6: Throughput Gain for convolutional code (constraint length = 9, code rate = 1/4) with MQAM. The decoding scheme is hard-decision Viterbi algorithm.

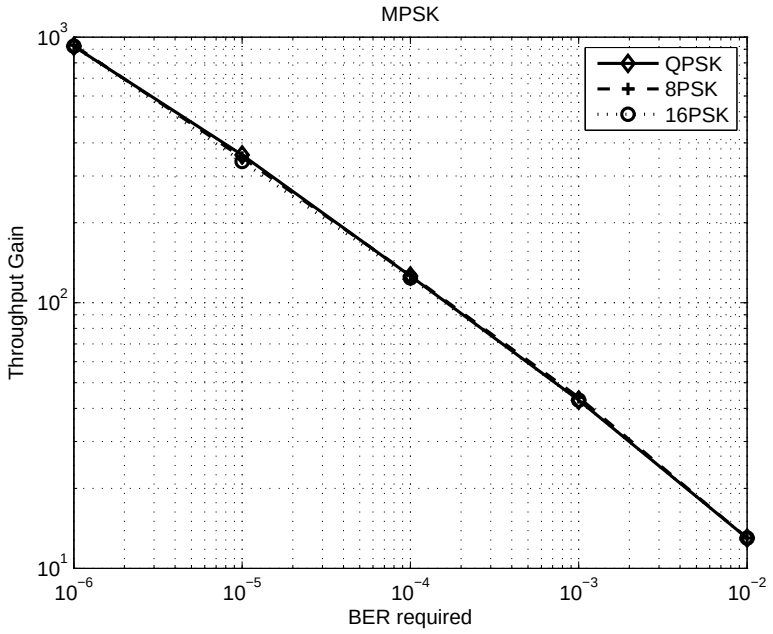

Figure 4.7: Throughput Gain for convolutional code (constraint length = 9, code rate = 1/4) with MPSK. The decoding scheme is hard-decision Viterbi algorithm.

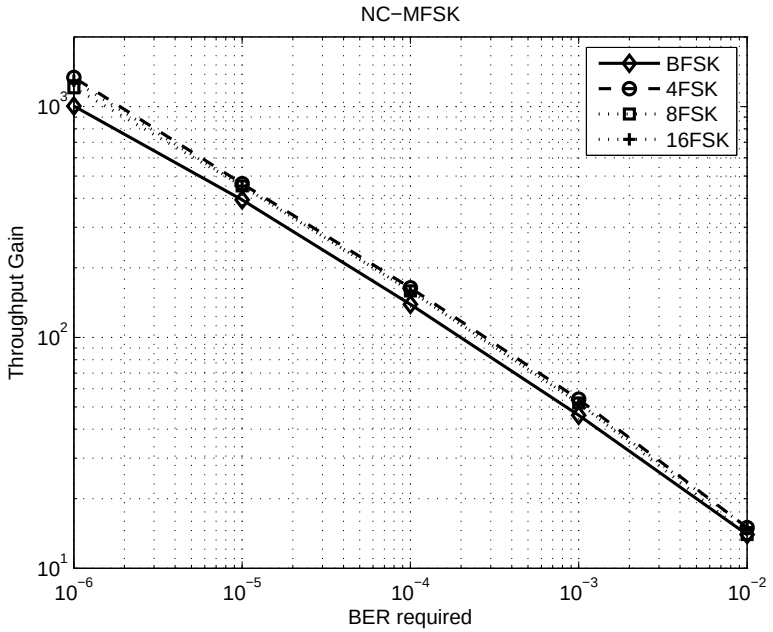

Figure 4.8: Throughput Gain for convolutional code (constraint length = 9, code rate = 1/4) with NC-MFSK. The decoding scheme is hard-decision Viterbi algorithm.

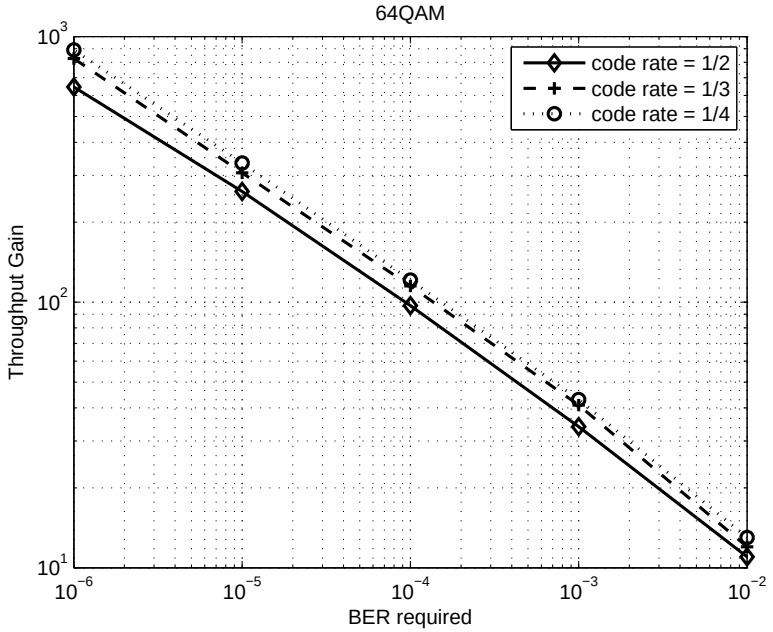

Figure 4.9: Throughput Gain of 64QAM and convolutional code (constraint length = 9) for code rates of 1/2,1/3 and 1/4. The decoding scheme is hard-decision Viterbi algorithm.

4.2.2 LDPC codes

Since the end of nineties, low density parity check (LDPC) code has drawn much attention because of its excellent error correction ability [43] [44] [45]. Some codes in the LDPC family have near Shannon limit performance [44] [46]. The throughput gain for BPSK with DVBS-S2 (the second generation satellite digital video broadcasting standard) LDPC code of 1/2 code rate was investigated by simulation. In the simulation, the maximum Doppler shift f_d was also set to 100Hz, and the information bit rate was set to 10^5 bps. The DVB-S2 LDPC code has the block length of 64800 bits and the code rates from 1/4 to 9/10. Reference [47] concludes that the DVB-S2 LDPC codes can approach the Shannon limit to within 0.6 – 0.8 dB over a Gaussian channel. The simulation results of throughput gain are shown in Figure 4.10. It is observed that the throughput gains are minor for all bit error probability requirements. There is little benefit to apply rapid duration adaptation with the DVB-S2 LDPC code. Although the DVB-S2 LDPC codes may be difficult to be applied in a wireless communication system such as the 3G CDMA networks, the result indicates that the throughput gain depends on the coding scheme. The stronger error correction ability a code has, the less throughput gain SBS adaptation can achieve with the code.

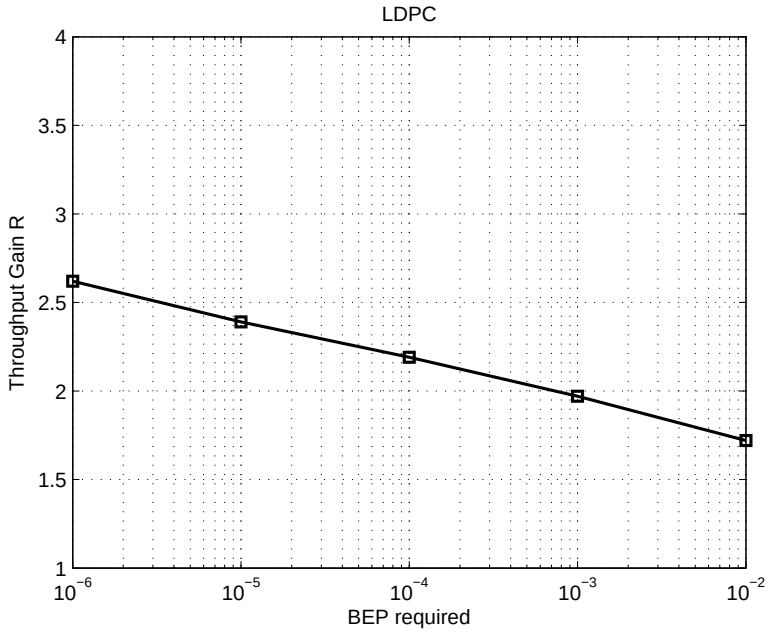

Figure 4.10: Throughput Gain of BPSK and LDPC code (DVB S.2 code, code rate = 1/2)

4.2.3 Other block codes

The throughput gains for some well-known block codes were also investigated. (31,26)Hamming code, (31,26) BCH code and (31,27) Reed-Solomon (RS) code were experimented with BPSK modulation. In simulation, the information bit rate was 10^4 bits/s and f_d was set to 100Hz. The throughput gain results are plotted in Figure 4.11. For all three codes, the throughput gains are also larger for the smaller BEP requirements. The Hamming code and BCH code result in almost identical throughput gains while the gains for the RS code are less.

Figure 4.12 plots the throughput gain for the (31,26) Hamming code combined with BPSK and MQAM. For small BER requirements, i.e., $\varepsilon_b = 10^{-5}$ and 10^{-6}, the throughput gain increases notably as the constellation size becomes larger; for $\varepsilon_b = 10^{-2}$ and 10^{-3}, the throughput gain is slightly smaller for the larger constellation size. Note that the bit error probability increases as the constellation size increases in both SBS rate adaptive system and non-adaptive system. However, the difference between the SNRs achieving a given BEP constraint ε_b in the SBS adaptive system and the non-adaptive system varies as the constellation size increases. In the case of (31,26) Hamming code, the variation is an increase for small ε_b values and a decrease for large ε_b values, resulting in the change of throughput gain with the constellation size we observe in Figure 4.12.

4.2.4 Interleaved channel

The throughput gain for interleaved Rayleigh fading channel was also investigated. The technique of interleaving is commonly used in modern wireless communication to break the channel time correlations. A channel with time correlation often brings burst errors to the communication system equipped with forward error correction (FEC) codes and thus degrades the performance. Interleaving spreads the burst errors around different code words, then the FEC codes have higher possibility to correct the errors. Figure 4.13 shows the system diagram to simulate the wireless communication system over the interleaved fading channel. At the transmitter, the coded sequence is first interleaved and then modulated. At receiver side, the demodulator output is deinterleaved and then fed to the decoder. By doing so, the adjacent coded bits are shuffled across different code words and the errors caused by deep fades are spread evenly.

The simulation applied block interleavers with the size 768 (12×64), 3072 (48×64),

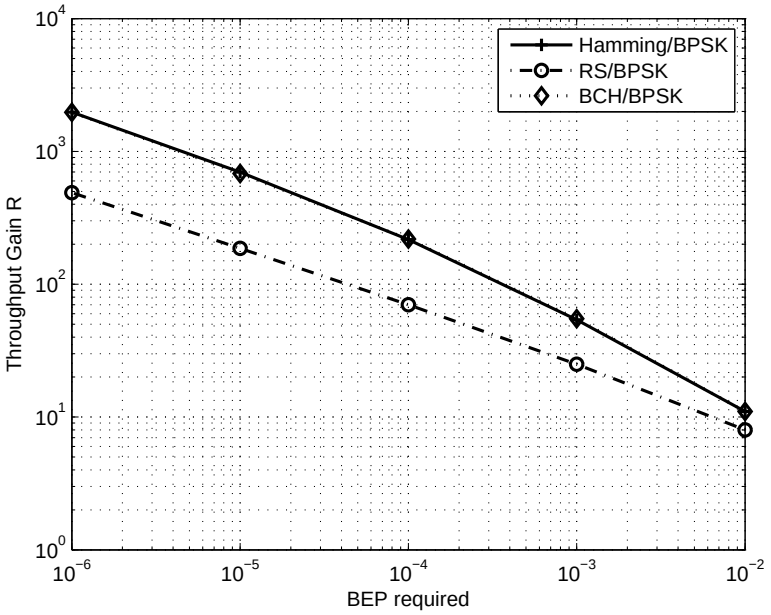

Figure 4.11: Throughput Gains of BPSK and Hamming code (31, 26), BCH code (31,26) and Reed-Solomon code (31,27).

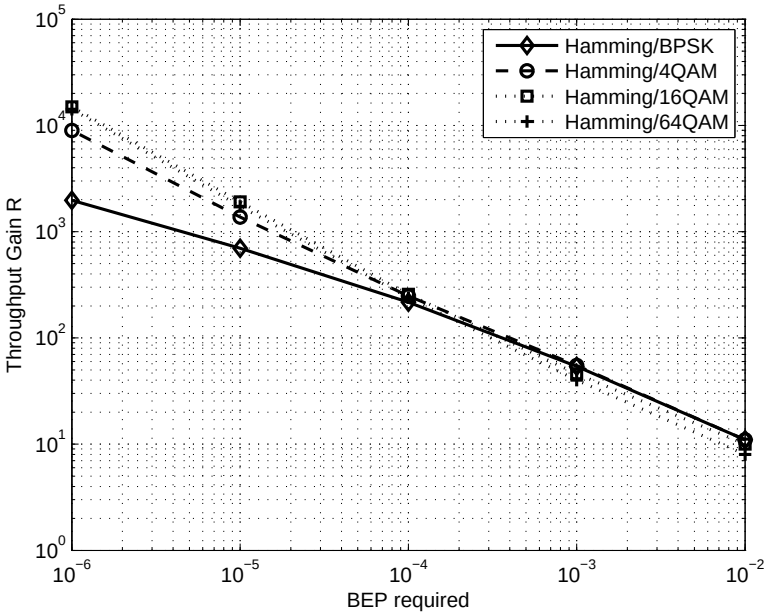

Figure 4.12: Throughput Gains of Hamming code (31, 26) with BPSK and MQAM.

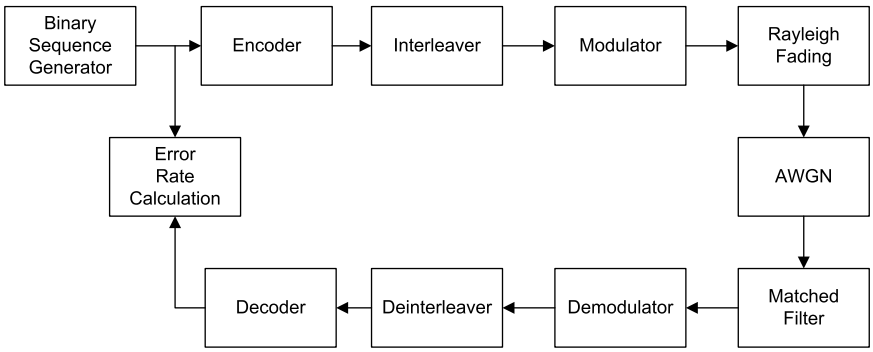

Figure 4.13: System diagram of the simulation to obtain the curve of $\tilde{H}_c(x)$, the BEP for expected receive SNR x over interleaved Rayleigh fading channel. The coded sequence is interleaved before modulation and the demodulated signal is deinterleaved before fed to the decoder.

and 18432 (48×384) bits and employed convolutional code with constraint length of 9 and code rate of 1/4. The coded bits are written into the interleavers column by column and read out row by row. In simulation, the information bit rate was set to be 38400 bps and the maximum Doppler shift was also set to be 100 Hz. Both the soft-decision and hard-decision Viterbi decoding algorithms were experimented. The modulation scheme is QPSK(4QAM) with Gray mapping. Figures 4.14 and 4.15 show the throughput gains with the three interleavers for soft-decision and hard-decision, respectively. In both figures, the throughput gains without interleaving and the throughput gains over uncorrelated Rayleigh channel are also plotted for comparison. It is observed that, as the interleaver size increases, the throughput gain dramatically decreases. This is consistent with the sensitivity of Viterbi decoders to burst errors [42]. The larger the interleaver is, the less time correlation of fading channel the symbol sequence experiences. In the case of our simulation channel (Jakes' model with $f_d = 100$ Hz), there is a significant time correlation of fading channels for neighboring symbols without an interleaver. Without an interleaver, there is a large gap between $\tilde{H}_c^{-1}(x)$ and $h_c^{-1}(x)$, so the rapid symbol duration adaptation can exploit it to improve the system throughput. With ideal interleaving (infinite sizes of interleaver), the channel gain becomes uncorrelated. So the throughput gains for uncorrelated channel are the lower bounds of the throughput gains for interleaved fading channel.

Figure 4.16 shows the throughput gains for Hamming code (31,26) and QPSK over the interleaved Rayleigh channel. The interleavers of 768 (12×64), 3072 (48×64) bits were experimented. The throughput gain decreases quickly as the interleaver size increases.

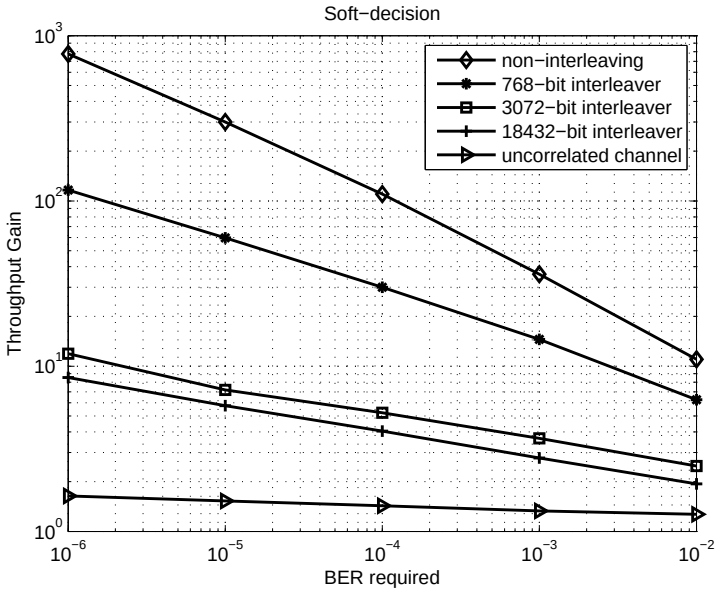

Figure 4.14: Throughput gains for QPSK with convolutional code (constraint length = 9, code rate = 1/4) and interleavers of the size of 768 (12×64), 3072 (48×64) and 18432 (48×384) bits. The decoding scheme is soft-decision Viterbi algorithm decoding. The throughput gain without interleaving and over uncorrelated Rayleigh fading channel is also plotted for the purpose of comparison.

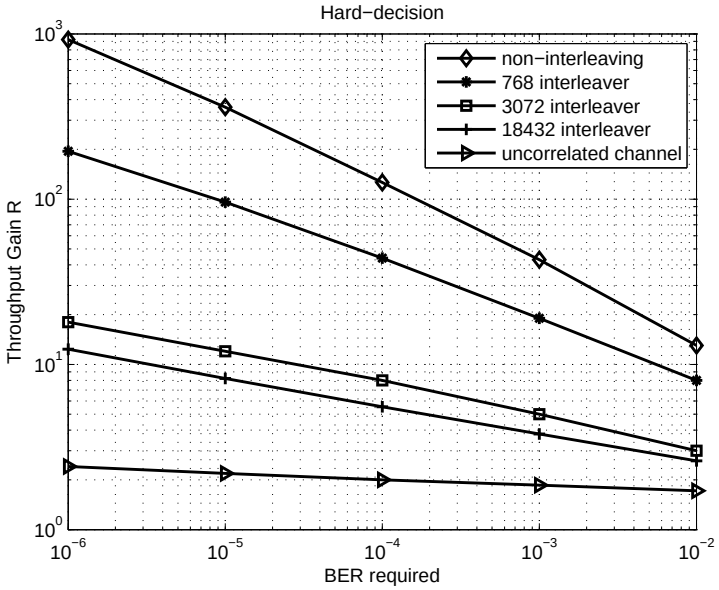

Figure 4.15: Throughput gains for QPSK with convolutional code (constraint length = 9, code rate = 1/4) and interleavers of the size of 768 (12×64), 3072 (48×64) and 18432 (48×384) bits. The decoding scheme is hard-decision Viterbi algorithm decoding. The throughput gain without interleaving and over uncorrelated Rayleigh fading channel is also plotted for the purpose of comparison.

It has been shown that throughput gain for a good LDPC code (e.g.,DVB-S2 code) is minor. Moreover, the gain is expected to decrease over interleaved fading channel. One interesting question is whether there is any throughput gain for LDPC code over interleaved channel. The answer is yes. Figure 4.17 shows the throughput gain for 1/2 DVB-S2 code and BPSK without interleaver, with 64800 (90×720) and 648000 (90×7200) bits interleavers, and over uncorrelated fading channel. It is again observed that the throughput gain decreases as the interleaver size increases. Note the interleaver of size 64800 bits affect the throughput gain very little. The DVB-S2 code has the block size of 64800 bits. The interleaver of size 64800 bits can only permute the code bits within the same codeword block. So it neither improves the bit error probability nor reduces the throughput gain. On the other hand, another interleaver has the size of 648000 bits, which is ten times of the codeword length. The interleaver can widely distribute the error bits caused by deep fades and thus improve the error probability. The throughput gain is therefore reduced. Nevertheless, the throughput gain dose exist though it is minor.

Interleaving does reduce the throughput gains achieved by SBS adaptation. Compared to rate adaptation, interleaving is a simple technique and fairly easy to implement. The problem of using interleaving technique is increasing latency because the interleaver/deinterleaver blocks must be filled up before the symbols can be output. If the coded system can tolerate the processing delay, interleaving should be a better choice for the system to improve the throughput.

4.2.5 Impact of f_d, the maximum Doppler shift

The numerical results of the throughput gain for coded systems presented so far in this chapter are all for the Rayleigh fading channel with 100Hz maximum Doppler shift . It is of interest how the throughput gain changes with f_d. Figure 4.18 illustrates how the throughput gain varies as f_d increases. The experiment system is equipped with QPSK and the 1/2 code rate convolutional code of constraint length 9. The decoding scheme is soft-decision Viterbi algorithm. The data rate of 14400 bps and f_d of 100, 200, 300, 500Hz were experimented. It is observed that the throughput gain decreases as f_d increases. In fact, the simulation results show that the bit error probability over the fading channel decreases as the f_d increases. As the maximum Doppler shift increases, the channel fluctuates faster. On the other hand, the duration of deep fades becomes shorter. The signal in turn suffers more deep fades but each deep fade corrupts fewer modulated symbols. Then forward error

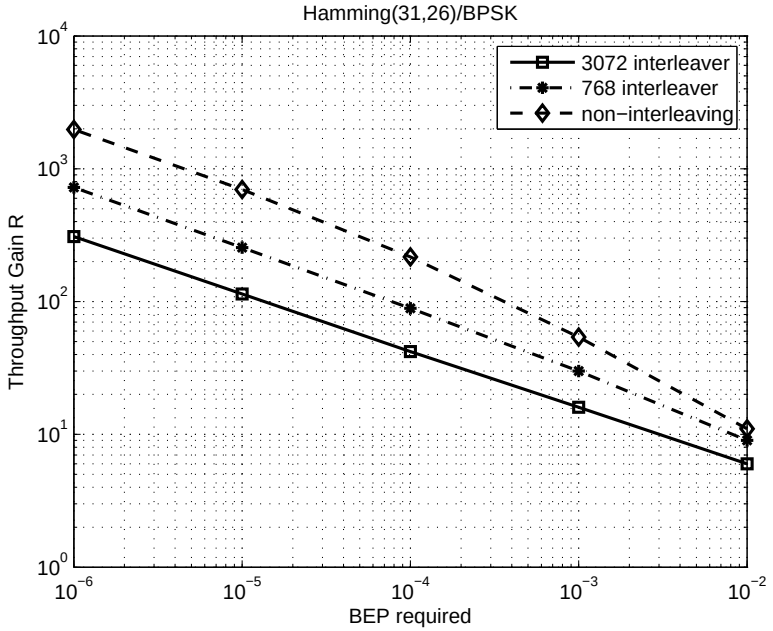

Figure 4.16: Throughput gains for QPSK with Hamming code (31, 26) and interleavers of the size of 768 (12×64), 3072 (48×64) bits. The throughput gains without interleaving are also plotted for the purpose of comparison.

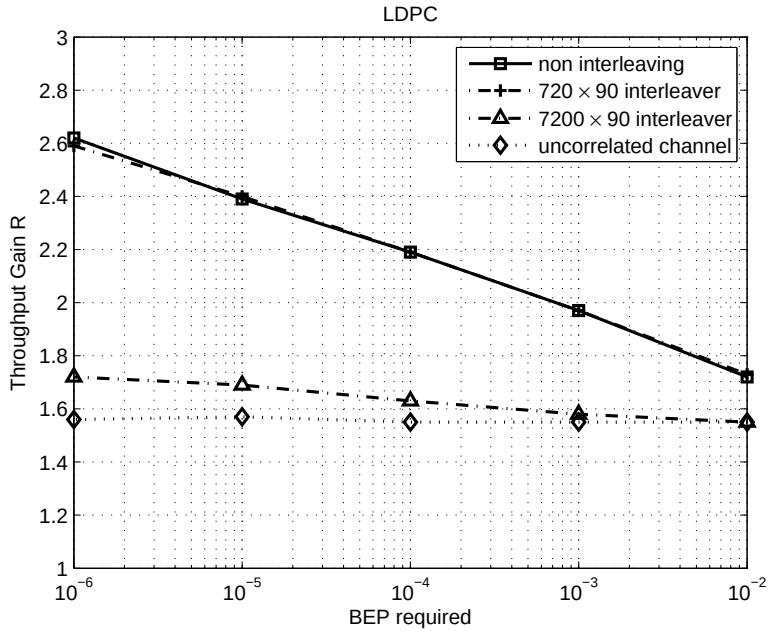

Figure 4.17: Throughput gains for BPSK with LDPC (1/2 code rate DVB-S2 code) and interleavers of the size of 64800 (90×720), 648000 (90×7200) bits. The throughput gains without interleaving and over uncorrelated Rayleigh fading channel are also plotted for the purpose of comparison.

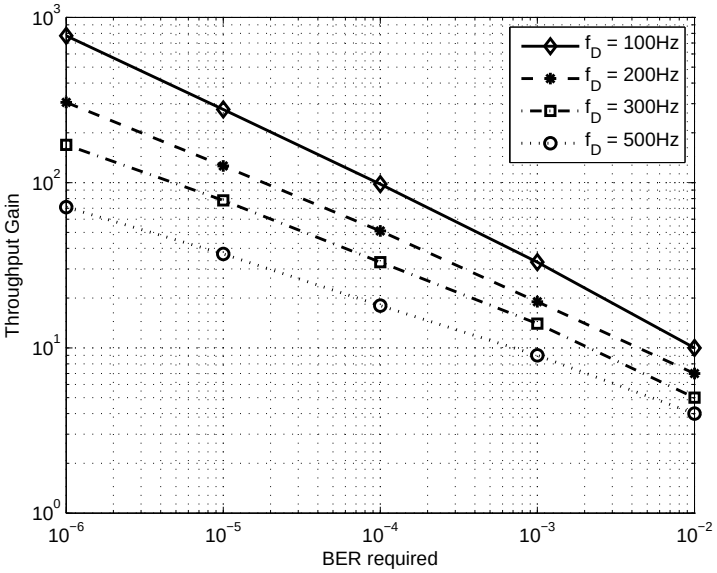

Figure 4.18: Throughput gains for QPSK and 1/2 code rate convolutional code of the constraint length of 9 over Rayleigh fading channels of maximum Doppler shift of 100, 200, 300 and 500 Hz. The decoding scheme is soft-decision Viterbi algorithm.

correction code has higher possibility to correct the errors. That is the reason why the bit error probability of non-adaptive system decreases as f_d increases. The bit error probability of SBS rate adaptation system is not affected by the change of f_d, so the resultant throughput gain decreases as f_d increases.

4.3 Chapter conclusion

In this chapter, the throughput gain achieved by rapid duration adaptation in coded systems is investigated by simulation. The simulation results show that the throughput gain for a coded system depends on the coding scheme and the associated interleaving technique. There is little benefit to apply rate adaptation with superior FEC codes like the DVB-S2 LDPC code or with large size interleavers. On the other hand, without interleaving, for some commonly used FEC codes, e.g., the convolutional code, SBS duration adaptation can achieve large throughput gain to FBF adaptation over the fast time-varying fading channel. Moreover, SBS duration adaptation achieves a higher throughput gain when the data rate in the system is higher. When the maximum Doppler shift of the channel increases, the throughput gain decreases.

Chapter 5

Throughput Gain with Imperfect Channel Information

In previous chapters, the performance of the symbol-by-symbol duration (rate) adaptation was analyzed and compared with the performance of the slow (frame-by-frame) adaptation. It was concluded that in uncoded systems the data throughput achieved by an SBS adaptation can be much higher than the throughput achieved by an FBF adaptation for the same data fidelity constraint. However, such throughput gains were derived under the ideal assumption that the transmitter's knowledge of the channel is perfect for each symbol. This chapter will examine whether SBS adaptation can achieve such a high throughput gain over FBF adaptation even if the transmitter's channel knowledge is imperfect. The analysis and results were first published in [48].

The system design under imperfect channel knowledge is challenging in many ways. One issue is how to best estimate/predict the channel conditions. Another is how to design a duration adaptation policy, which decides the duration of each symbol on the basis of its estimated/predicted channel condition. In this chapter, a very simple linear mean-square channel estimation/prediction is considered. As for the duration adaptation policy, the discussion is confined to policies in a simple linear form. Numerical results show significant gains in the error-constrained throughput of the uncoded system from symbol-by-symbol adaptation over frame-by-frame adaptation, even with the simple form of adaptation policy and the simple channel estimation/prediction scheme.

5.1 System model

Let $a(t)$ be a complex-valued random process that models the base-band complex-valued fading channel gain for the signal arriving at each time t. For analysis, an isotropic scattering channel model is employed, so accordingly $a(t)$ is assumed to be an ergodic zero-mean complex-valued random process with auto-correlation

$$E\left[a\left(t+\tau\right)a(t)^{*}\right]=E\left[\left|a\left(t\right)\right|^{2}\right]J_{0}\left(2\pi f_{D}\tau\right),\forall t,\tau \tag{5.1}$$

where J_0 is the zero-order Bessel function of the first kind and f_D is the maximum Doppler shift. In this model, the stationarity of complex process $a(t)$ implies [49, page 155] (see Appendix B)

$$E\left[a\left(t+\tau\right)a\left(t\right)\right]=0,\forall t,\tau \tag{5.2}$$

Let P_T be the transmit power. Under the assumption that receive power stays constant during the symbol duration, the instantaneous signal to noise ratio (SNR) per symbol at the receiver is $P_T|a(t)|^2T_s\Big/N_0$, where T_s is the symbol duration and N_0 is the spectral density of the additive noise (plus interference if there is any) power at the receiver. In the SBS adaptation, the duration of each symbol is determined by the transmitter based on the receive power $Y(t) = P_T|a(t)|^2$ at the time of the symbol's reception. Let the symbol duration (or rate) adaptation policy be represented by function $r_p(\cdot)$. The value $r_p(\hat{Y})$ represents the reciprocal of the symbol duration chosen by the transmitter in accordance with the policy $r_p(\cdot)$ for the symbol whose receive power is predicted to be $\hat{Y}$. (Assume that the receive power stays constant for each symbol duration.) The value $r_p(\hat{Y})$ can be interpreted as the instantaneous symbol rate, and the unit of $r_p(\cdot)$ is the number of symbols per second (or a unit time). For simplicity, the analysis only considers suboptimal policies in a linear form: $r_p(\hat{Y}) = q\hat{Y}$. Note that according to [28], in the case of perfect channel knowledge $\hat{Y} = Y$ for all symbols, optimal adaptation policy would be indeed linear $r_p(Y) = qY$ for some value of q.

5.2 Optimization of policy $r_p(\hat{Y}) = q\hat{Y}$

Let $f_{\hat{Y},Y}\left(\hat{y},y\right)$ be the joint probability density function (pdf) of $\hat{Y},Y$. The receiver estimates the channel gain at time t, $a(t)$, on the basis of the received signal up to time t. The receiver's estimation $a_{ES}(t)$ is fed back to the transmitter. Because of feedback and processing delay,

channel estimation $a_{ES}(t)$ is outdated for the symbol to be transmitted at time $t+\tau$. Time gap τ includes both processing and feedback delay in this model. Therefore, the duration of the symbol to be transmitted from time $t+\tau$ is determined on the basis of the predicted gain of the channel at time $t+\tau$, which is denoted by $\hat{a}(t+\tau)$. Consider a sub-optimal policy in the form of $r_p(\hat{Y}) = q\hat{Y}$ for some constant q, where $\hat{Y}$ is the predicted receive power, $P_T|\hat{a}\,(t+\tau)|^2$. Then, the problem of maximizing the error-constraint symbol throughput can be formulated as the following optimization:

$$\begin{aligned} &\max_{r_p(\hat{y})} \quad \int r_p\,(\hat{y}) f_{\hat{Y}}\,(\hat{y})\,d\hat{y} \\ &\text{subject to} \quad \frac{\int r_p\,(\hat{y}) h\left(\frac{y}{N_0 r_p(\hat{y})}\right) f_{\hat{Y},Y}\,(\hat{y},y)\,d\hat{y}dy}{\int r_p\,(\hat{y}) f_{\hat{Y}}\,(\hat{y})\,d\hat{y}} \leq \varepsilon \end{aligned} \tag{5.3}$$

where $h(\cdot)$ is the symbol error probability (SEP). The optimization formulation can also be written as:

$$\begin{aligned} &\max_{r_p(\hat{Y})} \quad E\left[r_p\left(\hat{Y}\right)\right] \\ &\text{subject to} \quad \frac{E\left[r_p\left(\hat{Y}\right) h\left(\frac{Y}{N_0 r_p(\hat{Y})}\right)\right]}{E\left[r_p\left(\hat{Y}\right)\right]} \leq \varepsilon \end{aligned} \tag{5.4}$$

Under the assumption of perfect channel knowledge, the policy $r_p(Y) = qY$ in [28] can be simply viewed as adjusting duration so that the SNR per symbol $y/\left(N_0 r_p\,(y)\right)$ is exactly $h^{-1}(\varepsilon)$. Under the assumption of imperfect channel, the policy in this form yields symbol throughput $E\left[r_p\left(\hat{Y}\right)\right] = qE\left(\hat{Y}\right)$. The symbol error probability is

$$\frac{E\left[r_p\left(\hat{Y}\right) h\left(\frac{Y}{N_0 r_p(\hat{Y})}\right)\right]}{E\left[r_p\left(\hat{Y}\right)\right]} = \frac{E\left[\hat{Y} h\left(\frac{Y}{N_0 q\hat{Y}}\right)\right]}{E\left[\hat{Y}\right]} \tag{5.5}$$

In accordance with (5.4), the average data throughput $E\left[r_p\left(\hat{Y}\right)\right] = qE\left(\hat{Y}\right)$ increases as q increases. However, (5.5) shows that SEP also increases as q increases. Therefore, the maximal adaptation policy takes the largest value of q such that the fidelity constraint ε is satisfied, i,e. the value of q that satisfies equality:

$$\frac{E\left[\hat{Y} h\left(\frac{Y}{N_0 q\hat{Y}}\right)\right]}{E\left[\hat{Y}\right]} = \varepsilon \tag{5.6}$$

The policy in this form yields symbol throughput

$$E\left[r_p\left(\hat{Y}\right)\right] = qE\left(\hat{Y}\right) = qP_T E\left(\left|\hat{a}\left(t+\tau\right)\right|^2\right) \tag{5.7}$$

The symbol error probability can be written as

$$\begin{aligned}
&\frac{E\left[r_p\left(\hat{Y}\right) h\left(\frac{Y}{N_0 r_p\left(\hat{Y}\right)}\right)\right]}{E\left[r_p\left(\hat{Y}\right)\right]} \\
&= \frac{E\left[qP_T\left|\hat{a}\left(t+\tau\right)\right|^2 h\left(\frac{P_T\left|a(t+\tau)\right|^2}{N_0 qP_T\left|\hat{a}(t+\tau)\right|^2}\right)\right]}{E\left[qP_T\left|\hat{a}\left(t+\tau\right)\right|^2\right]} \\
&= \frac{E\left[\left|\hat{a}\left(t+\tau\right)\right|^2 h\left(\frac{\left|a(t+\tau)\right|^2}{N_0 q\left|\hat{a}(t+\tau)\right|^2}\right)\right]}{E\left[\left|\hat{a}\left(t+\tau\right)\right|^2\right]}
\end{aligned} \tag{5.8}$$

For high data throughput the policy should choose the largest value of q that keeps SEP less than or equal to ε (the fidelity constraint)—that is, the value of q that satisfies the equality:

$$\frac{E\left[\left|\hat{a}\left(t+\tau\right)\right|^2 h\left(\frac{\left|a(t+\tau)\right|^2}{N_0 q\left|\hat{a}(t+\tau)\right|^2}\right)\right]}{E\left[\left|\hat{a}\left(t+\tau\right)\right|^2\right]} = \varepsilon \tag{5.9}$$

5.3 Suboptimal SBS adaptation policy for BFSK

The non-coherent BFSK modulation has the SEP function [49]

$$h\left(x\right) = \frac{1}{2}\exp\left(-\frac{x}{2}\right) \tag{5.10}$$

So from (5.9)

$$\frac{E\left[\left|\hat{a}\left(t+\tau\right)\right|^2 \frac{1}{2}\exp\left(-\frac{1}{2}\frac{\left|a(t+\tau)\right|^2}{N_0 q\left|\hat{a}(t+\tau)\right|^2}\right)\right]}{E\left[\left|\hat{a}\left(t+\tau\right)\right|^2\right]} = \varepsilon \tag{5.11}$$

To analyze this expected value, the relation between the prediction $\hat{a}(t+\tau)$ and the actual channel gain $a(t+\tau)$ is required. The receiver's channel estimation at time t is

$$a_{ES}\left(t\right) \equiv a\left(t\right) + a_v\left(t\right)$$

where $a(t)$ is the true channel gain at time t, and $a_v(t)$ is the estimation error (noise) in the receiver's channel estimation. Let the complex random processes $a(t)$ and $a_v(t)$ be modeled

as statistically mutually independent and zero-mean Gaussian processes. It is also assumed that these two complex random variables $a_{ES}(t)$ and $a(t+\tau)$ are jointly Gaussian. This joint Gaussian distribution grants that the MMSE (minimum mean square error) prediction of $a(t+\tau)$ based on $a_{ES}(t)$ is indeed the MMSE "widely linear" [50] estimator of $a(t+\tau)$ based on $a_{ES}(t)$. Moreover, from stationarity of zero-mean processes $a(t)$ and $a_v(t)$, and their statistical independence, we have

$$\begin{aligned} E\left[a\left(t+\tau\right)a_{ES}(t)^*\right] &= E\left[a\left(t+\tau\right)\{a\left(t\right)+a_v\left(t\right)\}^*\right] \\ &= E\left[a\left(t+\tau\right)a(t)^*\right]+E\left[a\left(t+\tau\right)a_v(t)^*\right] \\ &= E\left[\left|a\left(t\right)\right|^2\right]J_0\left(2\pi f_D\tau\right),\forall t,\tau \end{aligned} \tag{5.12}$$

Note that

$$E\left[a(t)a_v(t)\right]=E\left[a(t)\right]E\left[a_v(t)\right]=0$$

Therefore, we have

$$\begin{aligned} E\left[a_{ES}(t)^2\right] &= E\left[\left\{a\left(t\right)+a_\nu(t)\right\}^2\right] \\ &= E\left[a(t)\right]^2+2E\left[a(t)\right]E\left[a_v(t)\right]+E\left[a_v(t)\right]^2 \\ &= 0 \\ E\left[a\left(t+\tau\right)a_{ES}\left(t\right)\right] &= E\left[a\left(t+\tau\right)\{a\left(t\right)+a_v(t)\}\right] \\ &= E\left[a\left(t+\tau\right)a\left(t\right)\right]+E\left[a\left(t+\tau\right)a_v(t)\right] \\ &= 0 \end{aligned} \tag{5.13}$$

Thus, Equations (5.2) and (5.13) further grant that $\hat{a}(t+\tau)$, the MMSE predictor of $a(t+\tau)$ based on $a_{ES}(t)$, is simply a complex linear function of $a_{ES}(t)$:

$$\hat{a}\left(t+\tau\right)=\tilde{J}\left(\tau\right)a_{ES}\left(t\right) \tag{5.14}$$

where

$$\tilde{J}\left(\tau\right)=\frac{E\left[a\left(t+\tau\right)a_{ES}(t)^*\right]}{E\left(\left|a_{ES}\left(t\right)\right|^2\right)}=\frac{E\left(\left|a\left(t\right)\right|^2\right)J_0\left(2\pi f_D\tau\right)}{E\left(\left|a\left(t\right)\right|^2\right)+E\left(\left|a_v\left(t\right)\right|^2\right)} \tag{5.15}$$

The prediction $\hat{a}\left(t+\tau\right)=\tilde{J}\left(\tau\right)\left\{a\left(t\right)+a_\nu\left(t\right)\right\}$ is just a multiplication of a real number and random variable $a\left(t\right)+a_\nu\left(t\right)$, so again $\hat{a}(t+\tau)$ and $a(t+\tau)$ together form a zero-mean

complex Gaussian random vector. Moreover, the second-order statistics of these jointly Gaussian complex random variables have following special properties:

$$\begin{aligned} E\left[\hat{a}(t+\tau)^2\right] &= E\left[\left\{\tilde{J}\left(\tau\right)a_{ES}\left(t\right)\right\}^2\right] \\ &= \tilde{J}\left(\tau\right)^2 E\left[a_{ES}(t)^2\right] \\ &= 0 \\ E\left[a\left(t+\tau\right)\hat{a}\left(t+\tau\right)\right] &= E\left[a\left(t+\tau\right)\tilde{J}\left(\tau\right)a_{ES}\left(t\right)\right] \\ &= \tilde{J}\left(\tau\right)E\left[a\left(t+\tau\right)a_{ES}\left(t\right)\right] \\ &= 0 \end{aligned} \tag{5.16}$$

This joint complex Gaussian distribution between $\hat{a}(t+\tau)$ and $a(t+\tau)$ makes the conditional distribution of $a(t+\tau)$ for a particular condition $\hat{a}(t+\tau)=\hat{\alpha}$ also complex Gaussian. From (5.13) and (5.16) the conditional pdf [50] [51] can be expressed in the following simple form. Let us denote by a_R, a_Q the real and imaginary parts of random variable $a(t+\tau)$. Then, the joint pdf of a_R, a_Q conditioned on the event $\hat{a}(t+\tau)=\hat{\alpha}$ is

$$f_{a_R,a_Q|\hat{a}(t+\tau)}\left(\alpha_R,\alpha_Q\,|\hat{\alpha}\right) = \frac{1}{\pi\sigma^2}\exp\left[-\frac{|\alpha-\hat{\alpha}|^2}{\sigma^2}\right] \tag{5.17}$$

where $\alpha=\alpha_R+j\alpha_Q$ and σ^2 is the variance. The variance σ^2 is further given by [51]

$$\sigma^2 = E\left(|a\left(t+\tau\right)|^2\right) - \frac{E\left[a\left(t+\tau\right)\hat{a}(t+\tau)^*\right]E\left[\hat{a}\left(t+\tau\right)a(t+\tau)^*\right]}{E\left(|\hat{a}\left(t+\tau\right)|^2\right)} \tag{5.18}$$

Let us obtain a simple expression of σ^2.

$$\begin{aligned} & E\left[a\left(t+\tau\right)\hat{a}(t+\tau)^*\right] \\ =\ & E\left[a\left(t+\tau\right)\tilde{J}\left(\tau\right)a_{ES}(t)^*\right] \\ =\ & \tilde{J}\left(\tau\right)\,E\left[a\left(t+\tau\right)\{a(t)^*+a_\nu(t)^*\}\right] \\ =\ & \tilde{J}\left(\tau\right)E\left[a\left(t+\tau\right)a(t)^*\right] \\ =\ & \tilde{J}\left(\tau\right)J_0\left(2\pi f_D\tau\right)E\left(|a\left(t\right)|^2\right) \\ =\ & \Upsilon\left(\tau\right)E\left(|a\left(t\right)|^2\right) \end{aligned} \tag{5.19}$$

where

$$\Upsilon\left(\tau\right) = \tilde{J}J_0\left(2\pi f_D\tau\right) = \frac{E\left(|a\left(t\right)|^2\right)}{E\left(|a\left(t\right)|^2\right)+E\left(|a_v\left(t\right)|^2\right)}J_0(2\pi f_D\tau)^2 \tag{5.20}$$

Similarly, $E\left[\hat{a}\left(t+\tau\right)a(t+\tau)^{*}\right]=\Upsilon\left(\tau\right)E\left(\left|a\left(t\right)\right|^{2}\right)$. Also

$$\begin{aligned}
&E\left[\left|\hat{a}\left(t+\tau\right)\right|^{2}\right]\\
&=E\left[\tilde{J}\left(\tau\right)a_{ES}\left(t\right)\left(\tilde{J}\left(\tau\right)a_{ES}\left(t\right)\right)^{*}\right]\\
&=\tilde{J}\left(\tau\right)^{2}E\left[\left(a\left(t\right)+a_{\nu}\left(t\right)\right)\left(a\left(t\right)+a_{\nu}\left(t\right)\right)^{*}\right]\\
&=\tilde{J}\left(\tau\right)^{2}\left[E\left(\left|a\left(t\right)\right|^{2}\right)+E\left(\left|a_{v}\left(t\right)\right|^{2}\right)\right]\\
&=\Upsilon\left(\tau\right)E\left(\left|a\left(t\right)\right|^{2}\right)
\end{aligned}\tag{5.21}$$

Then by substituting (5.19) and (5.21) into (5.18), the variance is given by

$$\sigma^{2}=E\left(\left|a\left(t\right)\right|^{2}\right)\left[1-\Upsilon\left(\tau\right)\right]\tag{5.22}$$

(5.17) and (5.22) also indicate that the real and imaginary parts of $a(t+\tau)$ are statistically independent conditioned on the event $\hat{a}(t+\tau)=\hat{\alpha}$. Also the random variable $\left|a\left(t+\tau\right)\right|^{2}$, conditioned on the event $\hat{a}(t+\tau)=\hat{\alpha}$, has a non-central chi-square distribution with two degrees of freedom. Note that the Laplace transform of the chi-square distribution with two degrees of freedom is [49]

$$E\left\{\exp\left(-s|a\left(t+\tau\right)|^{2}\right)\,|\hat{a}\left(t+\tau\right)=\hat{\alpha}\right\}=\frac{1}{1+s\sigma^{2}}\exp\left[\frac{-s|\hat{\alpha}|^{2}}{1+s\sigma^{2}}\right]\tag{5.23}$$

Now, the expectation of the numerator of (5.11) can be written as

$$E\left[E\left\{\frac{\left|\hat{\alpha}\right|^{2}}{2}\exp\left(-\frac{1}{2}\frac{\left|a\left(t+\tau\right)\right|^{2}}{N_{0}q|\hat{\alpha}|^{2}}\right)\middle|\,\hat{\alpha}\right\}\right]\tag{5.24}$$

and first consider the conditional expectation

$$E\left\{\frac{\left|\hat{\alpha}\right|^{2}}{2}\exp\left(-\frac{1}{2}\frac{\left|a\left(t+\tau\right)\right|^{2}}{N_{0}q|\hat{\alpha}|^{2}}\right)\middle|\,\hat{a}=\hat{\alpha}\right\}\tag{5.25}$$

From (5.23) we have

$$\begin{aligned}
&E\left\{\exp\left(\frac{-\left|a\left(t+\tau\right)\right|^{2}}{2N_{0}q|\hat{\alpha}|^{2}}\right)\middle|\,\hat{a}\left(t+\tau\right)=\hat{\alpha}\right\}\\
&=\frac{1}{1+s\sigma^{2}}\exp\left(\frac{-s|\hat{\alpha}|^{2}}{1+s\sigma^{2}}\right)\Bigg|_{s=\frac{1}{2N_{0}q|\hat{\alpha}|^{2}}}\\
&=\frac{1}{1+\frac{\sigma^{2}}{2N_{0}q|\hat{\alpha}|^{2}}}\exp\left(\frac{-\frac{1}{2N_{0}q}}{1+\frac{\sigma^{2}}{2N_{0}q|\hat{\alpha}|^{2}}}\right)
\end{aligned}\tag{5.26}$$

$a_{ES}(t)$ is a stationary complex Gaussian process, so $|\hat{\alpha}|^2 = |\hat{a}(t+\tau)|^2 = \tilde{J}(\tau)^2 |a_{ES}(t)|^2$ is exponentially distributed with mean (5.21)

$$E\left[|\hat{a}(t+\tau)|^2\right] = \Upsilon(\tau) E\left(|a(t)|^2\right) = \frac{\Upsilon(\tau)}{1-\Upsilon(\tau)}\sigma^2 = \xi\sigma^2 \tag{5.27}$$

where

$$\xi \equiv \frac{\Upsilon(\tau)}{1-\Upsilon(\tau)} = \frac{\tilde{J}(\tau) J_0(2\pi f_D \tau)}{1-\tilde{J}(\tau) J_0(2\pi f_D \tau)} \tag{5.28}$$

Thus, we have

$$\begin{aligned}
&E\left[E\left\{\frac{|\hat{\alpha}|^2}{2}\exp\left(-\frac{1}{2}\frac{|a(t+\tau)|^2}{N_0 q|\hat{\alpha}|^2}\right)\middle|\hat{\alpha}\right\}\right] \\
&= E\left[\frac{|\hat{\alpha}|^2}{2}E\left\{\exp\left(-\frac{1}{2}\frac{|a(t+\tau)|^2}{N_0 q|\hat{\alpha}|^2}\right)\middle|\hat{\alpha}\right\}\right] \\
&= E\left[\frac{|\hat{\alpha}|^2}{2}\frac{1}{1+\frac{\sigma^2}{2N_0 q|\hat{\alpha}|^2}}\exp\left(\frac{-\frac{1}{2N_0 q}}{1+\frac{\sigma^2}{2N_0 q|\hat{\alpha}|^2}}\right)\right] \\
&= \int_0^\infty \frac{\sigma^2 y}{2}\frac{1}{1+\frac{\beta}{y}}\exp\left(\frac{-\beta}{1+\frac{\beta}{y}}\right)\frac{1}{\xi}\exp\left(-\frac{y}{\xi}\right)dy
\end{aligned} \tag{5.29}$$

where $\beta = 1/(2N_0 q)$. Then, from (5.11) the SEP constraint is

$$\begin{aligned}
&\frac{\int_0^\infty \frac{\sigma^2 y}{2}\frac{1}{1+\frac{\beta}{y}}\exp\left[\frac{-\beta}{1+\frac{\beta}{y}}\right]\frac{1}{\xi}\exp\left(-\frac{y}{\xi}\right)dy}{E\left[|\hat{\alpha}|^2\right]} \\
&= \frac{\int_0^\infty \frac{\sigma^2 y}{2}\frac{1}{1+\frac{\beta}{y}}\exp\left[\frac{-\beta}{1+\frac{\beta}{y}}\right]\frac{1}{\xi}\exp\left(-\frac{y}{\xi}\right)dy}{\xi\sigma^2} \\
&= \int_0^\infty \frac{y}{2}\frac{1}{1+\frac{\beta}{y}}\exp\left[\frac{-\beta}{1+\frac{\beta}{y}}\right]\frac{1}{\xi^2}\exp\left(-\frac{y}{\xi}\right)dy \le \varepsilon
\end{aligned} \tag{5.30}$$

The smallest $\beta = 1/(2N_0 q)$ that satisfies this constraint is numerically solved. Then, the error-constrained throughput for rapid adaptation policy $r_p(\hat{Y})$ is

$$\bar{r}_s = E\left[r_p\left(\hat{Y}\right)\right] = qP_T E\left(|\hat{a}(t+\tau)|^2\right) = \frac{P_T}{2N_0\beta}\Upsilon(\tau) E\left(|a(t)|^2\right) \tag{5.31}$$

From [28, eq.(23), eq.(29)] the error-constrained throughput for non-adaptive symbol duration (or approximately a frame-by-frame adaptation) is

$$r_F = \frac{P_T E\left(|a(t)|^2\right)}{N_0\left(\frac{1}{\varepsilon}-2\right)} \tag{5.32}$$

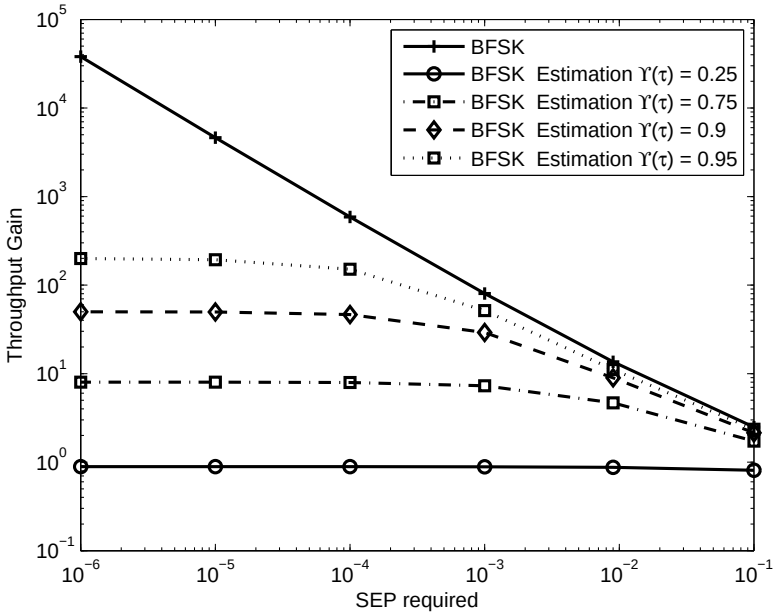

Figure 5.1: The throughput gain vs SEP required for BFSK with imperfect channel information.

Therefore, throughput gain is

$$\mathcal{R} = \frac{\bar{r}_s}{r_F} = \frac{\frac{P_T}{2N_0\beta}\Upsilon(\tau)\, E\left(|a(t)|^2\right)}{\frac{P_T E\left(|a(t)|^2\right)}{N_0\left(\frac{1}{\varepsilon}-2\right)}} = \frac{\Upsilon(\tau)}{\beta}\left(\frac{1}{2\varepsilon}-1\right) \tag{5.33}$$

The throughput gain $\mathcal{R} = \bar{r}_s/r_F$ can be interpreted as the throughput gain of SBS adaptation with imperfect CSI over FBF adaptation for a frame length that is relatively long compared to $1/(2f_D)$. The numerical evaluation of the ratio $\mathcal{R} = \bar{r}_s/r_F$ for NC-BFSK is shown in Figure 5.1. In the figure, it is observed that the throughput gain degrades as $\Upsilon(\tau)$ becomes smaller. The value of Υ reflects the correlation between $\hat{a}(t+\tau)$ and $a(t+\tau)$, the channel gain prediction and the true channel gain at time $t+\tau$. The higher the correlation is, the larger the throughput gain is achieved. To explore the benefit of SBS adaptation, reliable and accurate channel estimation/prediction technique is needed.

5.4 Chapter conclusion

This chapter presents the gains in throughput achieved by applying a rapid symbol duration adaptation in an uncoded system with outdated and imperfect channel estimation. The results show that SBS adaptation has promising gain over FBF adaptation even with very basic estimation/predictions schemes and a suboptimal adaptation policy.

Chapter 6

Conclusions and Discussion

In this thesis, the error-constrained throughput that is theoretically achievable by adjusting the duration of each symbol to the fast time-varying channel condition was analyzed. In accordance with the analysis results, such a rapid adaptation has the potential for significant throughput gain in uncoded systems. In coded systems, the throughput gain depends on the coding scheme and the interleaver size adopted by the system.

In Chapter 2, the throughput gain within the finite discrete duration set for the uncoded system was studied. We assumed that the symbol durations that the adaptive system can choose is within a finite discrete set and the durations are different powers of 2 CDMA chips. This is the case of dynamic spreading gain control [16] [25] [27] that applies a finite OVSF code set to adjust the symbol duration. In the adaptation policy of chapter 2, the range of receive power corresponds to the channel power gain is divided into a number of regions by thresholds. Each region is mapped to a duration in the duration set in accordance with the adaptation policy. When the receive power falls into a region, the corresponding duration is chosen for the symbol. The thresholds are optimized such that the throughput for SBS duration adaptation is maximized while a target average BEP is maintained. The numerical results of chapter 2 shows that for a required BEP, adjusting symbol duration within a finite discrete set can achieve throughput gain similar to that achieved with continuous duration as long as the dynamic range of the discrete duration set is sufficient. In another word, the discrete duration set does not degrade the throughput gain. The dynamic range of the discrete duration set is the upper bound of the achievable throughput gain.

In Chapter 3, we consider a channel model that is more realistic than the one in Chapter 2. The fading channel is no longer assumed to stay constant during each symbol duration.

Instead, the channel is assumed to remain unchanged for each chip duration but vary from chip to chip. The adaptation policy chooses a symbol duration among a discrete duration set such that a target instantaneous BEP requirement is satisfied. The numerical results show that, for a specified BEP requirement, adjusting the symbol duration within a fairly small duration set in an uncoded system can achieve the throughput gain from tens to over one hundred, which is still promising.

Chapter 4 extended the throughput gain study to coded systems. The throughput gain for a number of coding and modulation combination is investigated by simulations. We consider a rate adaptation policy which is linear to the received power, so it is ideally assumed that the symbol duration is not chosen from a finite discrete set but can take any positive real values. The simulation results shows that the throughput gain depends on the coding scheme and interleaver size. There is little merit to apply SBS duration adaptation with superior FEC codes (e.g., DVB.S2 LDPC codes) or with large size interleavers. On the other hand, without interleaving, the achievable throughput gain is still large for many commonly used coding scheme (e.g., convolutional codes).

Chapter 5 presented the preliminary study on the throughput gain with outdated and imperfect channel state information (CSI). In the analysis of Chapter 2 to Chapter 4, we assumed that the CSI known by the receiver and transmitter is perfect. In reality, the estimation/prediction process and feedback make the channel information at the transmitter side outdated and imperfect. The channel information at the transmitter is a set of information related to true channel condition. In Chapter 5, it is demonstrated that the higher the correlation between CSI and the true channel condition is, the larger throughput gain is achieved. During the analysis of Chapter 5, we consider a simple linear MMSE prediction scheme based on a single sample of the channel gain. The achievable throughput gain is promising since sophisticated estimation/prediction techniques available today can provide CSI highly correlated with the true channel condition [52].

Although the achievable throughput gain for uncoded systems is attractive, actual implementation of such a rapid adaptation seems challenging, as is the case with many adaptive transmission ideas. The idea of how to build a symbol-by-symbol adaptive transmission has been introduced in chapter 1 and its full detail was presented in references [1] [27]. In the proposed scheme, the CDMA chip duration is fixed, and symbols with different durations are spread by orthogonal-variable-spreading-factor (OVSF) codes of different lengths.

The data stream from an individual user will occupy bandwidth in excess of what is necessary for its momentary symbol rate. The same bandwidth is shared by many users whose signals are separated with OVSF codes and pseudo-random codes, which means that bandwidth efficiency does not suffer collectively, as is the case with most CDMA systems. Thus, the scheme can achieve higher error-constrained throughput without sacrificing bandwidth efficiency. However, the throughput gains to be achieved by using the SBS adaptation protocols will not be as high as those specified in previous chapters because of overhead of implementing an SBS adaptation. In the adaptation mechanism introduced in [27] and chapter 1, the control information is carried implicitly by the choice of spreading codes. The modulated symbols are only used to represent the user's data. By doing so, the frequent control information and rapid channel feedback occupy little transmission time. Thus, the throughput gain will not be reduced much after compensating the overhead and feedback of SBS adaptation. The price to be paid for this gain would be an increase in processing complexity.

In this thesis, the adaptation of symbol duration is discussed under the assumption that the transmission power is constant. An envisioned application of this assumption is in multi-user environment in which there is no centralized control of adaptation or global knowledge of all channels' states. The feedback architecture of SBS adaptation allows for symbol-by-symbol adaptation of both transmission power and the symbol duration if a centralized power control is available. The symbol-by-symbol distributed power and rate control in a multi-user CDMA system with multi-user interference, without knowledge of all channels' states and centralized control, is a complicated problem and is beyond the scope of this thesis. Consider another kind of multi-user CDMA system, in which frames are all synchronized and a frame-by-frame power control is exercised by each user. Then, an individual user's transmission power during each frame is constant, so the symbol-by-symbol spreading gain adaptation results are applicable under the assumption that the Doppler shift f_D is high in relation to the frame duration, i.e., the fading channel is fast time-varying. This frame-by-frame power adaptation symbol-by-symbol duration adaptation system can exploit the much of the throughput gain and hence improve the spectrum efficiency of the fast time-vary fading channels.

Another thought about the frame-by-frame duration adaptation is that, if the frame duration is reduced (i.e., increase the frequency of adaptation), the error-constrained throughput will increase, even though the adaptation is not as rapid as SBS adaptation. However,

the throughput gain will be less than that of the SBS adaptation. Intuitively speaking, the shorter the frame length is, the higher the throughput will be. On the other hand, the shorter the frame length is, the higher the overhead will be. The trade off between the overhead and the throughput in FBF duration adaptation is left for future study.

Appendix A

Derivation of Channel Power Gain Autocorrelation

Let us derive the first equation in (3.17). We assume the normalized complex channel gain $g_1, g_2, \ldots, g_i, \ldots$ is a stationary random process. Let $g_i = g_i^I + jg_i^Q$, where g_i^I and g_i^Q are zero-mean real Gaussian variables with $E\{(g_i^I)^2\} = E\{(g_i^Q)^2\} = 1/2$ such that g_i is a zero-mean complex Gaussian variable with $E(|g_i|^2) = 1$. The autocorrelation of g_i is

$$\begin{aligned} E\left(g_i g_k^*\right) &= E\left\{\left(g_i^I + jg_i^Q\right)\left(g_k^I + jg_k^Q\right)^*\right\} \\ &= E\left\{\left(g_i^I + jg_i^Q\right)\left(g_k^I - jg_k^Q\right)\right\} \\ &= E\left(g_i^I g_k^I\right) + E\left(g_i^Q g_k^Q\right) - jE\left(g_i^I g_k^Q\right) + jE\left(g_i^Q g_k^I\right) \end{aligned} \tag{A.1}$$

For the stationary random process $g_1, g_2, \ldots, g_i, \ldots$, we have $E\left(g_i^I g_k^I\right) = E\left(g_i^Q g_k^Q\right)$ and $E\left(g_i^I g_k^Q\right) = -E\left(g_i^Q g_k^I\right)$ [38] [49, Page 155]. Then (A.1) further becomes

$$E\left(g_i g_k^*\right) = 2E\left(g_i^I g_k^I\right) + j2E\left(g_i^Q g_k^I\right) \tag{A.2}$$

The power of channel gain is $|g_i|^2 = (g_i^I)^2 + (g_i^Q)^2$. The correlation of the channel power gain is given by

$$\begin{aligned} E\left\{|g_i|^2|g_k|^2\right\} &= E\left\{\left(\left(g_i^I\right)^2 + \left(g_i^Q\right)^2\right)\left(\left(g_k^I\right)^2 + \left(g_k^Q\right)^2\right)\right\} \\ &= E\left\{\left(g_i^I\right)^2\left(g_k^I\right)^2\right\} + E\left\{\left(g_i^Q\right)^2\left(g_k^Q\right)^2\right\} \\ &\quad + E\left\{\left(g_i^I\right)^2\left(g_k^Q\right)^2\right\} + E\left\{\left(g_i^Q\right)^2\left(g_k^I\right)^2\right\} \end{aligned} \tag{A.3}$$

For the zero-mean real Gaussian variables g_i^I, g_i^Q, g_k^I and g_k^Q, Isserlis' theorem [53] can be applied to compute the 4th-order moments [1]. We have

$$\begin{aligned}
E\left\{(g_i^I)^2(g_k^I)^2\right\} &= E\left\{(g_i^I)^2\right\}E\left\{(g_k^I)^2\right\} + 2\left[E\left\{g_i^I g_k^I\right\}\right]^2 = \frac{1}{4} + 2\left[E\left\{g_i^I g_k^I\right\}\right]^2 \\
E\left\{(g_i^Q)^2(g_k^Q)^2\right\} &= E\left\{(g_i^Q)^2\right\}E\left\{(g_k^Q)^2\right\} + 2\left[E\left\{g_i^Q g_k^Q\right\}\right]^2 = \frac{1}{4} + 2\left[E\left\{g_i^Q g_k^Q\right\}\right]^2 \\
E\left\{(g_i^I)^2(g_k^Q)^2\right\} &= E\left\{(g_i^I)^2\right\}E\left\{(g_k^Q)^2\right\} + 2\left[E\left\{g_i^I g_k^Q\right\}\right]^2 = \frac{1}{4} + 2\left[E\left\{g_i^I g_k^Q\right\}\right]^2 \\
E\left\{(g_i^Q)^2(g_k^I)^2\right\} &= E\left\{(g_i^Q)^2\right\}E\left\{(g_k^I)^2\right\} + 2\left[E\left\{g_i^Q g_k^I\right\}\right]^2 = \frac{1}{4} + 2\left[E\left\{g_i^Q g_k^I\right\}\right]^2
\end{aligned} \tag{A.4}$$

Hence the autocorrelation of the channel power gain is

$$\begin{aligned}
E\left\{|g_i|^2|g_k|^2\right\} &= 1 + 2\left[E\left\{g_i^I g_k^I\right\}\right]^2 + 2\left[E\left\{g_i^Q g_k^Q\right\}\right]^2 + 2\left[E\left\{g_i^I g_k^Q\right\}\right]^2 + 2\left[E\left\{g_i^Q g_k^I\right\}\right]^2 \\
&= 1 + 4\left[E\left\{g_i^I g_k^I\right\}\right]^2 + 4\left[E\left\{g_i^I g_k^Q\right\}\right]^2
\end{aligned} \tag{A.5}$$

The channel is assumed to be the Clarke's two-dimensional isotropic scattering model of which the channel gain autocorrelation is give by

$$E\left[g_i g_k^*\right] = J_0\left(2\pi f_D(k-i)T_c\right) \tag{A.6}$$

Note that for this channel model [38],

$$E\left\{g_i^I g_k^Q\right\} = 0 \tag{A.7}$$

By Equation (A.2), we further have

$$E\left\{g_i^I g_k^I\right\} = \frac{1}{2}E\left\{g_i g_k^*\right\} = \frac{1}{2}J_0\left(2\pi f_D(k-i)T_c\right) \tag{A.8}$$

By substituting (A.7) and (A.8) into (A.5), the channel power gain correlation is

$$E\left\{|g_i|^2|g_k|^2\right\} = 1 + 4\left[E\left\{g_i^I g_k^I\right\}\right]^2 = 1 + J_0^2\left(2\pi f_D(k-i)T_c\right) \tag{A.9}$$

which is the first line of (3.17).

---

[1] Let $\bar{X} = [X_1, X_2, \ldots, X_N]$ be a zero-mean real Gaussian random vector. The 4th-order moments are given by

$$E\left\{X_i X_j X_k X_n\right\} = E\left\{X_i X_j\right\}E\left\{X_k X_n\right\} + E\left\{X_i X_k\right\}E\left\{X_j X_n\right\} + E\left\{X_i X_k\right\}E\left\{X_j X_n\right\}$$

where $i,\ j,\ k,\ n = 1,\ 2,\ \ldots,\ N$. Specially,

$$E\left\{X_i^2 X_j^2\right\} = E\left\{X_i X_i X_j X_j\right\} = E\left\{X_i^2\right\}E\left\{X_j^2\right\} + 2E\left\{X_i X_j\right\}$$

Appendix B

Proof of Equation (5.2)

Let $a(t)$ be a stationary complex-valued random process that models the base-band complex-valued fading channel gain for the signal arriving at each time t. Let $x(t)$ and $y(t)$ be the In-phase and Quadrature components of $a(t)$, i.e., $a(t) = x(t) + jy(t)$. Let $n(t)$ be the narrowband band-pass process [49] corresponding to $a(t)$, i.e.,

$$n(t) = \mathrm{Re}\left[a(t)e^{j2\pi f_c t}\right] \tag{B.1}$$

$n(t)$ can also be represented by

$$n(t) = x(t)\cos 2\pi f_c t - y(t)\sin 2\pi f_c t \tag{B.2}$$

Then the autocorrelation of $n(t)$ is given by

$$\begin{aligned}
E\{n(t)n(t+\tau)\} &= E\{[x(t)\cos 2\pi f_c t - y(t)\sin 2\pi f_c t] \\
&\quad \times [x(t+\tau)\cos 2\pi f_c(t+\tau) - y(t+\tau)\sin 2\pi f_c(t+\tau)]\} \\
&= E\{x(t)x(t+\tau)\}\cos 2\pi f_c t \cos 2\pi f_c(t+\tau) \\
&\quad + E\{y(t)y(t+\tau)\}\sin 2\pi f_c t \sin 2\pi f_c(t+\tau) \\
&\quad - E\{x(t)y(t+\tau)\}\cos 2\pi f_c t \sin 2\pi f_c(t+\tau) \\
&\quad - E\{y(t)x(t+\tau)\}\sin 2\pi f_c t \cos 2\pi f_c(t+\tau) \\
&= \frac{1}{2}\left[E\{x(t)x(t+\tau)\} + E\{y(t)y(t+\tau)\}\right]\cos 2\pi f_c \tau \\
&\quad + \frac{1}{2}\left[E\{x(t)x(t+\tau)\} - E\{y(t)y(t+\tau)\}\right]\cos 2\pi f_c(2t+\tau) \\
&\quad - \frac{1}{2}\left[E\{y(t)x(t+\tau)\} - E\{x(t)y(t+\tau)\}\right]\sin 2\pi f_c \tau
\end{aligned}$$

$$-\frac{1}{2}\left[E\{y(t)x(t+\tau)\}+E\{x(t)y(t+\tau)\}\right]\sin 2\pi f_c(2t+\tau) \tag{B.3}$$

Since $n(t)$ is also stationary, the autocorrelation of $n(t)$ must be independent of t. This condition can only be satisfied if

$$E\{x(t)x(t+\tau)\}=E\{y(t)y(t+\tau)\} \tag{B.4}$$

and

$$E\{x(t)y(t+\tau)\}=-E\{y(t)x(t+\tau)\} \tag{B.5}$$

Therefore, we have

$$\begin{aligned} E\{a(t)a(t+\tau)\} &= E\{[x(t)+jy(t)]\,[x(t+\tau)+jy(t+\tau)]\} \\ &= E\{x(t)x(t+\tau)\}-E\{y(t)y(t+\tau)\} \\ &\quad + j\left[E\{x(t)y(t+\tau)\}+E\{y(t)x(t+\tau)\}\right] \\ &= 0 \end{aligned} \tag{B.6}$$

Bibliography

[1] L. Tsaur and D. Lee, "Symbol rate adaptation and blind rate detection using FOSSIL (forest for OVSF-sequence-set-inducing lineages)," in *proc. of IEEE International Conference on Communication*, vol. 6, 2001, pp. 1754–1759.

[2] ——, "Symbol-by-symbol rate adapting wireless communication systems: architecture," in *Rail Conference, 2003. Proceedings of the 2003 IEEE/ASME Joint*, April 2003, pp. 109–131.

[3] J. Hayes, "Adaptive feedback communications," *IEEE Transactions on Communication Technology*, vol. 16, no. 1, pp. 29–34, 1968.

[4] J. Cavers, "Variable-rate transmission for Rayleigh fading channels," *Communications, IEEE Transactions on Communications*, vol. 20, no. 1, pp. 15–22, 1972.

[5] A. Goldsmith and P. Varaiya, "Capacity of fading channels with channel side information," *IEEE Transactions on Information Theory*, vol. 43, no. 6, pp. 1986–1992, 1997.

[6] G. Caire and S. Shamai, "On the capacity of some channels with channel state information," *IEEE Transactions on Information Theory*, vol. 45, no. 6, pp. 2007–2019, 1999.

[7] S. Chung and A. Goldsmith, "Degrees of freedom in adaptive modulation: a unified view," *IEEE Transactions on Communications*, vol. 49, no. 9, pp. 1561–1571, 2001.

[8] A. Goldsmith and S. Chua, "Variable-rate variable-power MQAM for fading channels," *IEEE Transactions on Communications*, vol. 45, no. 10, pp. 1218–1230, 1997.

[9] J. Cavers, "An analysis of pilot symbol assisted modulation for Rayleigh fading channels," *IEEE Trans. Veh. Technol*, vol. 40, no. 4, pp. 686–693, 1991.

[10] S. Otsuki, S. Sampei, and N. Morinaga, "Square-QAM adaptive modulation/TDMA /TDD systems using modulation level estimation with Walsh function," *Electronics Letters*, vol. 31, no. 3, pp. 169–171, 1995.

[11] W. Webb and R. Steele, "Variable rate QAM for mobile radio," *IEEE Transactions on Communications*, vol. 43, no. 7, pp. 2223–2230, 1995.

[12] J. Hagenauer, "Rate-compatible punctured convolutional codes (RCPC codes) and their applications," *IEEE transactions on Communications*, vol. 36, no. 4, pp. 389–400, 1988.

[13] G. Ungerboeck, "Channel coding with multilevel/phase signals," *IEEE Transactions on Information Theory*, vol. 28, no. 1, pp. 55–67, 1982.

[14] A. Goldsmith and S. Chua, "Adaptive coded modulation for fading channels," *IEEE Transactions on Communications*, vol. 46, no. 5, pp. 595–602, 1998.

[15] C. LI and K. Sabnani, "Variable spreading gain CDMA with adaptive control for true packet switching wireless network," in *Proceedings of the IEEE ICC Conference*, vol. 2, 1995, pp. 725–730.

[16] S. Oh and K. Wasserman, "Dynamic spreading gain control in multiservice CDMA networks," *IEEE Journal on Selected Areas in Communications*, vol. 17, no. 5, pp. 918–927, 1999.

[17] T. Lee and J. Wang, "Admission control for variable spreading gain CDMA wireless packet networks," *IEEE Transactions on Vehicular Technology*, vol. 49, no. 2, pp. 565–575, 2000.

[18] IEEE, *IEEE Standard for Information technology –Telecommunications and information exchange between systems–Local and metropolitan area networks–Specific requirements Part 11: Wireless LAN Medium Access Control (MAC) and Physical Layer (PHY) specifications Amendment 4: Further Higher Data Rate Extension in the 2.4 GHz Band.* http://ieeexplore.ieee.org, 2003.

[19] C. Heegard, J. Coffey, S. Gummadi, P. Murphy, R. Provencio, E. Rossin, S. Schrum, M. Shoemake, and T. Instruments, "High performance wireless Ethernet," *IEEE Communications Magazine*, vol. 39, no. 11, pp. 64–73, 2001.

[20] IEEE, *IEEE Standard for Information technology –Telecommunications and information exchange between systems–Local and metropolitan area networks–Specific requirements Part 11: Wireless LAN Medium Access Control (MAC) and Physical Layer (PHY) specifications High-speed Physical Layer in the 5 GHz Band.* http://ieeexplore.ieee.org, 2003.

[21] J. Andrews, A. Ghosh, and R. Muhamed, *Fundamentals of WiMAX.* Prentice Hall USA, 2007.

[22] H. Holma, A. Toskala *et al.*, *WCDMA for UMTS: Radio access for third generation mobile communications.* Wiley New York, 2000.

[23] S. Yang, *3G CDMA2000: wireless system engineering.* Artech House Publishers, 2004.

[24] E. Dahlman, B. Gudmundson, M. Nilsson, and A. Skold, "UMTS/IMT-2000 based on wideband CDMA," *IEEE Communications magazine*, vol. 36, no. 9, pp. 70–80, 1998.

[25] F. Adachi, M. Sawahashi, and K. Okawa, "Tree-structured generation of orthogonal spreading codes with different lengths for forward link of DS-CDMA mobile radio," *Electronics Letters*, vol. 33, no. 1, pp. 27–28, 1997.

[26] M. Fong, V. Bhargava, and Q. Wang, "Concatenated orthogonal/PN spreading sequences and their application to cellular DS-CDMA systems with integrated traffic," *IEEE Journal on Selected Areas in Communications*, vol. 14, no. 3, pp. 547–558, 1996.

[27] L. Tsaur and D. Lee, "Closed-loop architecture and protocols for rapid dynamic spreading gain adaptation in CDMA networks," *IEEE/ACM Transactions on Networking (TON)*, vol. 14, no. 4, p. 834, 2006.

[28] D. LEE and L. TSAUR, "Gains achieved by symbol-by-symbol rate adaptation on error-constrained data throughput over fading channels," *Journal of Communication and Networks*, vol. 9, no. 3, pp. 213–218, 2007.

[29] L. Tsaur and D. Lee, "Gain achieved by symbol-by-symbol rate adaptation on error-constrained data throughput over fading channels," in *proc. of IEEE International Conference on Communication*, 2001, pp. 213–218.

[30] M. Naeem and D. Lee, "On convexity of MQAM's and MPAM's bit error probability functions," *International Journal of Communications*, vol. 22, pp. 1465–1477, 2009.

[31] L. Hanzo, S. Ng, T. Keller, and W. Webb, *Quadrature amplitude modulation.* John Wiley, 2004.

[32] K. Cho and D. Yoon, "On the general BER expression of one- and two-dimensional amplitude modulations," *IEEE Transactions on Communication*, vol. 50, no. 7, pp. 1074–1080, 2002.

[33] M. Simon and M. Alouini, *Digital communication over fading channels.* IEEE, 2005.

[34] A. Goldsmith, *Wireless communications.* Cambridge Univ Pr, 2005.

[35] M. Alouini and A. Goldsmith, "A unified approach for calculating error rates of linearly modulated signals over generalized fading channels," *IEEE Transactions on Communications*, vol. 47, no. 9, pp. 1324–1334, 1999.

[36] P. Lombardo, G. Fedele, and M. Rao, "MRC performance for binary signals in Nakagami fading with general branch correlation," *IEEE Transactions on Communications*, vol. 47, no. 1, pp. 44–52, 1999.

[37] A. Annamalai and C. Tellambura, "A moment-generating function (MGF) derivative-based unified analysis of incoherent diversity reception of M-ary orthogonal signals

over independent and correlated fading channels," *International Journal of Wireless Information Networks*, vol. 10, no. 1, pp. 41–56, 2003.

[38] G. Stüber, *Principles of mobile communication.* Kluwer Academic Pub, 2001.

[39] D. Lee and S. Xue, "Gains in Error-Constrained Data Throughput for Extreme Fast Adaptation of symbol Durations Over Multi-Path Fading Channel: Coded and Uncoded systems," *IEEE Transactions on Communication*, accepted.

[40] T. Cover and J. Thomas, *Elements of information theory.* wiley, 2006.

[41] J. Devore, *Probability and Statistics for Engineering and the Sciences.* Thomson Learning, 2004.

[42] J. Hagenauer, "Viterbi decoding of convolutional codes for fading-and burst-channels," in *Proc. Int. Zurich Seminar*, 1980.

[43] D. MacKay and R. Neal, "Near Shannon limit performance of low density parity check codes," *Electronics letters*, vol. 33, no. 6, pp. 457–458, 1997.

[44] T. Richardson, M. Shokrollahi, and R. Urbanke, "Design of capacity-approaching irregular low-density parity-check codes," *IEEE Transactions on Information Theory*, vol. 47, no. 2, pp. 619–637, 2001.

[45] J. Hou, P. Siegel, and L. Milstein, "Performance analysis and code optimization of low density parity-check codes on Rayleigh fading channels," *IEEE Journal on Selected areas in Communications*, vol. 19, no. 5, pp. 924–934, 2001.

[46] S. Chung, G. Forney Jr, T. Richardson, R. Urbanke, A. Inc, and M. Chelmsford, "On the design of low-density parity-check codes within 0.0045 dB of the Shannon limit," *IEEE Communications Letters*, vol. 5, no. 2, pp. 58–60, 2001.

[47] M. Eroz, F. Sun, and L. Lee, "DVB-S2 low density parity check codes with near Shannon limit performance," *International Journal of Satellite Communications and Networking*, vol. 22, no. 3, pp. 269–279, 2004.

[48] D. Lee, M. Naeem, and S. Xue, "On Error-Constrained Data Throughput of Rapid Symbol Duration Adaptation with Imperfect Channel Information," in *IEEE International Networking and Communications Conference, 2008. INCC 2008*, 2008, pp. 96–100.

[49] J. Proakis, *Digital communications 4th Edition.* McGraw-hill New York, 2001.

[50] B. Picinbono and P. Chevalier, "Widely linear estimation with complex data," *IEEE Transactions on Signal Processing*, vol. 43, no. 8, pp. 2030–2033, 1995.

[51] B. Picinbono, "Second-order complex random vectors and normal distributions," *IEEE Transactions on Signal Processing*, vol. 44, no. 10, pp. 2637–2640, 1996.

[52] A. Duel-Hallen, S. Hu, and H. Hallen, "Long-range prediction of fading signals," *IEEE Signal Processing Magazine*, vol. 17, no. 3, pp. 62–75, 2000.

[53] L. Isserlis, "On a formula for the product-moment coefficient of any order of a normal frequency distribution in any number of variables," *Biometrika*, vol. 12, no. 1-2, p. 134, 1918.